A New Sheet Metal Forming System Based on Incremental Punching

LUO, Yuanxin

A Thesis Submitted in Partial Fulfillment

of the Requirements for the Degree of

Doctor of Philosophy

in

Automation and Computer-Aided Engineering

The Chinese University of Hong Kong

July 2010

UMI Number: 3446007

Thesis/ Assessment Committee

Professor Michael Yu Wang (Chair)

Professor Ruxu Du (Thesis Supervisor)

Professor Yangsheng Xu (Committee Member)

Professor Wingbun Lee (External Examiner)

Abstract

Stamping is one of the most commonly used manufacturing processes. Everyday, millions of parts are formed by this process. The conventional stamping is to form a part in one or several operations with a press machine and a set / sets of dies. It is very efficient but is not cost effective for small batch production parts and prototypes as the dies are expensive and time consuming to make. Recently, with the increasing demands for low-volume and customer-made products, a die-less forming method, Incremental Sheet Metal Forming (ISMF), has become one of the leading R&D topics in the industry.

ISMF uses a small generic tool to apply a sequence of operations along the given path to deform the sheet incrementally. These small deformations accumulate to form the final shape of the part. As a result, different parts can be made by the same setup. Despite of some 30 years of research and development, however, ISMF technology is still premature for industrial applications due to the following reasons: The accuracy of the part is limited; the surface roughness is poor; and the productivity is low. This motivates the presented research.

In this research, a new incremental forming system based on incremental punching is designed and built. The system consists of a 3-axes CNC platform, a high speed hydraulic cylinder with a hemispherical forming tool, and a PC-based CNC control system. The hydraulic system provides the forming force to deform the sheet metal with constant stokes, while the CNC system positions the part. When forming a part, the forming tool punches the sheet metal along the given contour of the part punch by punch; when one layer of the part is completed, the forming tool moves down to the next layer; and the process is finished till all layers are completed. The CNC control system works with standard NC code, and hence, is easy to use.

In order to ensure the desirable performance of the machine, dynamic analysis of the machine is necessary. The analysis is conducted by the mean of computer simulation in consideration of applying a large impulsive force. This study validates the machine stability and accuracy.

One of the keys to successful application of sheet metal forming is to be able to predict the deformation and the strain / stress of the part incurred during the forming process. Because of the complexity of the ISMF process, it is not possible to derive an analytical method. The alternative is to use Finite Element Analysis (FEA). However, based on our experience, it takes about one week to solve a simple case. A mechanics model is therefore developed. It consists of two steps. The first step is to computer the final shape: the initial geometric surface is obtained using the punch positions; then using the minimum energy principle, the virtual forces drive the nodes of geometric surface to their lowest energy positions, which gives the final shape of the forming part. The second step is to predict the strain and stress distributions. This is done using the inverse Finite Element Modeling (FEM). An in-house computer software is developed using MATLAB®.

In order to verify the new mechanics model, numerical and experimental studies are conducted using the new incremental punching system. The final shape and thickness distributions of parts are compared to verify the mechanics model. It is found that the model prediction fits the experiment result well. Forming parameters are also investigated.

To evaluate the capability of the presented ISMF process, the formability is studied by the means of theory and experiment. A modified M-K model is proposed for predicting the forming limit of the formed part which is undergoing a very complicated strain path. The maximum forming angle is also investigated by experiments.

摘　要

冲压是使用最广泛的制造工艺之一，大量的零件都是由冲压方法成形。其过程就是在压力机上安装一套或几套模具，通过一次或几次操作就可生产出一个零件。因而，冲压成形具有很高的效率，但对于小批量和零件试制而言，其单件成本就非常高。近年来，随着小批量和客户定制零件的需求不断上升，一种无模成形方法，薄板渐进成形技术已成为冲压领域研究的热点之一。

薄板渐进成形方法是采用一个小成形工具，沿着给定的轨迹在工件上逐点作用产生一系列的小变形，通过累积得到零件的最终形状。因此，用同一套装置可以生产出不同的零件。尽管经过近 30 年的研究开发，但是薄板渐进成形技术还存在几个方面问题：成形精度不高，表面质量差，而且效率很低。所以，该技术仍待发展才广泛应用于工业领域，这亦是本课题研究的出发点。

本研究设计一套新的基于渐进冲压的成形系统，可为制造小批量板料成形提供一种解决方案。该成形系统包括三轴 CNC 运动平台，高速液压系统和与之相连的球形成形工具，以及基于 PC 的 CNC 控制系统。液压系统将以固定行程往复运动，为金属变形提供所需的冲压力，而 CNC 运动系统用于定位加工工件。其加工过程是，成形工具按照给定轨迹逐点敲击产生局部小变形，完成当前层轨迹后，成形工具将下移一层直到整个零件加工完成。该 CNC 系统可以读入标准数控代码。

为了确保能够达到预期的性能，须对机械系统的动力学进行分析。本研究分别对三个进给轴系进行动力学建模，采用计算机数值方法进行分析，并考虑到冲压力等外载的影响。该研究确保了运动系统的稳定性和精度。

准确预测加工过程的工件的应变或应力，是金属成形方法得到成功应用的关键因素之一。但是，由于薄板渐进成形过程较复杂，很难运用解析法进行准确预测。

虽然，运用商业有限元工具可以对整个成形过程进行模拟，但是计算一个很简单的算例亦须耗时一周左右。因此，本研究提出一个基于最小能量原理的力学模型，由已给定的冲头位置和形状，运用几何关系计算出理想状态下工件的初始几何面，然后定义曲面上节点的虚拟势能，通过虚拟节点力驱动几何面的节点移动到其最低势能位置，以得到零件的最终形状。然后采用逆有限元方法，根据计算出的形状，计算出工件的最终应变和应力。最后运用 MATLAB®编写了一套计算程序。

本研究运用上述程序进行大量算例的数值模拟，并利用我们的渐进冲压的成形系统制作了样件。测量样件的最终形状和厚度，与数值模拟结果进行对比以验证所提出的力学模型。结果表明，理论预测与实验分析具有很好一致性。同时，研究了加工参数的影响。

为了评估该工艺的成形能力，本研究对其成形能力进行理论分析和实验研究。提出一种改进的 M-K 模型，可对在该成形过程中工件复杂的应变历程进行分析。此外，还通过实验的方法得到了最大成形角。

Acknowledgement

First, I would like to express my sincere gratitude to my supervisor, Prof. Ruxu Du, for his great support and patient guidance through all these three years. From him I have learned a lot of knowledge, research methodology, and skills as well as positive attitude towards life, which are very helpful in my future career. I really appreciate him for giving me the opportunity to study in CUHK.

I also want to say thanks to other people who played vital roles in completing this thesis. Special thanks go to Prof. Yang-sheng Xu, Prof. Michael Wang and Prof. Wing-bun Lee who took the time to serve on my dissertation committee and provided insightful comments and ideas to further improve this dissertation.

I am grateful to all the people who have helped me through the process, especially Dr. Tom Kong, Dr. Kai He and Dr. Wu-jiao Xu for their encouragement and valuable advice thought the process. I wish to thank Mr. Peng Zhang for his suggestions on the mechanics model, Mr. Jiu-hua Li for his FEA simulation results, Dr. Shi-qing Liu for his help to develop the control system. I am also grateful to other colleagues at Institute of Precision Engineering, CUHK. I enjoy the study and life in IPE. I will treasure the wonderful time and the friendship forever.

Finally, with great love and respect, I would like to deeply appreciate the continuous and strong support from my family and my girl friend.

Table of Contents

List of Notations

$S(x, y)$ middle surface of the sheet metal

$E(S(x, y))$ energy of the surface

a_{11} stretching stiffness in the x direction

a_{22} stretching stiffness in the y direction

β_{11} bending stiffness in the x direction

β_{12} bending stiffness in the x and y directions

β_{22} bending stiffness in y direction

$\Delta x_{i,j}$ grid distance in the x direction

$\Delta y_{i,j}$ grid distance in the y direction

S_{ij} energy of node i, j

F_{ij} driven force of node i, j

n_0 initial normal vector of the node

n normal vector of a final state element

$(x\ y\ z)$ initial position of a node

$(X\ Y\ Z)$ final position of a node

$\vec{x}_1, \vec{x}_2$ vectors of the first two edges of a element in initial state

$\vec{X}_1, \vec{X}_2$ vectors of the first two edges of a element in final state

$\vec{t}$ translation vector between initial state and final state

$[R]$ rotation matrix

$[u]$ displacement matrix of a final state element

$[\lambda]$ true strains matrix of a final state element

$[\sigma]$ stresses matrix of a final state element

$[A]$ shape matrix of the initial element

$[W]$ the constants matrix

$[\varepsilon]$ logarithmic strain matrix of a element

$[m]$ rotation matrix of principle strains

$[P]$ material properties matrix

(x_k, y_k, z_k)	a punch location
r_t	radius of the forming tool (mm)
$G(x, y)$	geometric surface
E	young's module
v	poisson ratio
r	lankford value
$\bar{\sigma}$	effective stress
$\bar{\varepsilon}_p$	effective strain
F	resultant feed rate of in X-Y direction
a	feed step in X-Y direction
f	punch speed
h	layer thickness / feed step in Z direction
δ	geometric error
R	local curvature of the part contour in X-Y direction
R'	local curvature of the part contour in Z direction
t	thickness of a part formed
t_0	initial thickness of the blank
θ	slope angle of the part in Z direction

List of Tables

List of Figures

Acronym

CAD	computer-aided design
CAM	computer-aided manufacturing
CNC	computer numerical controlled
CST	constant strain triangular
FEA	finite element analysis
FEM	finite element modeling
FLC	forming limit curve
FLD	forming limit diagram
ISMF	incremental sheet metal forming
M-K	Maricniak and Kuczynski
NC	numerical control
PC	personal computer
PLC	programmable logic controller
SPM	stroke per minute
3D	three dimensional

Chapter 1:

Introduction

1.1 Motivation

Modern continuous rolling mills produce large quantities of sheet metals as thin hot roll strip or cold rolled sheet with low cost [Marciniak, Duncan and Hu, 2002]. Sheet metal forming, also called the stamping, is the secondary process in which the sheet metal is converted to another shape without change in the mass or composition of the material. It is one of most commonly used manufacturing processes and plays an important role in the modern society. Everyday millions of parts are made by stamping; therefore, even a small improvement may add a significant corporative gain. Traditional stamping includes a variety of sheet metal forming processes, such as punching, blanking, drawing, bending, flanging, and coining. It could be a single stage operation where every stroke of the press produce a part with desired form, or could be a multi-stage operation forming progressively [Pearce, 1991]. Most of the conventional means of forming sheet metals into finished shapes involve the use of expensive press machine and dies. Their high cost and long leading time militate against the customer demands for reduced cost and shortened the production time.

Die-less forming, also called Incremental Sheet Metal Forming (ISMF), is a recently invented die-less forming method, which is quite different to the traditional methods. In ISMF, a piece of sheet metal is formed to the desired shape by a series of small incremental deformations. As it does not use dies, ISMF is effective for small batch production and prototypes. In recent years, it has become one of the leading R&D topics in the industry.

Despite several benefits over conventional sheet metal forming process for prototyping and small batch production, ISMF has achieved only limited success in industry [http://www.thefabricator.com]. Current studies have shown that the key concerns are:

Firstly, the accuracy of the final parts; secondly, the thickness variations which resulting poor surface quality; and thirdly, the low production rate. In order for the industry to accept this technology, dramatic improvements are imperative. Moreover, the prediction of the forming process is also a must.

In this thesis, a new ISMF system for sheet metal forming known as Incremental Punching is proposed. It involves the use of a sphere punch tool driven by high frequency hydraulic system to punch the sheet metal to form the part progressively. The controlled movement of the tool is done through a CNC machine. The new system can make various sheet metal parts directly from a 3D CAD model without the conventional intermediate stage of die design and manufacture. This research also develops the mechanics model of the ISMF process. An in-house computer simulation program is developed that can predict the final shape and the strain / stress distributions of the part. The prediction helps to avoid failure during the forming process before the part is being made. Also, it helps to examine process variables such as the layer thickness, feed step, surface finish and dimensional accuracy. Finally, the formability of the process is investigated by both of theoretical method and experimental method.

To sum up, the arm of this thesis are two folders, which are to develop the new sheet metal forming process and to develop a mechanics model to predict the final shape and strains / stress distributions in the forming process.

1.2 Organization of the Thesis

This thesis is divided into eight chapters. The rest of the thesis is organized as follows.

Chapter 2 presents a literature review on various ISMF methods. The history and working principle of ISMF are introduced. The mechanics models and numerical studies are also studied.

In Chapter 3, the incremental punching process is described and studied by geometric method and Finite Element Analysis (FEA).

Chapter 4 presents a mechanics model of the proposed forming process, which uses minimum energy principle for predicting the final shape, and use inverse FEA for calculating the strains and stress distributions. The algorithms are detailed in this chapter.

Chapter 5 presents the design and control of the incremental punching machine. The dynamic model of the motion system is developed, and the effect of punching force is investigated. Also, the control system and the hydraulic system are studied.

In Chapter 6, two sample parts are studied by numerical and experimental methods. Comparisons of the design, numerical and experimental results are also conducted to verify the mechanics model as well as investigate the forming parameters.

Chapter 7 investigates the formability of incremental punching process. A modified M-K method is proposed to compute the forming limit. Also, the maximum forming angle is tested by series of experiments. It guarantees the success of achieving the final product.

Finally, Chapter 8 gives the conclusions as well as the future work.

Chapter 2:

Literature Survey

2.1 Review of Dieless Sheet Metal Forming Processes

Classical sheet metal forming process includes a variety of sheet metal forming processes, such as punching, blanking, drawing, bending, flanging, coining, *etc* [Marciniak *et al.*, 2002]. These processes could be a single stage operation where desired shape are formed on the sheet metal part in every stroke of the press, or could incrementally produce through a series of stages. Most of these means of forming sheet metals into finished shapes have to use an expensive press machine and stamping dies. For example, in drawing process, a blank of sheet metal is clamped around the edges, while the middle section is forced by a punch into a die to stretch the metal into the desired shape. Hence, it requires a press machine to provide sufficient force to push the sheet metal into a die punch to form a part. Moreover, a set / sets of dedicated dies are needed to be used for different parts.

It is well known that it is expensive and time-consuming to design and make the dies, to speed up the prototyping process and lower the cost for the low volume production, various kinds of die-less forming methods that can produce the sheet metal parts without dedicated dies were proposed. These methods include laser forming, flexible spinning, multi-point forming, incremental forming, shot peen forming, *etc*. Today, the die-less forming methods have been hot topics in the research of industry. Each method has its advantages and limitations which will lead to different applications.

Laser Forming technique has recently been developed and applied in the metal industries. The basic feature of laser forming is the forming by thermal stresses, induced by irradiation of a laser beam [Gieger and Vollertsen, 1993]. These internal stresses induce plastic strains that bend the material or result in local elastic/plastic buckling. Based on energy conservation, Arnet and Vollertsen [1995] proposed three basic modes

in the laser forming of sheet metals. They were defined quantitatively as temperature gradient, buckling and shortening mechanisms [Abbott, 1999; Shi *et al.*, 2006; Edwards, 2010]. This is illustrated in Figure 2.1.
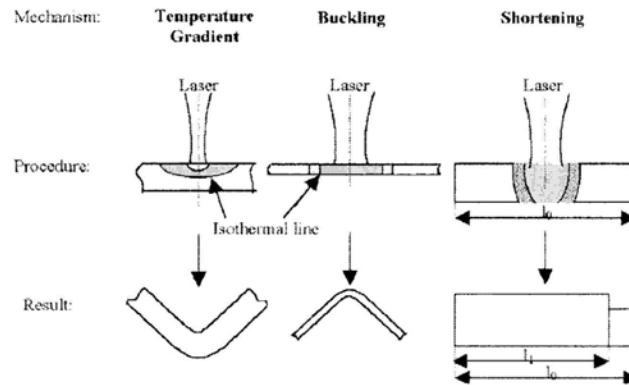
Figure 2.1: The forming principles of laser forming [Shi *et al.*, 2006]

Laser forming process is widely used in ship building industry, however, it should be noted that some limitations has been found [Abbott, 1999]. First, Current research has shown that it can produce parts with 2-D bends, however, it is more complicated to make a 3-D part, and not all of materials are amenable to the laser forming process [Nal and Kim, 2008]. Also, this process is with low product rate, and hence for some components, it is more cost effectively produced by conventional manufacturing processes.

Shot Peen Forming is a die-less sheet forming process that uses a stream of small hard shot with sufficient kinetic energy to bombard the surface of a metal sheet for forming a specific shape. This forming process is a derived from the shot peening surface treatment, which is usually used to enhance the fatigue strength of sheet metal parts for some special applications, especially for aerospace industry [Aggarwal *et al.*, 2006; Kim *et al.*, 2010]. In shot peen forming, the shot is usually made up of steel balls which are accelerated to a specific velocity and directed in a desired pattern. The size of balls is about $\Phi 0.05{\sim}2$ mm in diameter [Hong *et al.*, 2008]. They impact on the sheet metal thousands of times in a random manner. During impacts of the shots, a certain amount of its kinetic energy is transformed into plasticication of the component. When shot

velocity is fairly low, only a thin layer of the component's material is elongated, resulting in a convex curvature. If shot velocity is increased, concave curvatures are produced. The mechanism of shot peen forming is shown in Figure 2.2.
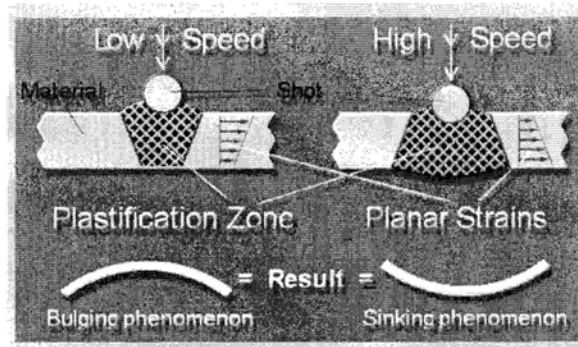
Figure 2.2: Mechanism of shot peen forming
[http://www.abrasivefinishingcompany.com]

The shot peen forming process generally has lower manufacturing costs because there is no need for dies and presses or subsequent thermal processes, and once the process parameters have been determined, the process is easily reproducible [Wang *et al.*, 2006]. It also has better adaptability to modern aircraft designs, for example, the capability to form single and double curved shapes and virtually any size of parts [Kishor *et al.*, 1981; Kopp and Schulz, 2008]. In addition, it can provide beneficial performance to the peen-formed component like the general shot peen hardening process [Guagliano and Vergnai, 2004].

Multi-point Forming is to form the sheet metal with a press machine with a reconfigurable discrete dies. The concept of discrete-pin die that was used for forming sheet metal was first introduced about 30 years ago [Hardt *et al.*, 1981]. Hardt and Walczyk [Hardt *et al.*, 1982; Walczyk *et al.*, 1998; Walczyk and Hardt, 1998] explored a discrete-die mechanical design for rapid response production of sheet metal parts. However, with the advance of computer control technology, this technology was conducted to industry applications in recent year [Li *et al.*, 2008]. It will be found extensive applications in sheet metal forming fields such as airplane skin panel, vehicle

6

body skin panel, medical engineering, *etc.,* and also in plate forming fields such as shipbuilding, pressure vessel, metal sculptures, modern architectures, etc. especially for small lot products. To obtain both flexible die and stamp the multi-point method is investigated by Jilin University in China [Li *et al.,* 2002]. It involves several hydraulic cylinders working against each other to shape a detail. The working principle of Multi-forming is to control the tool system setting a matrix of threaded rods to approximate the designed shape, and then the geometric surfaces of the matrix of threaded rod converts to a dedicated discrete die. The configured discrete die removes from the setting machine and clamps into a rigid stretch forming tool. Hence, the flexibility of this process is largely depending on the resolution of discrete die. Figure 2.3 shows a reconfigurable discrete die.
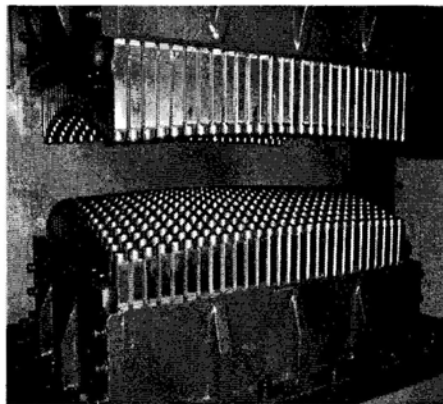
Figure 2.3: A reconfigurable discrete die [Li *et al.,* 2002].

Multi-point forming provides a forming system that can quickly change the set up of the forming tool. The better result will be achieved when the punch size is small [Cai *et al.,* 2009]. For the parts with large curvature, the shape errors will be large. Also, the small punch size will make the machine more complicated and expensive.

Flexible Bending is a flexible process developed from the general bending process. General bending process bends the workpiece across an entire cross-section using a dedicated die. However, the flexible bending process has two differences against to general bending: 1) allow control of the bend angle at a particular location, and 2)

control the distribution of the bend over some length of the product. Yang and Shima [1991] explored the first approach for bending sheets along a line. Yang *et al.* [1998] also applied a related method to 'L-bending' with an intelligent punch tool. Both of these methods are used for creating single sharp bends, but in the second approach, continuous sheet bending is achieved by three-roll bending. Mori *et al.* [1995] reported on the optimal control of this process. The control system included a 'fuzzy learning process' to allow for control of plates and sheets with unknown properties. However, the equipment is expensive. Ong *et al.* [1997] also used fuzzy-set based methodology to determine the optimal bending sequences for the brake forming of sheet metal components, considering the relative importance of handling and accuracy. Yoon and Yang [2005] also proposed a new incremental forming process using an adjustable punch set and used it to make a doubly curved sheet metal part. Allwood and Utsunomiya [2006] summarized the flexible bending method as shown in Figure 2.4. It was reported that Hu *at al.* [2009] used three bendable rollers to form 3-D surface parts.
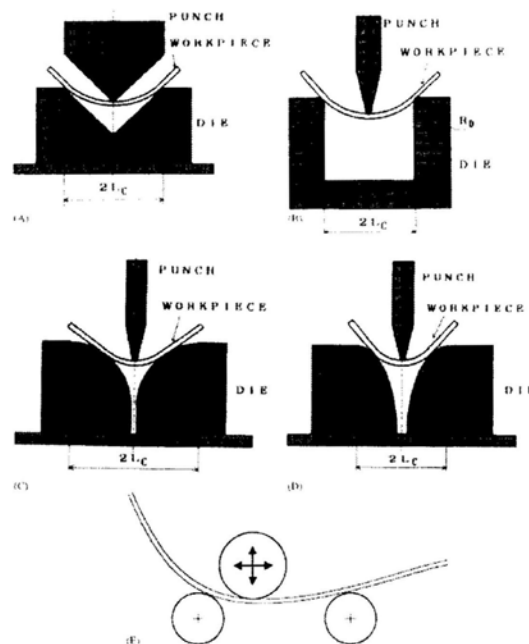
Figure 2.4: Flexible bending of sheets with: (A) conventional V-bending, (B) air bending, (C) a curved die, (D) an oval die and (E) three roll bending [Allwood and Utsunomiya, 2006]

8

Flexible Spinning: Conventional spinning is using rotating tool and a specific mandrel for each product, and hence it is not a flexible process. This technique is being applied for the production of many key components, especially for the automotive industry [Wong *et al.*, 2003]. Kitazawa *et al.* [1994], Shima *et al.* [1996] and Matsubara [1994] have explored three approaches to make this process flexible. The ability to enable metal to flow in complicated paths using simple tools not only eliminates multi-production stages on presses, thus reducing costs, but also offers the potential for the production of lightweight, net shape parts. Kawai *et al.* [2007] conducted experiment to investigate the technological possibility of the shear spinning of truncated hemispherical shells with a cylindrical mandrel for general purposes using A1050-H and A1050-O commercially pure aluminum sheets of 1 mm thickness. Figure 2.6 illustrate a typical experimental setup in their research.
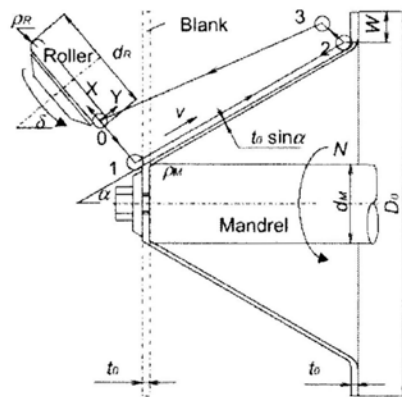
Figure 2.6: Scheme of shear spinning of truncated conical shell with a cylindrical mandrel for general purposes [Kawai *et al.*, 2007]

As we known, the conventional spinning can only make axisymmetrical sheet metal parts. Recently, some researchers attempted to make non-axisymmetrical part using this process. Arai [2005] designed a new apparatus for asymmetric spinning with force feedback control to secure the workpiece (metal sheet) onto a mandrel with an asymmetric shape. This apparatus can be used to produce hollow products with various asymmetric shapes. The process of the 3D non-axisymmetrical tube spinning was simulated theoretically and analyzed experimentally by Xia *et al.* [2006]. Shimizu [2010] proposed a new method to form asymmetric aluminum sheets by synchronous spinning.

The roller path was traced using a control software by taking into account the errors caused by the step pulse control. The design of synchronous spinning machine is shown in Figure 2.8.
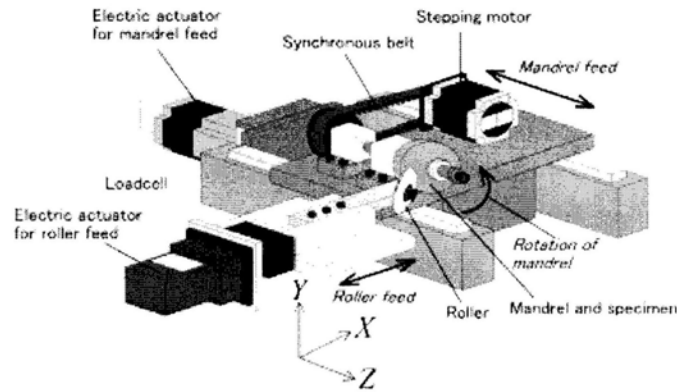
Figure 2.8: Synchronous spinning machine [Shimizu, 2010]

In spinning process, a forming tool with small contact area moves across the workpiece, and hence this process is regarded as the ancestor of incremental sheet mental forming (ISMF) process, which will be discussed in the next section in details.

2.2 Review of the Incremental Sheet Metal Forming

2.2.1 A Short History

The basic idea of incremental sheet metal forming was patented almost 40 years ago by Leszak [1967], but it became one of the leading R&D topics in the sheet metal forming industry today and were put into practice until recently. This is probably because of the development of the computer numerically controlled (CNC) technology and the increasing need of the low volume production. Similar to spinning, ISMF process is to form sheet metal into final shape by a series of small incremental deformations. Presently, the ISMF machine has become a viable product in the market.

According to literature survey, Nakajima [1979] first proposed the concept of flexible computer controlled forming process and anticipated the development of incremental forming being done in 1979. A number of significant developments followed in 1990s

[Tanaka *et al.,* 1999; Murata, 1999; Iseki *et al.,* 1996]. With the advances in CAD, CAE and CNC, this process has since been developed in response to the low volume product and rapid prototyping in the field of sheet metal forming industry. It offers several advantages over the conventional sheet metal forming methods [Allwood and Utsunomiya, 2006]. These advantages include: (a) much reduced tooling cost, (b) shortened production time, (c) easy modification of the part, and (d) highly improved the formability.

Based on different incremental forming mechanism, it can be divided into two categories: a). Based on CNC milling machine with rotary tool (hereafter is CNC ISMF machine), and b). Based on robot arm with punch (hereafter is Robot ISMF machine). In this section, the two methods will be summarized respectively.

2.2.2 CNC ISMF Process

According to literature survey, most of the researches were based on CNC ISMF process forming method. The equipment they used was rebuilt based on CNC milling machine, using a hemisphere head tool instead of the milling tool. In general, the geometry of the part is converted from CAD data through CAM to NC data. It is downloaded to a 3-axis numerical controlled system. The working principle of the process is shown in Figure 2.9. It consists of a number of components: a blank (the sheet metal); a clamp plate, a XY table, a fixture, and a forming tool mounted on the Z axis.
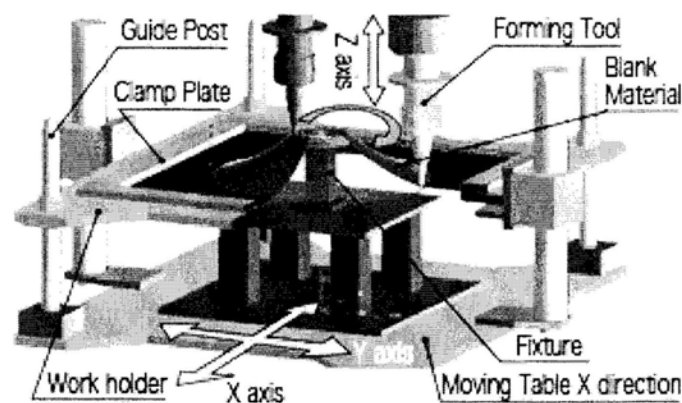
Figure 2.9: Illustration of a typical ISMF system [http://www.aminonac.ca]

It should be noted that the support is used to enforce the local deformation during the forming process. Form the point view of using support, ISMF methods can be divided into three types: fully support (specific support), simple support (unspecific support), and no support, as shown in Figure 2.10. In all the cases, the blank is clamped at the edge by a blank-holder.

(a) Fully support   (b) Simple support   (c) No support
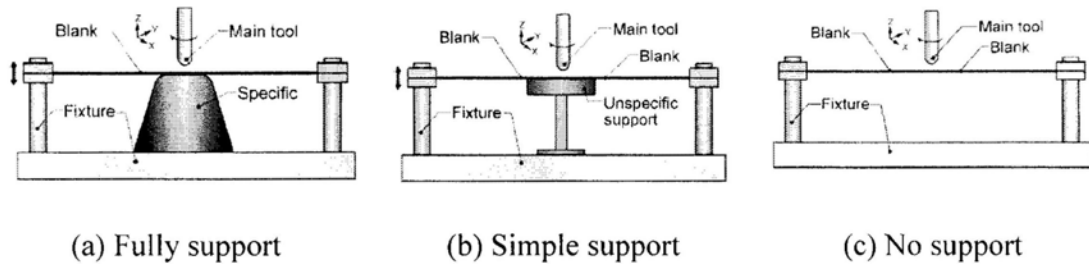
Figure 2.10: The three types of ISMF in the view of support [Shanka *et al.*, 2005]

The CNC based ISMF process has received much attention. Ambrogio *et al.* [2005] made a high customized medical product by ISMF process using a CNC machine and achieved a good produce that satisfied the desired application. Hussain and Gao [2007] used a three axis CNC milling machine tool to form parts by without support. Hirt *et al.* [2004] demonstrated the ISMF process is with capable of producing complex sheet components by the CNC movement of a simple tool in combination with simplified dies. Henrard [2008] used a 3-axis CNC ACIERA milling machine with a horizontal spindle to form a part in the speed of 2000mm/min in his Ph. D thesis.

Some other researchers built special experimental setups for further experimental studies on this forming process. For example, Allwood *et al.* [2005] designed and built a new incremental sheet forming machine in Cambridge University and was commissioned in October 2004. The machine is integrated with sensors to measure the force and the final shape of the part. Moreover, Fillice *et al.* [2006] designed an on line control of ISMF system though punch fore monitoring. A close loop control system was also developed in their experiments [Allwood *et al.*, 2009]. The machine is shown in Figure 2.11.
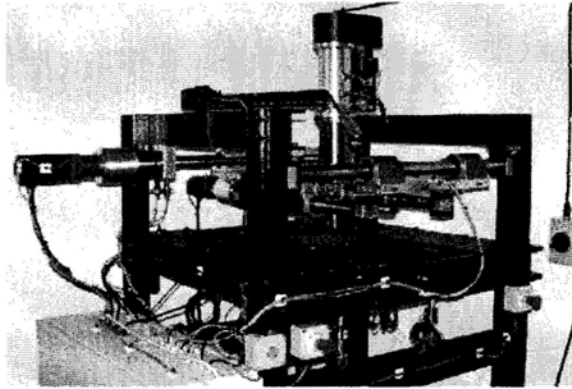
Figure 2.11: A close loop controlled ISMF system in Cambridge University
[Allwood *et al.*, 2005]

Based on this working principle, Amino Co. built a specialized CNC machine with a hemispherical end tool, as shown in Figure 1.4. Presently, the machine is variable in market. The maximum production capacity of the machine is about 500 pieces a month, varying widely on the size and geometry of formed products.
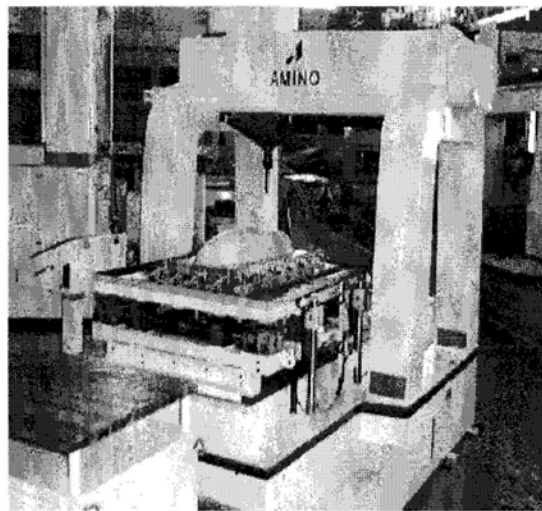
Figure 2.12: CNC ISMF system [http://www.aminonac.ca]

2.2.3 Robot ISMF Process

Hammering is of course an ancient process, and it is done manually using wooden positive die and hammer. Robot ISMF process is developed form hammering that is

moved by a computer-controlled process. From a hardware point of view, many research works were carried out using a robot, as it is easily available. For example, Tanaka *et al.* [1999] designed a special incremental stamping process. In his experiment, the workpiece was held on a frame that can be moved by a robot. The hammering was carried out by a set of upper and lower tools of various shapes. The robot presented the sheet to the hammer and a simple hemispherical part was made. Mori *et al.* [1996] proposed a concept of new incremental forming method, in which the forming was carried out by a series of movements of a hemispherical hammer head to hammering the metal sheet into a 3D shape. In that case, a die was employed as the support. He also considered the problem as an optimization problem and used Genetic Algorithm (GA) to solve it. Lamminem *et al.* [2005] built the test equipment based on a strong arm robot and a moving forming table, where a sheet metal blank was attached. The tool continuously pressed on the sheet and incrementally formed the desired shape. The robot was capable of 5-axis forming, which enabled forming of inwards curved forms. Schafer and Schaft [2005] used an industry robot with a general tool to form aluminum sheet in the Frauhofer Institute of Manufacturing and Automation. Figure 2.13 shows the robot incremental forming system and its forming tools. Puzik [2008] used a robot with handling payloads of 400 kg to conduct this experiment.

Figure 2.13: An ISMF system based on industrial robot and a hammer
[Schafer and Schaft, 2005]

Micari *et al.* [2007] used two robots to form the sheet on double side. The principle of the procedure was based on flexible shaping by means of a freely programmable path-synchronous movement of two robots. The final shape was produced by the incremental infeed of the forming tool in depth direction and its movement along the contour in lateral direction on each level. Callegari *et al.* [2008] used a parallel robot in stead of conventional industrial robot which does not have the required stiffness and the capability of applying the necessary forces to the blank. The forming tool was still kept the rotary tool as shown in Figure 2.14. Rauch *et al.* [2009] developed a tool path programming optimization for incremental sheet metal forming and applied on a parallel robot.
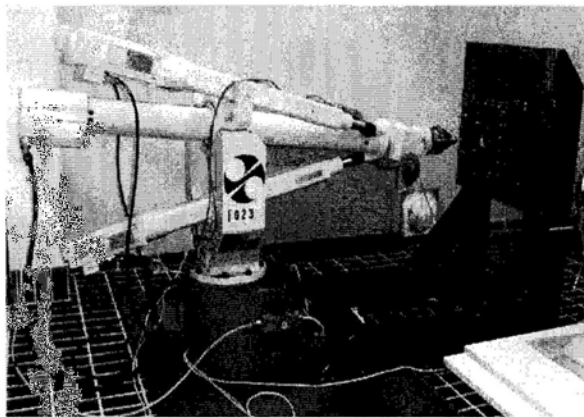
Figure 2.14: An ISMF system based on parallel robot and a rotary tool

[Callegari *et al.*, 2008]

Comparison of the CNC based ISMF process and robot based ISMF process has been done by Vihtonen *et al.* [2008]. Both of the methods are able to form same features, and neither one of them is more capable in terms of geometrical features. However, the punching forming can be used to form a sheet metal with holes, which is not possible with the pressing forming. Also, the Robot based ISMF is not affected by friction and does not need lubrication and cooling.

2.2.2 ISMF Parts

During the past decade, the ISMF processes have been studied in the means of theoretical analysis, numerical simulations and experiments. And a wide variety of parts were made to illustrate the possibilities of ISMF processes. Figure 2.15 shows some example parts achieved by the others researchers. Some of these parts are difficult to form in conventional stamping due to the complex shape (see Figure 2.15 (a) and (d)), high strain ratio (Figure 2.15 (b)) or large scale (Figure 2.15 (c)). Noted that most of these parts are made by using a dedicate support.

(a) Complex formed steel-component
[http://www.msm.cam.ac.uk]
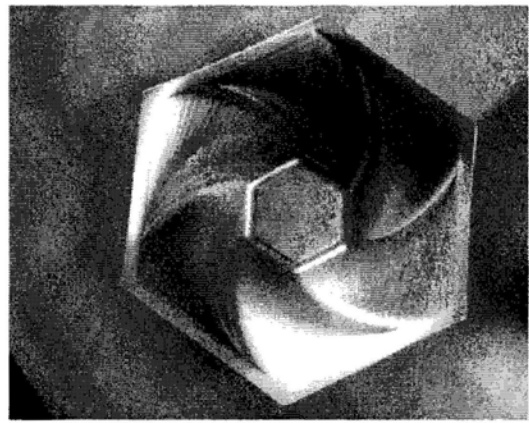
(b) asymmetric shapes
[Allwood *et al.,* 2007]
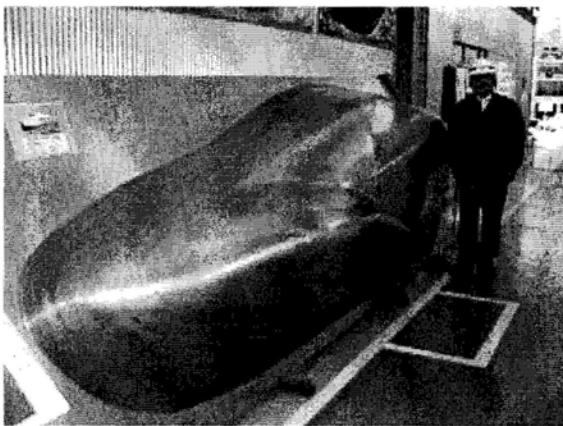
(c) A large scale part (Amino Co.)
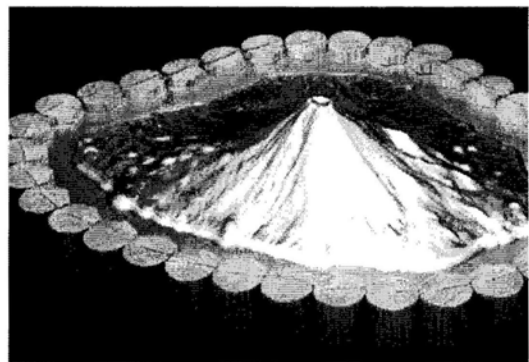
(d) A complex formed part (Amino Co.)

Figure 2.15: Sample parts of ISMF

2.2.3 Limitation of ISMF Process

ISMF Forming is suitable for one-piece and low volume production. It can also be used as a prototyping method for sheet metal products produced in large series. Based on the first ISMF machine built by Amino Co. [http://www.aminonac.ca], ISMF method has some limitations in compared with conventional stamping method:

- The production capacity of the ISMF machine is about 500 pieces a month;
- The maximum thickness of the sheet is 2mm for mild steel, and 4 mm for aluminum;
- Maximum forming angle is about $70°$;
- The surface quality is good when the feed step is less than 1mm; and
- In general, it is cost efficient when amount of production is less than 1000 pieces.

In summary, it is seen that the current research issues include: (a) improving the productivity, (b) improving accuracy and reducing springback, (c) using rollers or spherical balls at the moving tool tip to minimize friction, (d) using hydraulic counter pressure against the deforming tool to increase formability, and (e) using thick sheet or plate for shipbuilding and similar applications.

2.3 Review of the Mechanics Modeling of ISMF

2.3.1 Use Commercial FEA Packages

The key to success in application of sheet metal forming processes is to be able to predict the deformation and the strain / stress of the part incurred during the forming process. In general, it is difficult to predict the thickness strain distribution of the initial state of a deformation after the accumulation of numerous incremental deformation passes. One option to predict the deformation and strains during the whole process is by using FEA. According to literature survey, there are several commercial FEA packages available for special sheet metal forming processes, such as ABAQUS®, LS-DYNA®, PAMSTAMP® and SUPERFORM®, etc. For example, Wang et al. [2006] used ABAQUS® to simulate only several steps in shot peen forming. Hong et al. [2008] also

used ABAQUS® to investigate single/ multiple shots impact on the sheet metal. Similarly, these software systems also can be used for ISMF process.

Kim and Park [Kim and Park, 2000; Shim and Park, 2001; Kim and Park, 2002; Kim and Park, 2003] used a commercial FEA code, PAM-STAMP® produced by ESI Group [http://www.esi-group.com], for the analysis of ISMF process. Strano et al. [2005] conducted FEA for the incremental forming with a spherical punch hammer using PAM-STAMP®. He studied the process parameters that affected the formability and validated the results by experiments. It was found that FEA results were in good agreement with physical tests.

Iseki [2001] studied the ISMF process used Abaqus® developed by Abaqus Inc. [http://www.abaqus.com], with both of implicit or explicit finite element code. He compared the experimental results with FEA results and approximate deformation analysis. Meier et al. [2009] computed the Robot ISMF process using four node shell elements with reduced integration which are available in the ABAQUS® finite element analysis code. Modeling of the contact between the sheet metal and the tools is a penalty node-to-surface contact method. Whenever a node of one body penetrates a segment of the other one, forces are applied to the slave nodes (sheet metal) to oppose the penetration, while equal and opposite forces act on the rigid tool surfaces at the penetration point.

LS-DYNA® is explicit FEA code that supports adaptive remeshing and will refine the mesh during the analysis, as necessary, to increase accuracy and save time. It is developed by Livermore Software Technology Corp [http://www.lstc.com]. Filicel et al. [2002] used PC-Dynaform® as preprocess tool to define the CNC ISMF process, and computed the final shape as well as thickness distributions in LS-DYNA®. Araghi et al. [2009] defined a finite element model set-up in LS-DYNA for forming of the grooved sphere in both of pure ISMF process and the combined of ISMF and stretching process. In the FE model, the sheet was meshed with 13,500 shell elements for the first forming stage. Automatic remeshing was applied in the AISF forming step which yielded

approximately 30,000 elements at the end of the simulation. The CPU time for the simulation of the stretch forming step was 2 h, while the simulation of the forming of the groove took approximately 6 days on a two processor machine. If a fine mesh with 30,000 elements were to be used from the beginning, 39 days were needed to simulate the whole ISMF process.

DEFORM® is a process simulation system developed by Scientific Forming Technologies Corporation [http://www.deform.com], for analyzing the three-dimensional flow of complex metal forming processes. It is used relatively widely in metal forming industry. Hwang and Altan [2002] used it for simulation of tube hydro-forming process. Ceretti *et al.* [2004] conducted several FEM simulations, using DEFORM® software, to identify the maximum load applied to the tool and the stress and strain distributions in the sheet. These values are fundamental in determining the correct tool dimensions and stiffness, the elastic spring coefficient and its pre-load value in order to avoid punch plastic deflection during the deformation and also overloads on the machine spindle. The FEM analyses aimed to identify the magnitude of the loads acting on the punch. The maximum load is greater than 1000N when the tool is with a preload. However, they did not simulate the whole deformation process. Some others such as, ANSYS® was used by Pohlak *et al.* [2004], DYNA3D® was used by Yamashita *et al.* [2008], *etc.*

Compared with the others sheet metal forming processes, the ISMF process has a simple deformation mechanism, but the whole process is much complicated. Commercial FEM software is available for simulating conventional sheet metal forming process, but it will face some difficulties when applied to the ISMF process. It will take a lot of effort to setup the boundary conditions. The most critical problem is the large number of calculation steps, which means very long time for calculation. Hence, some researchers implored the analytic solution and approximate mechanics model for simulating the ISMF process.

2.3.2 Approximate Mechanics Model

A large number of papers were devoted to the study of ISMF process by experimental method and FEM simulation. But it takes a long time to simulate the ISMF process by using commercial FEM software, some researchers tried to develop the analytical solutions to model this complicated forming process. However, a quite limited amount of literature dealing with the mechanics model of ISMF process can be found until recently.

For example, Iseki [2001] gave an approximate model for the incremental bulging of sheet metal. A method of calculating for the approximate distribution of thickness strain and the maximum bulging height has been proposed using a plane-strain deformation model [Iseki and Naganwa, 2002]. A simplified FEM model was also developed by Kim and Yang [2000]. Dai *et al.* [2000] presented the mapping relationship between the metal in the specimen with an even strain distribution and the metal on its blank. It was pointed out that the main characteristics of CNC ISMF process are: 1). the sheet is formed according to a given locus, 2). the deformation of the sheet is point-by-point, and 3) the deformation of every step is small. It also point out the factors should be considered the effect of springback and the situation that current deformed region should more or less affect the other region. Raithatha *et al.* [2006] proposed a new method for determining plastic deformation of sheet metal. However, it can only deal with a simple case with several forming steps. Callegari *et al.* [2007] studied the mechanics of two ISMF processes: one with punch hammer and the other with rotation tool. In their study, both analytical approximation and FEM are employed. The analytical solution is only available for some simple cases. Silva *et al.* [2008] proposed the first closed-form analytical model of ISMF process. It based on membrane model with bi-directional in-plane contact friction and can only deal with for rotational symmetric. Moreover, Strain hardening and anisotropy were not taken into consideration while bending effects were only indirectly included in the analysis. The extreme modes of deformation those were likely to be found in single point ISMF [Martins *et al.,* 2008]. The ISMF process was applied to form the tailored blanks produced by friction stir welding [Silva *et al.,* 2009]. Jackson and Allwood [2009] studied the two ISMF process: single point forming and

two-point forming using the sine law. It was observed that observed mechanisms of two methods differ from the mechanism of pure shear

It is difficult to applying the analytical solution in the design due to a typical part is too complicated to analyze by this method. And these approximate FEM model is still need improvement to fulfill the requirements of simulating the ISMF process: (1). reduce the computing load, (2). the accuracy is acceptable, and (3). with capability of prediction on the potential failure of the part.

2.4 Review of the Formability Studies

Before application to industry, the formability is one of the mainly concerned issues in the new sheet metal forming process. Hence, it was studied in two methods: maximum forming angle and forming limit diagram (FLD). These researches are introduced below.

The formability can be expressed as the *maximum forming angle* (θ_{max}) that a sheet would endure without fracturing. Lots of investigations on the formability of this process have been done using this method. Cerro *et al.* [2006] conducted experiment and a 75° wall angle square-based pyramid was formed from aluminum sheet for the study of different forming strategies. Gao *et al.* [2007] conducted experiments to evaluate the forming angle of aluminum in the condition described in the article. The maximum forming angle is 66°. It was also reported by Takano *et al.* [2008] that the forming angle of aluminum is 65°~70° in CNC ISMF process. Doflou *et al.* [2008] summarized the maximum forming angel of several kinds of sheet metal formed by ISMF with a tool diameter of 10 mm, as shown in Table 2-1.

Martins *et al.* [2008] also pointed out that the increased formability compared to conventional stamping and deep drawing operations is provided through the utilization of fracture forming limit diagrams based on the onset of fracture instead of the conventional forming limit diagrams based on the onset of necking. This result is in close agreement with the typical loci of failure strains in conventional sheet-forming processes, where the slope of the fracture forming line is often about -1 [Kim and Park.,

2003; Gao *et al.*, 2008]. Eyckens *et al.* [2009] presented the formability predictions using an M-K type of forming limit model. The method can well predict the fracture, however, it should account for anisotropic yielding and anisotropic hardening at strain path changes, as well as an accurate description of the complex deformation path.

Table 2-1: Maximum wall angles for cones [Doflou *et al.*, 2008]

Material	Thickness[mm]	Max. wall angle [°]
AA3003-O	1.2	71
AA3003-O	2.0	76
AA3103	0.85	71
AA3103	1.5	75
Ti Grade	2.0	47
DC01	1.0	67
AISI 304	0.4	63

It has been reported that friction increases the formability in SPIF [Allwood *et al.*, 2007] and [Jackson and Allwood, 2008]. However, this finding is valid for a certain level of friction and the excessive friction causes wear of sheet reduces formability [Kim and Park, 2002]. Multistage forming is considered by many researchers to improve the formability of incremental forming [Hirt *et al.*, 2004; Skjoedt *et al.*, 2008; Verbert *et al.*, 2008; Duflou *et al.*, 2008]. Cui and Gao [2010] developed three multistage tool path strategies to optimize the formability of a hole flange.

Chapter 3:

Studies on Incremental Punching Process Using Geometric Method and Commercial Finite Element Packages

3.1 Introduction

Sheet metal stamping is one of the most commonly used manufacturing processes. Everyday, millions of parts are formed by stamping. The conventional stamping method is to form a part in one or several operations. It is very efficient but is not cost effective for small batch production parts and/or prototypes as the dies are expensive and time consuming to make. In recent years, Incremental Sheet Metal Forming (ISMF) received much attention. As it does not depend on special tool and hence is cost effective for small batch production parts and prototypes. In ISMF, a small generic tool is used to apply a sequence of operations to deform the sheet incrementally. These small deformations accumulate to form the final shape of the part. As a result, different parts can be made by a same setup.

According to literatures, a number of ISMF methods have been developed. From the view of forming tools, many variations have been explored, but by far the most widely used tool is a solid hemispherical indenter. From the machine point of view, the two most common configurations of ISMF are CNC ISMF system [Allwood and Utsunomiya, 2006] and robot ISMF system [Schafer and Schaft, 2005; Callegari et al., 2008]. The former is based on a CNC machine while, the later is based on a robot arm. Each has its advantages and limitations. The CNC based system is easy to use, while the using robot based system is not affected by friction force and would have large envelop.

A new ISMF process is proposed based on incremental punching. It will take some advantages of the two above mentioned methods. In this chapter, we will first briefly introduce the proposed forming process in Section 2. The relevant motion of the forming

tool is controlled by the punch path, which will largely determine final shape of the part. Hence, the tool path generation method is presented in Section 3 and the errors between the punch path and the designed part is studied in the means of geometry in Section 4. Finally, as the sheet metal will experience plastic deformation and elastic deformation causing the changes in thickness and material properties (strain-hardening) during this forming process. FEM simulations are conducted to demonstrate the how the incremental punching process works. Two typical cases are presented for 2D and 3D respectively.

3.2 Incremental Punching Process

Recently, Du's group in the Institute of Precision Engineering at the Chinese University of Hong Kong developed a new ISMF system that is incremental punching machine [Luo *et al.*, 2008; Luo, He and Du, 2009]. Its mainly components include: (1) slider，(2) workpiece, (3) blankholder, (4) high frequency punch and forming tool, and (5) X-Y table, which are shown in Figure 3. 1. The details of the design will be presented in Chapter 5. In incremental punching process, a simple tool punches on the sheet metal that produces local plastic deformations which is accumulated to a large deformation. The tool path is similar to single point incremental forming (SPIF), but the forming tool is rather different that using a punching tool instead of a rotating tool.

The forming method is in fact rather similar to that of an old craftsman. The initial sheet metal is flat. The punch head moves up and down driven by the hydraulic system in high speed to stamp on the sheet metal. When forming a part, the forming tool punches the sheet metal along the contour of the part punch by punch; when one layer of the part is completed, the forming tool move down to the next layer; and the process is completed till all layers are completed. Hence, the final shape of the part is largely depended on the tool path.
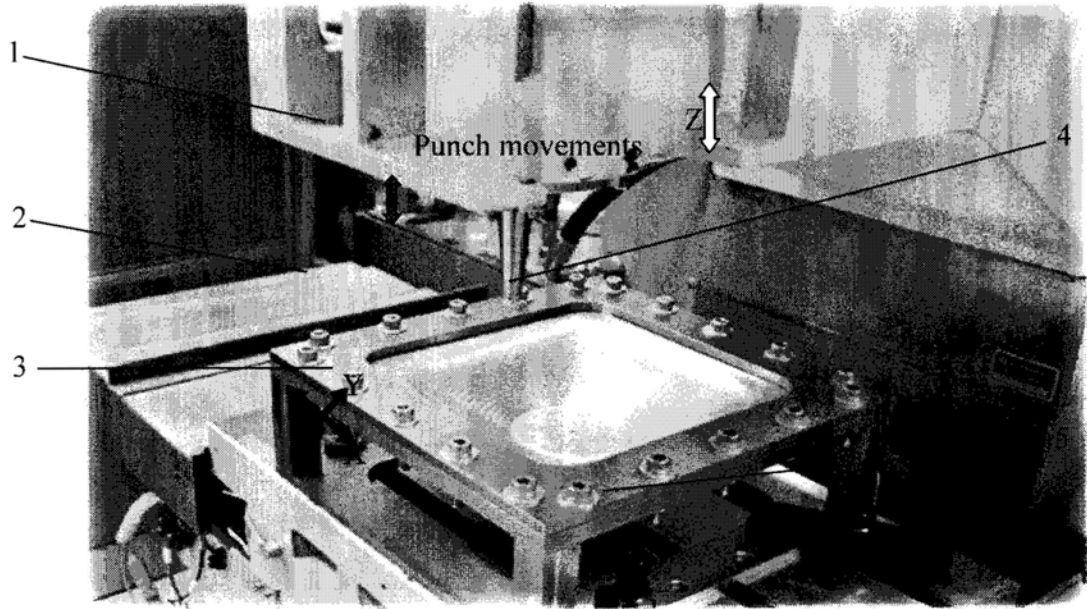
Figure 3.1: Illustration of incremental punching setup

Similar to existing ISMF processes, this forming process will have two variants: with support or without support, which are shown in Figure 3.2. It should be mentioned that former is simpler, though the later could give better accuracy and make more complex parts.
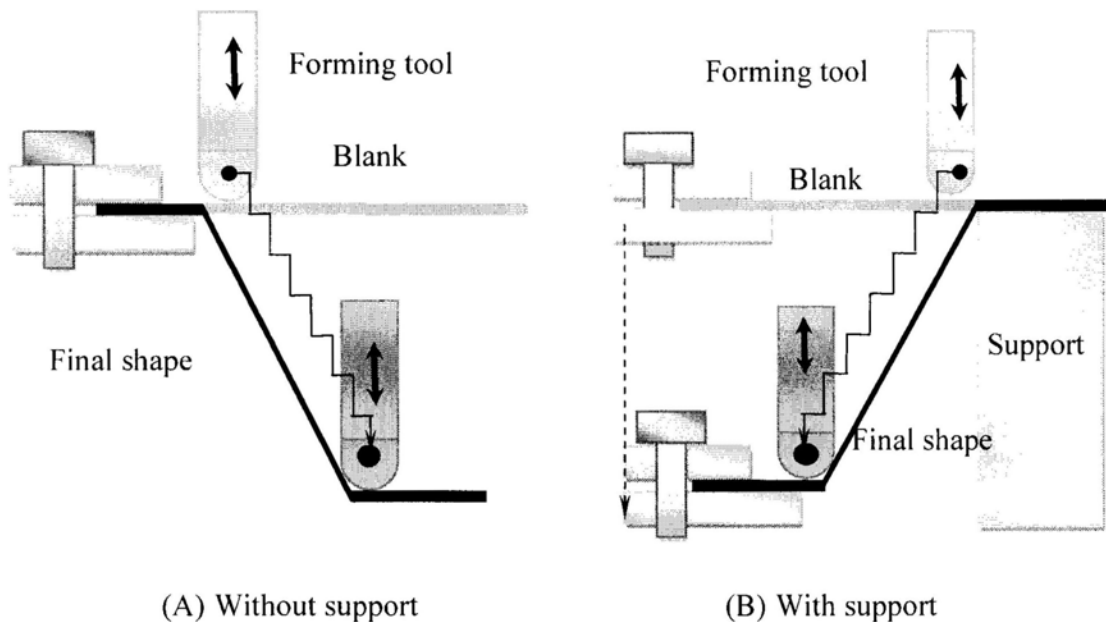
(A) Without support   (B) With support

Figure 3.2: Working principle of incremental punching system

3.3 Tool Path Generation

Compared with conventional stamping, the proposed ISMF method is formed by a serious of deformation by the high frequency hydraulic punch in incremental layers. The operation of our ISMF machine is rather similar to that of an experienced smith. The workpiece is mounted on the fixture. Along the depth of the part, the part is divided into a number of layers. At each layer, from the top to the bottom, the workpiece is punched step by step along the contour of the layer. When one layer is done, the Z slider moves down. The whole operation is finished when the all the layers are done. Punch path has a direct impact on the dimensional accuracy, surface finish, formability, thickness variation and processing time. To control the machine to forming a three dimensional part using ISMF, the proposed method is rather similar to cutter path generation in NC machining. Schafer and Schraft [2005] proposed a method to generate the punch trajectories. The process is shown in Figure 3.3.
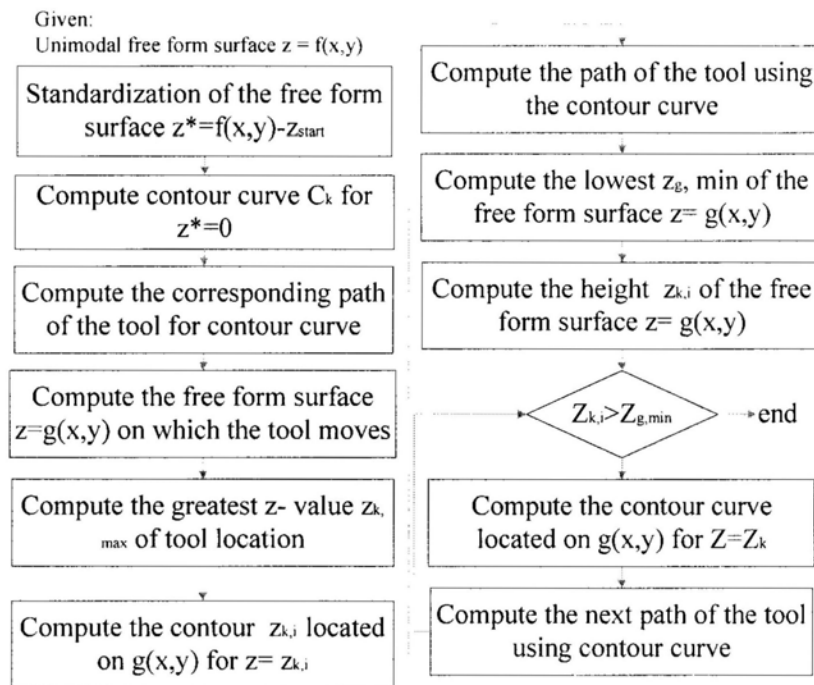
Figure 3.3: Tool path generation process [Schafer and Schraft, 2005]

Figure 3.4 shows the generation of punch locations for a typical part. In order to make this part, we first slice the part into a number of sections, as shown in Figure 3.4(b). Note that the thickness of the slice depends on the curvature of the part.

(a) Step 1 A typical part
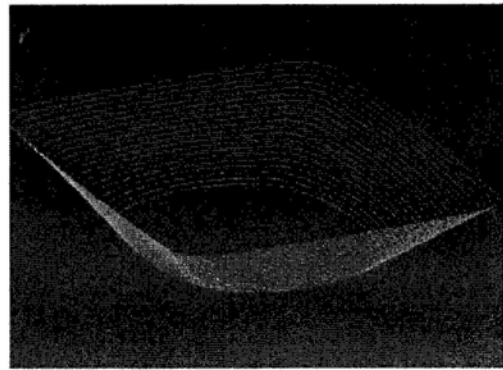
(b) Step 2 Sections
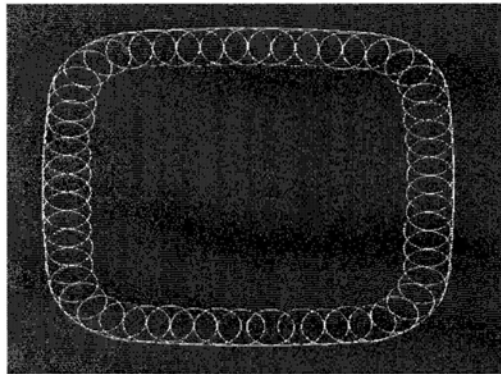
(c) Step 3 A contour
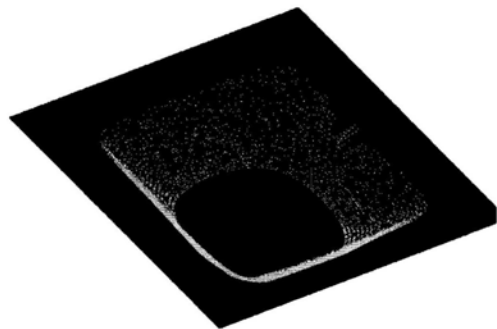
(d) Step 4 Punch locations

Figure 3.4: The punch path generation process

The incremental step-down size (step size, Δh, mm) is the amount of material deformed for each revolution of the forming tool. (It is similar to cut depth in machining). Feed step (denoted as a, mm) is the distance between two adjacent punch locations. The feed rate in the XY direction (the horizontal direction feed) is calculated based on the following equation:

$$F = \frac{a \times f}{60} \, (\text{mm/min}) \tag{3-1}$$

where, a is the feed step (mm) and f is the punch speed (SPM). Since the hydraulic punch of our machine is *300 CPM* (cycle per minute), the feeding speed of forming tool moved a long the path can be determined by: *feed step $\times$ 300 CPM*.

Although commercial CAD/CAM package has been used to generate tool path for incremental forming, it may not represent the requirements of incremental forming realistically enough. Jie *et al.* [2004] developed special software for path generation for ISMF based on STL files. In this experiment, the punch paths were generated by using commercial software systems, such as MasterCAM®. Since the ISMF process is quite similar to CNC machining, for practically, the forming tool path also can be done in commercial CAM software, such as, MasterCAM®, EdgeCAM®, UG®, and *etc*. Figure 3.5 illustrates the punch path of a typical part generated by MasterCAM®.
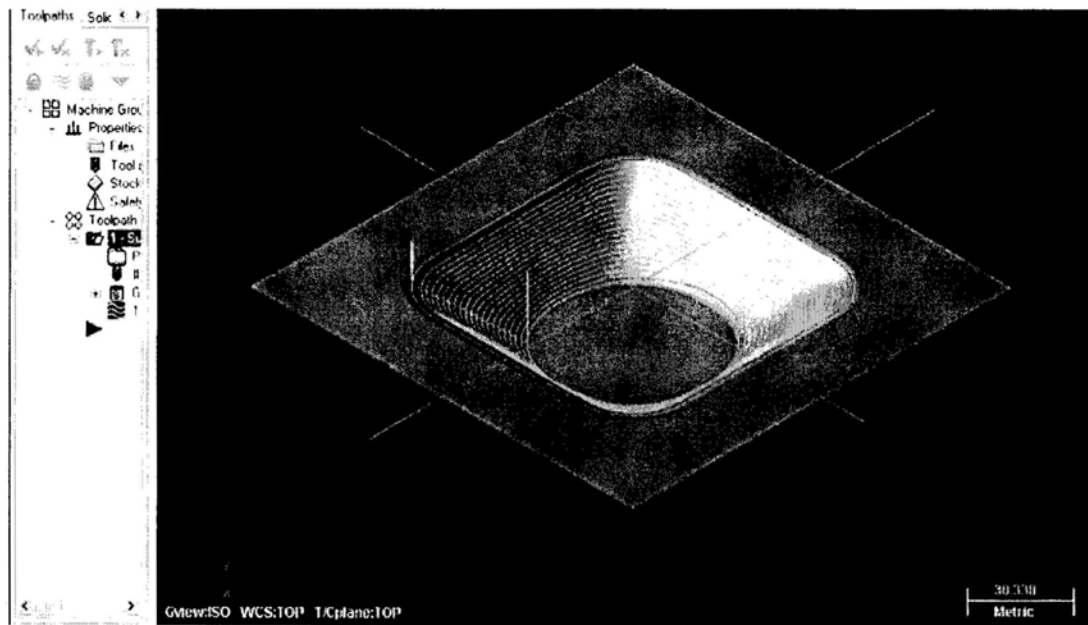
Figure3.5: Tool path generated by MasterCAM®

3.4 Geometric Errors

Both step-down size and feed step had a direct impact on the machine time for forming. Moreover, they also affect the machine time and the surface quality. In this study, we considered a special case that the punches have sphere heads of different sizes. For a given part and its punch path, the geometric error can be found based on the geometry. The geometric errors include the section error, and the contour error because of the spherical punch head. Given the layer thickness, Δh, and the feed step size a, the resulting geometric error can be calculated. Figure 3.6 illustrates the geometric relationship of a part contour along the horizontal direction and the ball-end punch. It can be shown that the geometric error, δ, is as Figure 3.6.
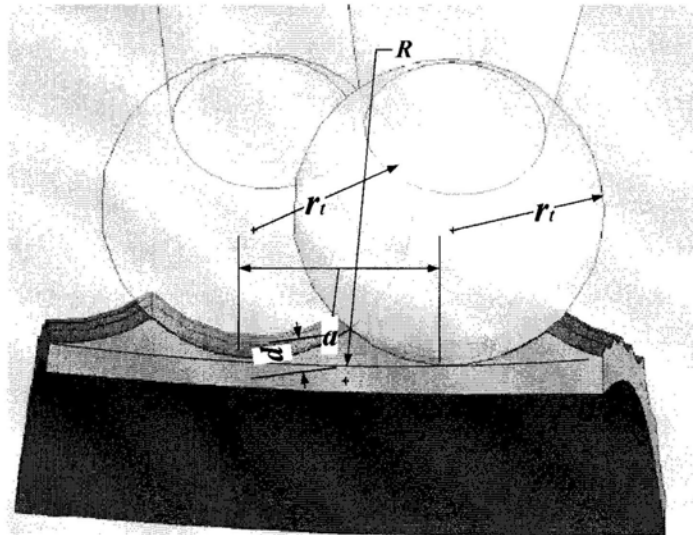
Figure 3.6: The geometric error in a contour

Figure 3.6 also shows the geometric relation of a part contour, and the punch spherical head with its locations. It can be shown that the geometric error can be described as follows:

29

$$\sigma = \begin{cases} r_t - \sqrt{r_t^2 - \dfrac{a^2}{4}} & R = 0 \\[3mm] R - \sqrt{(r_t - R)^2 - \dfrac{a^2}{4}} - \sqrt{r_t^2 - \dfrac{a^2}{4}} & R > 0 \\[3mm] \sqrt{(r_t - R)^2 - \dfrac{a^2}{4}} - \sqrt{r_t^2 - \dfrac{a^2}{4}} + R & R < 0 \end{cases} \qquad (3\text{-}2)$$

where, a is the feeding step; r_t is the diameter of the punch spherical head, and R is the curvature of the part contour. Hence, for a given maximum geometric tolerance, σ_{max}, the maximum step can be defined as:

$$a = \frac{\sqrt{s \cdot (s - r_t)(s - R + r_t)(s - R + \sigma_{max})}}{2(R - \sigma_{max})} \qquad (3\text{-}3)$$

Similarly, along the vertical sections, the geometric error can be found from the geometric relations as shown in Figure 3.7.
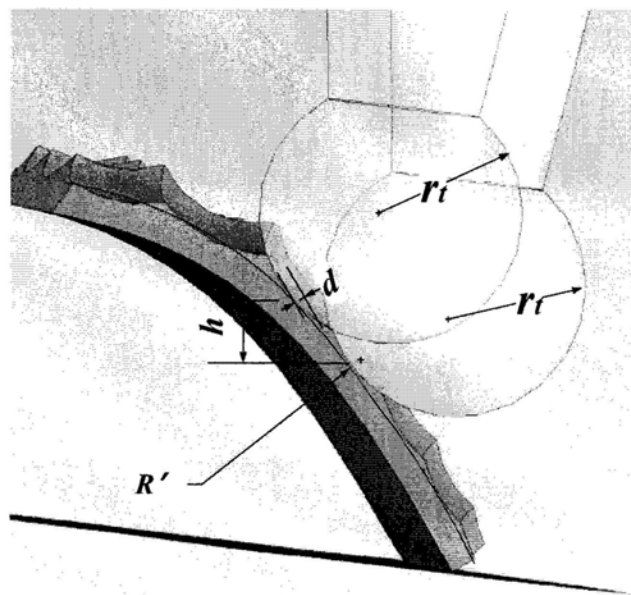
Figure 3.7: The geometric error in vertical cross section

$$\delta = \begin{cases} r_t - \sqrt{r_t^2 - \dfrac{h^2}{4}} & R' = 0 \\[2ex] R' - \sqrt{(r_t - R')^2 - \dfrac{h^2}{4}} - \sqrt{r_t^2 - \dfrac{h^2}{4}} & R' > 0 \\[2ex] \sqrt{(r_t - R')^2 - \dfrac{h^2}{4}} - \sqrt{r_t^2 - \dfrac{h^2}{4}} + R' & R' < 0 \end{cases} \qquad (3\text{-}4)$$

where, h is the thickness of the layers; R' is the radius of curvature in the cross section plane. When the maximum geometric tolerance is defined as σ_{max}, the maximum thickness of each layer is,

$$\Delta h = \frac{\sqrt{s \cdot (s - r_t)(s - R' + r_t)(s - R' + \sigma_{max})}}{2(R' - \sigma_{max})} \qquad (3.5)$$

where, $s = R' - \dfrac{\sigma_{max}}{2}$.

As mentioned earlier, when the feeds are decided, the punch path can be generated using commercial CAM software systems, such as MasterCAM®. It takes only a few minutes. The surface finish can also be estimated using above mentioned method. Following the aforementioned example, with the feeding step ($a = 2\ mm$), layer thickness ($\Delta h = 2\ mm$), and the punch size ($r_t = 5\ mm$), the geometric error map of the part can be calculated as shown in Figure 3.8.
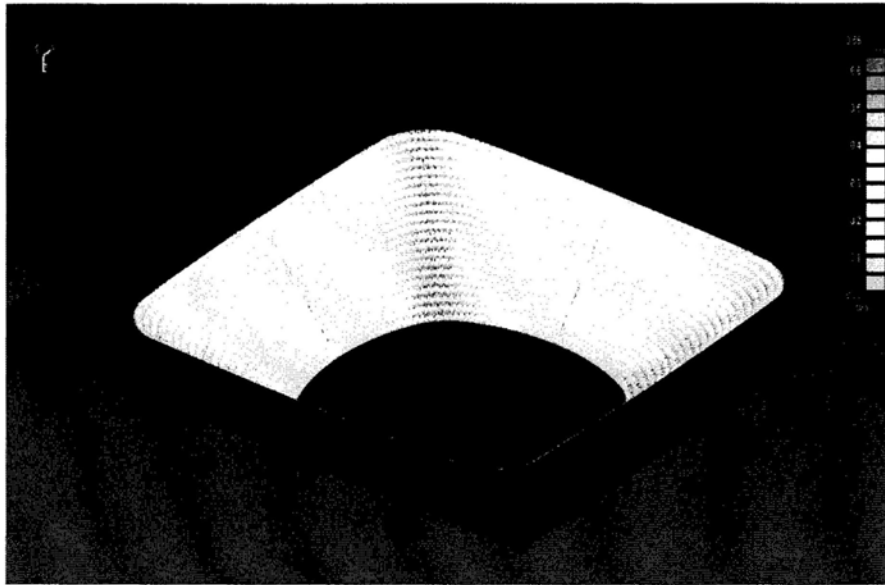
Figure 3.8: The geometric error map of the part

The geometric error analysis can be used for selecting the forming parameters, such as feeding step and layer thickness. However, the forming process is rather complicated. This is because that the sheet metal will experience plastic deformation and elastic deformation causing the changes in thickness and material properties (strain-hardening) during a stamping process. These effects shall be considered in the subsequent Finite Element Method (FEM) analysis.

3.5 FEM Simulation Using Commercial Software

FEM is one of the powerful tools in virtual manufacturing which includes the sheet mental forming process, such as deep drawing and bending [Hortig *et al.*, 2001]. After decades of development, there are some commercial softwares, such as Dynaform®, Ansys®, and Surperform®, are available for modeling and simulating these processes. A lot of fundamental researches on metal forming are conducted by FEM simulations for investigating the deformation mechanics and material behavior [Batoz, 2005; Khelifa, 2008]. In this study, the commercial FEM package, DYNAFORM®, are used to model and verify a special workpiece formed by a typical process of the proposed ISMF.

32

Firstly, a case of two dimensional incremental stamping is studied. In this case, a square workpiece is clamped on its edges is being punched incrementally along the edges with an offset. This is illustrated in Figure 3.9(a). It is well known that owing to the complexity of the stamping process, there is no analytical solution for the workpiece deformations. Though, FEM could be used to analyze the entire stamping process punch by punch. Figure 3.9(b) shows the workpiece deformation with the strain distribution and the stress distribution respectively.
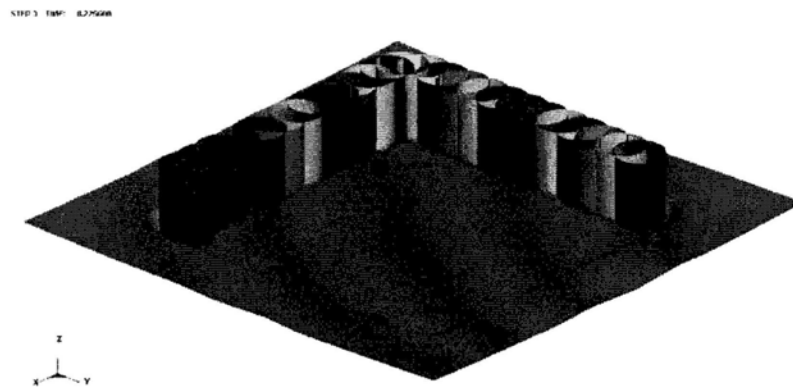
(a) A typical setup
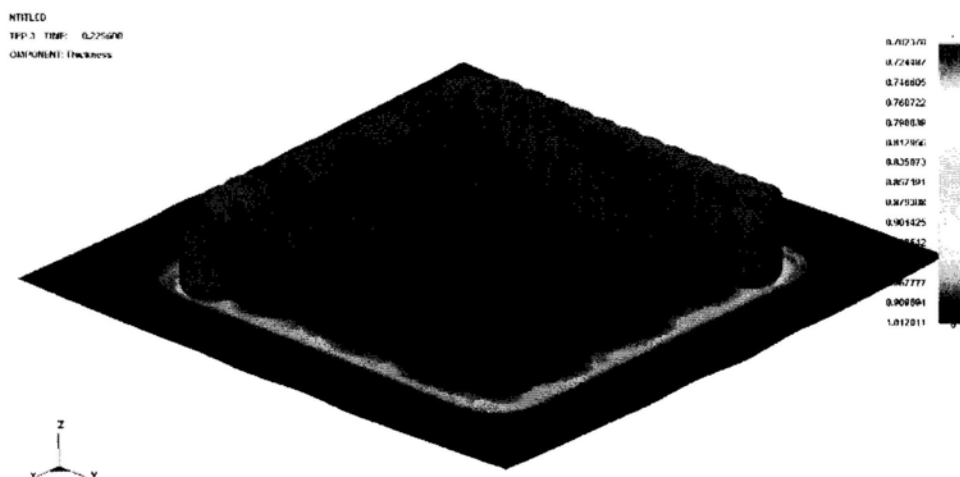
(b) The workpiece deformation with strain distribution
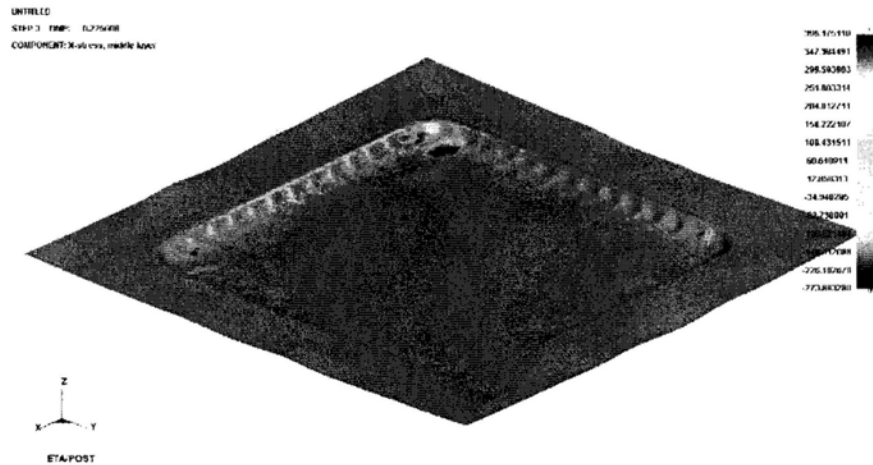
(c) The workpiece deformation with stress distribution

Figure 3.9: A typical setup of 2D incremental punching and FEM results

As an example, the simulation of a 3D ISMF is shown in Figure 3.10. In this case, the layer thickness is 3mm and the feeding step is 3 mm. Figure 3.10(a) shows the setup of the simulation. Figure 3.10(b) and Figure 3.10(c) show the plastic strain distribution and the thickness of the part respectively. Figure 3.10(d) shows the formability prediction in forming the designed part using incremental punching.
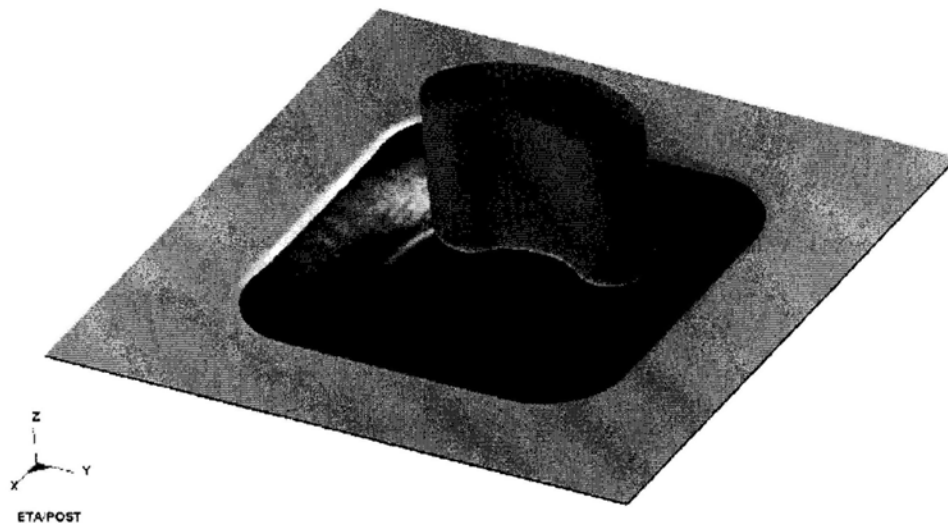
(a) A typical setup of 3D ISMF

34
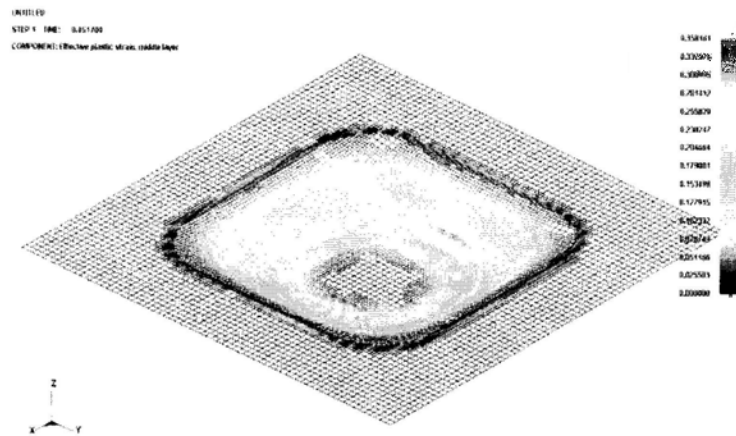
(b) The plastic strain of a typical workpiece
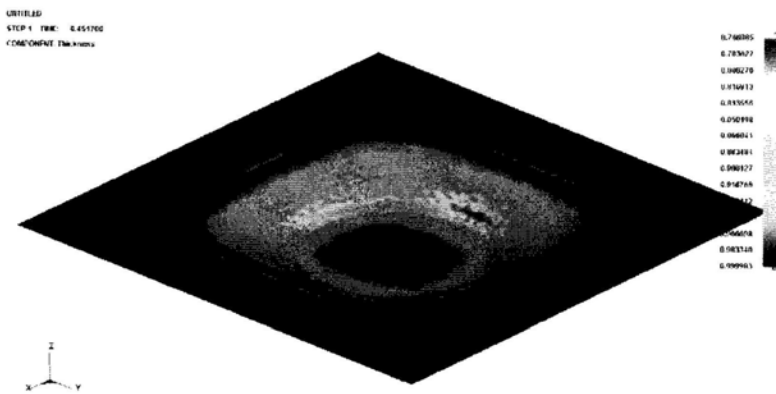
(d) The thickness of final part
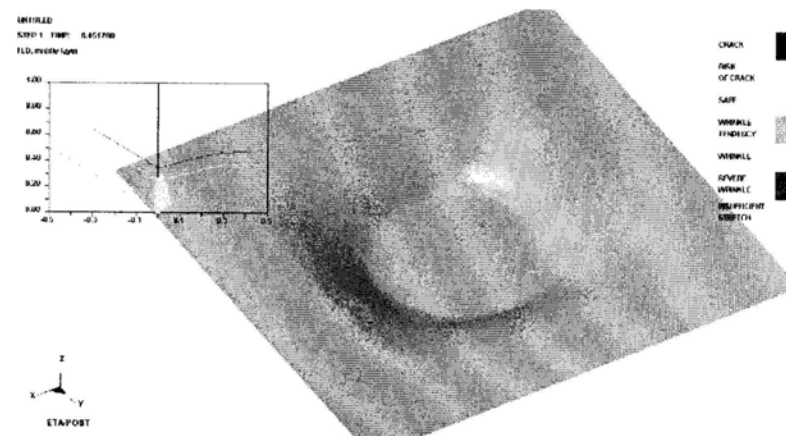
(e) Formability prediction of the process

Figure 3.10: A typical setup of 3D incremental punching and FEM results

From FEM analysis, it is seen that the part can be successfully made by ISMF. However, it should be noted that the FEM simulation is time consuming. It takes more than 5 days on a work station（HP xw8400: CPU: 2.33^3 GHz, Memory: 16GB）for this case.

3.6 Summary

In this chapter, the proposed ISMF forming process based on incremental punching is briefly introduced. It's pointed out that the punch path is rather similar to CNC milling. Hence, the punch path can be generated by using commercial CAM software, *eg.* MasterCAM®. The forming parameters, such as feeding speed, step-down size (layer thickness), tool diameters, *et.,* are studied in the mean of geometry. And the relations between these parameters and geometric error are given. FEM simulations are conducted to simulate two typical formed parts for 2D and 3D respectively. Based on the discussions above, following conclusions can be made:

- The punch path and geometric error studies can be use to define the feed step and layer thickness; and
- The FEM analysis can be use to simulate ISMF process and predict the shape of final part. However, it's time consuming to simulation ISMF process using commercial FEM software.
- The proposed process will be an effective method to make a sheet metal part without support.

Chapter 4:

Mechanics Model of Incremental Punching

4.1 Introduction

As mentioned in Chapter 2, it is difficult to predict the whole incremental forming process due to complex of the problem. In the old days, trial and error method was always used to improve the design of dies in conventional stamping. Tuomi and Lamminen [2004] presented a general production process of ISMF that can be utilized for most of existing ISMF process. However, the quality improvement will be depended on experience of the worker. This is illustrated in Figure 4.1.
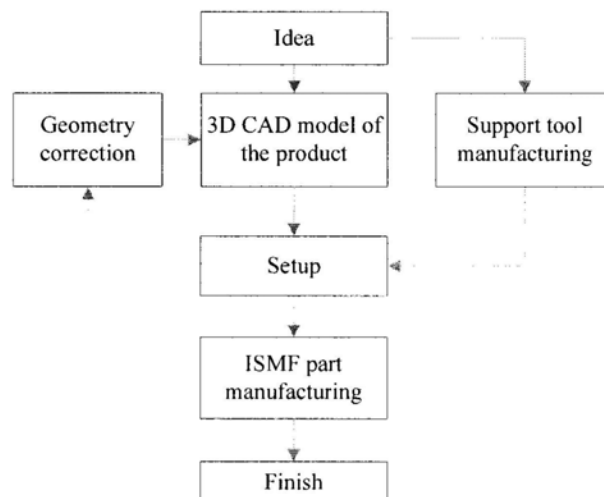
Figure 4.1: A general production process of ISMF

It's reported that the commercial FEM packages can be used to simulate the forming process instead of trial-and-error method. A modified process is proposed for the whole forming process, which is shown in Figure 4.2. In this process, firstly, a CAD model is build based on the conception of desired part. Secondly, the initial tool path is generated in the CAM software according to the geometric relations. Thirdly, FEA simulation is conducted to predict the final shape and the strain / stress distributions. If the prediction

is failure, then the go back to second / third step to modified the design / punch path. This process can be iterated several times till the prediction is success. The fixture and the support are made according to the prediction results. Finally, the part is manufactured successfully.
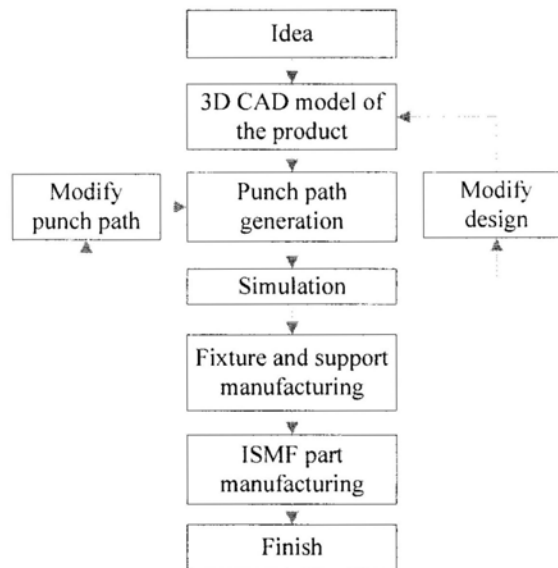
Figure 4.2: The proposed ISMF process

Note that the key to success application of this process to incremental punching process is to be able to predict the deformation and the strain / stress of the part incurred during the forming process. Because of the complexity of the problem, analytical models and solutions may not possible to compute the some processes. It is possible to use commercial FEM packages for establishing quantitative relations between the forming parameters and local deformation of the formed part. But incremental punching is a very complex process in which a huge numbers of contacts between the tool and workpiece (more than say 5000 punches) are involved in forming a typical part. According to our experience, it takes more than 5 days for computing a case with 100 punches. Hence, a fast computing model is required to fulfill the above mentioned process.

In this chapter, a fast computing method is proposed based on minimum energy principle and inverse FEM for predicting the incremental punching process. The rest of

the chapter is organized as follows. Section 2 presents a method to find the final shape based on minimum energy principle. Section 3 presents a method to compute the strain and stress distribution using Inverse FEM. Section 4 describes the implementation procedure. Section 5 gives two numerical examples. Finally, Section 6 contains conclusions.

4.2 Finding the Final Shape Based on Minimum Energy Principle

As above mentioned, the new incremental punching process can be described as follows: A sheet metal blank is secularly clamped by a blank holder and is incrementally stretched by the punch to reach the final shape punch by punch. In each punch, the punch force is sufficient for the sheet metal to deform. Punches on different locations will result in different amount of deformation. Also, in each punch, the contact region and the blank holder region is constrained. The rest of sheet metal beyond the vicinity of the contact area of the sheet metal are free; however, it may have plastic deformation when its effective stress is large than the yield stress. As a result, for a single punch, its effect region is not only to the contact area, but also the region nearby. As the process goes, the sheet metal attempts to reach a minimum energy state forming the shape. Figure 4.3 shows a simple case of two punches. The thick line is the geometric profile, while the dash line is the predicted profile. Note that the geometric profile follows the punch positions while the predicted profile is resulted from the minimum energy state of the sheet metal. This method has been used by a number of researchers, such as Tang *et al.* [2007].
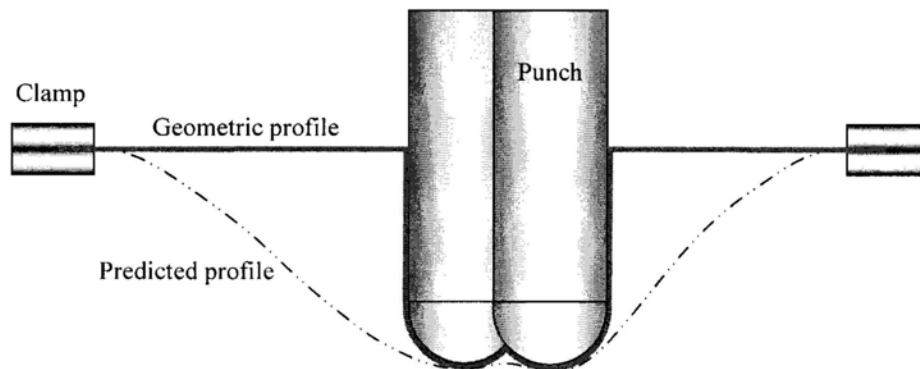
Figure 4.3: Illustration of a deformed sheet metal

To model our ISMF process, following assumptions are made:

(1) In the entire process, the sheet metal is secularly clamped by the blank holder;

(2) Because the punching takes place in a very short period of time, the effect of friction due to the contact between the punch hammer and the sheet metal is negligible (this assumption is the same as the conventional one punch stamping);

(3) The initial energy of the sheet metal is zero;

(4) The sheet metal blank can be described by its middle surface;

(5) The dynamic effect of each punching is negligible (*i.e.*, the vibration of the sheet metal is negligible);

(6) The volume of the sheet metal is conserved throughout the process; and

(7) The material will not fracture during the process.

As stated in the previous section, during the ISMF process, the sheet metal will deform to its lowest energy state. At the mean time, it must satisfy the boundary conditions, including the geometric surfaces of punches, as well as the clamping condition. Accordingly, the final shape of the surface can be found. To model the mechanics of the process, the energy function of the deformed sheet metal should be defined. Hu *et al.* [2001] defined the energy function for NURBS surfaces. It is utilized to model deformed sheet metal here. Denote the middle surface of the sheet metal as $S(x, y)$, the energy function of the deformed sheet metal can be represented as follows:

$$E(S(x,y)) = \iint \left(\alpha_{11} \frac{\partial S^T}{\partial x} \frac{\partial S}{\partial x} + \alpha_{22} \frac{\partial S^T}{\partial y} \frac{\partial S}{\partial y} + \beta_{11} \frac{\partial^2 S^T}{\partial x^2} \frac{\partial^2 S}{\partial x^2} + \beta_{12} \frac{\partial^2 S^T}{\partial x \partial y} \frac{\partial^2 S}{\partial x \partial y} + \beta_{22} \frac{\partial^2 S^T}{\partial y^2} \frac{\partial^2 S}{\partial y^2} \right) dxdy$$

$$(4\text{-}1)$$

where, a_{11} is the stretching stiffness in x direction, a_{22} the stretching stiffness in y direction, β_{11} the bending stiffness in x direction, β_{12} the bending stiffness in x and y direction, and β_{22} the bending stiffness in y direction. These parameters can be calculated based on the material properties of the sheet metal.

Although Equation (4-1) has no analytical solution, it can be solved numerically. Express the surface in discrete grids, the energy function can then be written in discrete form:

$$E(S) = \alpha_{11}\left(\sum_{i,j}^{n,m}\left(\frac{S_{i+1,j} - S_{i,j}}{\Delta x_{i,j}}\right)^2 + \sum_{i,j}^{n,m}\left(\frac{S_{i,j} - S_{i-1,j}}{\Delta x_{i,j}}\right)^2\right)$$

$$+ \alpha_{22}\left(\sum_{i,j}^{n,m}\left(\frac{S_{i,j+1} - S_{i,j}}{\Delta y_{i,j}}\right)^2 + \sum_{i,j}^{n,m}\left(\frac{S_{i,j} - S_{i,j-1}}{\Delta y_{i,j}}\right)^2\right)$$

$$+ \beta_{11} \cdot \sum_{i,j}^{n,m}\left(\frac{(2 \cdot S_{i,j} - S_{i-1,j} - S_{i+1,j})}{\Delta x_{i,j}^2}\right)^2 + \beta_{22} \cdot \sum_{i,j}^{n,m}\left(\frac{(2 \cdot S_{i,j} - S_{i,j-1} - S_{i,j+1})}{\Delta y_{i,j}^2}\right)^2$$

$$+ \beta_{12}\sum_{i,j}^{n,m}\left(\frac{S_{i+1,j+1} - S_{i-1,j+1} - S_{i+1,j-1} + S_{i-1,j-1}}{4\Delta x_{i,j} \cdot \Delta y_{i,j}}\right)^2$$

(4-2)

where, n and m are the number of nodes in x and y directions. $\Delta x_{i,j} = \dfrac{|x_{i+1,j} - x_{i-1,j}|}{2}$ and

$\Delta y_{i,j} = \dfrac{|y_{i,j+1} - y_{i,j-1}|}{2}$ are the distances between the nodes in x and y directions

respectively (by central difference).

Based on the minimum energy principle, for a point, S_{ij}, not in its lowest energy state, it will be driven to its lowest energy state. From the Equation (4-2), the energy of S_{ij} is:

$$E(S_{ij}) = \alpha_{11}\left(\left(\frac{S_{i+1,j} - S_{i,j}}{\Delta x_{i,j}}\right)^2 + \left(\frac{S_{i,j} - S_{i-1,j}}{\Delta x_{i,j}}\right)^2\right)$$

$$+ \alpha_{22}\left(\left(\frac{S_{i,j+1} - S_{i,j}}{\Delta y_{i,j}}\right)^2 + \left(\frac{S_{i,j} - S_{i,j-1}}{\Delta y_{i,j}}\right)^2\right)$$

$$+ \beta_{11} \cdot \left(\frac{(2 \cdot S_{i,j} - S_{i-1,j} - S_{i+1,j})}{\Delta x_{i,j}^2}\right)^2 + \beta_{22} \cdot \left(\frac{(2 \cdot S_{i,j} - S_{i,j-1} - S_{i,j+1})}{\Delta y_{i,j}^2}\right)^2$$

$$+ \beta_{12}\left(\frac{S_{i+1,j+1} - S_{i-1,j+1} - S_{i+1,j-1} + S_{i-1,j-1}}{4\Delta x_{i,j} \cdot \Delta y_{i,j}}\right)^2$$

(4-3)

The resulting force on the node is

$$F_{ij} = \frac{\partial E(S_{ij})}{\partial S_{ij}} = 2\alpha_{11}\frac{2S_{i,j} - S_{i+1,j} - S_{i-1,j}}{\Delta x_{i,j}^2} + 2\alpha_{22}\frac{2S_{i,j} - S_{i+1,j} - S_{i-1,j}}{\Delta y_{i,j}^2}$$
$$+ 2\beta_{11} \cdot \frac{2 \cdot S_{i,j} - S_{i-1,j} - S_{i+1,j}}{\Delta x_{i,j}^4} + 2\beta_{22} \cdot \frac{2 \cdot S_{i,j} - S_{i,j-1} - S_{i,j+1}}{\Delta y_{i,j}^2} \tag{4-4}$$

Using Equation (4-4), the minimum energy state of S_{ij}, can be found through iterative searching:

$$S_{ij}(t) = S_{ij}(t-1) + c \cdot F_{ij}(t-1) \tag{4-5}$$

where, t is the times of iterations, c is a positive constant, the driven force, F_{ij} is positive in the positive direction of z.

Note that some points are constrained by the boundary conditions, including the contacting points of the punch, and the contacting points to the blank holder. These points will be invariant in the process. In addition, Equation (4-5) assumes the minimum energy state, S'_{ij}, has the same position as S_{ij} in x and y directions. This may cause some error. However, the error shall be small when the forming angle in z direction is less than 70°.

4.3 Finding the Strain / Stress Distribution Using Inverse FEM

The other major concern is the strain and stress incurred in the forming process. Overstress may cause the sheet metal fracture and hence, shall be avoided. The inverse FEM, also called the one-step FEM, is used to compute the strains and the stresses. Different from the conventional FEM, it simulates the entire sheet metal forming process in one-step and hence, is very fast; though its accuracy is not as good. According to

42

literatures, Batoz *et al.* [1998] first developed an inverse FEM approach with simple triangular shell elements. Lee and Huh [1998] introduced a new inverse FEM approach to predict blank shape and strain distribution. More recently, Du *et al.* [2006] discussed several important issues in inverse FEM. Lan *et al.* [2005] derived a new model to predict the thickness strain distribution and Naceur *et al.* [2004] made some improvements for the inverse FEM. These research results lay the foundation for our research.

In our ISMF process, the part is formed punch by punch. In each punch, there is deformation (both plastic and elastic), stress build-up and strain-hardening. In addition, the result of each punch is dependent on the previous punches. However, the final shape of the part shall follow the minimum energy state. Based on the final shape of the part, the inverse FEM can predict the thickness strain distribution with reasonable accuracy.

4.3.1 The Kinematics of the Inverse FEM

In order to simplify the problem, it is assumed that the strain is membrane strain and the thickness is perpendicular to the sheet metal surface. In addition, the effect of elastic deformation is negligible. Following the discussion above, the minimum energy state is used as the final shape. To find the strain and the stress, the inverse FEM starts from the final shape and projects the final shape back to the sheet metal blank. The difference between the projection and the original shape is caused by the deformation and hence, can be used to compute the strain and stress.

Figure 4.4 shows the geometric relation of a typical element on the final shape and its project (the guess solution) on the blank. It should be noted that the guess solution is an approximation of the actually 'initial states'. The two states is essentially a transformation between the part coordinate system (x, y, z) (the local coordinate system) and the original blank coordinate system (X, Y, Z) (the global coordinate system). Assume the element is a three-node triangle with straight sides (the so-called Constant Strain Triangle or CST), then, the elongation strain distribution of the element can be computed as shown below [Becker, 2004].
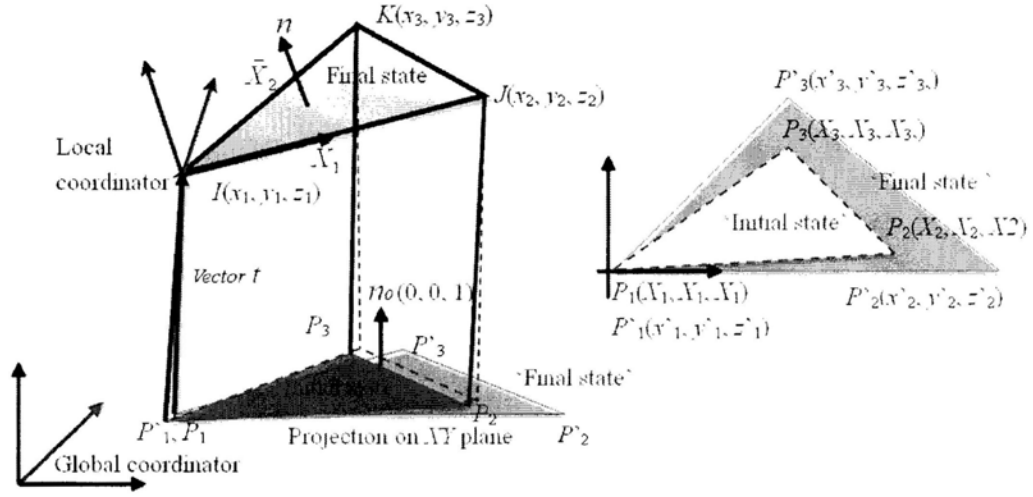
Figure 4.4: Illustration of the mapping in the inverse FEM

First, as shown in the figure, the upper element is the 'final state' and the lower element is taken as the 'initial state'. The initial state is in the XY plane, and its normal vector is $n_0 = (0, 0, 1)$. On the other hand, the normal vector of the final state element in the global coordinator is:

$$n = \bar{X}_1 \times \bar{X}_2 = K_x i + K_y j + K_z k \tag{4-6}$$

where, $\bar{X}_1$ and $\bar{X}_2$ are the vectors of the two edges of the final state element. They can be expressed as follows:

$$\bar{X}_1 = J - I = \langle (x_2 - x_1), (y_2 - y_1), (z_2 - z_1) \rangle$$
$$\bar{X}_2 = K - I = \langle (x_3 - x_1), (y_3 - y_1), (z_3 - z_1) \rangle \tag{4-7}$$

Moreover, the angels between the two elements in the YZ plane, α, and the XZ plane, β, can be described by using the two normal vectors:

44

$$\alpha = \arccos \frac{\langle K_y, K_z \rangle \cdot \langle 0,1 \rangle}{\left|\langle K_y, K_z \rangle\right| \cdot \left|\langle 0,1 \rangle\right|} \tag{4-8}$$

$$\beta = \arccos \frac{<K_x, K_z> \cdot <0,1>}{\left|<K_x, K_z>\right| \cdot \left|<0,1>\right|} \tag{4-9}$$

Though, since n_0 is perpendicular to the *XY* plane, it cannot be used to compute the angel in the *XY* plane. Fortunately, the angle can be found by using the two vectors $\bar{x}_1$ and $\bar{X}_1$, which are the first edges of elements in the initial and the final states.

$$\theta = \arccos \frac{<(x_2 - x_1),(y_2 - y_1)> \cdot <(X_2 - X_1),(Y_2 - Y_1)>}{\left|<(x_2 - x_1),(y_2 - y_1)>\right| \cdot \left|<(X_2 - X_1),(Y_2 - Y_1)>\right|} \tag{4-10}$$

With the three angles, the rotation matrix can then be found:

$$[R] = \begin{bmatrix} r_{xx} & r_{xy} & r_{xz} \\ r_{yx} & r_{yy} & r_{yz} \\ r_{zx} & r_{zy} & r_{zz} \end{bmatrix} \tag{4-11}$$

where,

$$r_{xx} = \cos\beta\cos\theta$$

$$r_{xy} = \sin\alpha\sin\beta\cos\theta - \cos\alpha\sin\theta$$

$$r_{xz} = \cos\alpha\sin\beta\cos\theta + \cos\alpha\sin\theta$$

$$r_{yx} = \sin\alpha\sin\beta\cos\theta - \cos\alpha\sin\theta$$

$$r_{yy} = \cos\theta\sin\theta$$

$$r_{yz} = \cos\alpha\sin\beta\sin\theta - \cos\alpha\sin\theta$$

$$r_{zx} = -\sin\beta$$

$$r_{zy} = \sin\alpha\cos\beta$$

$$r_{zz} = \cos\alpha\cos\theta$$

To compute the strain, the coordinate system of the final state needs to align to the coordinate system of the initial state. This requires the movement X_i' expressed below:

$$X_i' = [R]X_i + \bar{t} \tag{4-12}$$

where, X_i, $i = 1, 2, 3$, are position of the node in final state; $\bar{t}$ is the vector of the translation of the fist node between final state and the initial state.

Having aligned the finial state element in the XY plane, the element can be then considered as a 2D element (since z_i' are 0). In this case, the displacement$[u]$, the true strains$[\lambda]$, and the stresses $[\sigma]$ are defined as [Becker, 2004]:

$$[u] = \begin{bmatrix} u_x \\ u_y \end{bmatrix} ; \quad [\lambda] = \begin{bmatrix} \lambda_{xx} \\ \lambda_{yy} \\ \lambda_{zz} \end{bmatrix} ; \quad [\sigma] = \begin{bmatrix} \sigma_{xx} \\ \sigma_{yy} \\ \sigma_{zz} \end{bmatrix} \tag{4-13}$$

Since the element is CST, the displacement will be linear over the element. The displacements in terms of x and y can be written as:

$$\begin{aligned} u_x(x, y) &= W_1 + W_2 x + W_3 y \\ u_y(x, y) &= W_4 + W_5 x + W_6 y \end{aligned} \tag{4-14}$$

where, W_i are the constants.

The displacement of the element can be expressed as:

$$[u] = \begin{bmatrix} u_{x1} \\ u_{y1} \\ u_{x2} \\ u_{y2} \\ u_{x3} \\ u_{y3} \end{bmatrix} = \begin{bmatrix} x_1' - x_1 \\ y_1' - y_1 \\ x_2' - x_2 \\ y_2' - y_2 \\ x_3' - x_3 \\ y_3' - y_3 \end{bmatrix} \qquad (4\text{-}15)$$

Or:

$$\begin{bmatrix} u_{x1} \\ u_{y1} \\ u_{x2} \\ u_{y2} \\ u_{x3} \\ u_{y3} \end{bmatrix} = \begin{bmatrix} 1 & x_1 & y_1 & 0 & 0 & 0 \\ 0 & 0 & 0 & 1 & x_1 & y_1 \\ 1 & x_2 & y_2 & 0 & 0 & 0 \\ 0 & 0 & 0 & 1 & x_2 & y_2 \\ 1 & x_3 & y_3 & 0 & 0 & 0 \\ 0 & 0 & 0 & 1 & x_3 & y_3 \end{bmatrix} \begin{bmatrix} W_1 \\ W_2 \\ W_3 \\ W_4 \\ W_5 \\ W_6 \end{bmatrix} \qquad (16)$$

Furthermore, Equation (4-16) can be abbreviated to:

$$[u] = [A][W] \qquad (4\text{-}17)$$

where, $[A]$ is the shape matrix of the initial element, and $[W]$ is the constants matrix. The constants matrix can be solved using the following equation:

$$[W] = [A^{-1}][u] \qquad (4\text{-}18)$$

Based on the definition of strains and displacement, the element strains can be determined as follows:

47

$$\begin{bmatrix} \lambda_{xx} \\ \lambda_{yy} \\ \lambda_{zz} \end{bmatrix} = \begin{bmatrix} \dfrac{\partial u_x}{\partial x} \\[2mm] \dfrac{\partial u_y}{\partial y} \\[2mm] \dfrac{\partial u_y}{\partial x} + \dfrac{\partial u_x}{\partial y} \end{bmatrix} = \begin{bmatrix} W_2 \\ W_6 \\ W_3 + W_5 \end{bmatrix} \tag{4-19}$$

The direction of the principle strains is given by:

$$\varphi = \frac{1}{2} \arctan \frac{2\lambda_{xy}}{\lambda_{xx} - \lambda_{yy}} \tag{4-20}$$

so that,

$$[m] = \begin{bmatrix} \cos\varphi & \sin\varphi & 0 \\ -\sin\varphi & \cos\varphi & 0 \\ 0 & 0 & 1 \end{bmatrix} \tag{4-21}$$

Hence, the principle strain is:

$$\begin{bmatrix} \lambda_1 \\ \lambda_2 \\ \lambda_3 \end{bmatrix} = [m^{-1}][\lambda][m^{-1}]^T \tag{4-22}$$

To expressed large deformation in sheet metal forming, the logarithmic strain is usually used. It can be expressed as:

$$[\varepsilon] = \begin{bmatrix} \varepsilon_1 \\ \varepsilon_2 \\ \varepsilon_3 \end{bmatrix} = \begin{bmatrix} \ln\lambda_1 \\ \ln\lambda_2 \\ \ln\lambda_3 \end{bmatrix} \tag{4-23}$$

The logarithmic strain in the local coordinator is:

$$\begin{bmatrix} \varepsilon_{xx} & \varepsilon_{xy} & 0 \\ \varepsilon_{xy} & \varepsilon_{yy} & 0 \\ 0 & 0 & \varepsilon_{zz} \end{bmatrix} = [m][\varepsilon][m]^{T} \tag{4-24}$$

4.3.2 Material Continuation Descriptions and Stress

As the inverse FEM only considers the 'initial state' and the 'final state' of the sheet metal, the resultant strain is independent from the loading history. Thus, the assumption of proportional loading is applied. According to Hency-Ilyushin's law, the Hill's anisotropic yield criterion can be written as:

$$f(\sigma) = [\sigma][P][\sigma]^{T} - \bar{\sigma}^{2} = 0 \tag{4-25}$$

where $[\sigma] = [\sigma_{xx} \quad \sigma_{yy} \quad \sigma_{xy}]$ is the Cauchy plane stress, and $\bar{\sigma}$ is the equivalent stress. With the Lankford value $r = (r_0 + 2r_{45} + r_{90})$, the anisotropic matrix can be written as:

$$[P] = \begin{bmatrix} 1 & -\dfrac{r}{1+r} & 0 \\ -\dfrac{r}{1+r} & 1 & 0 \\ 0 & 0 & \dfrac{2(1+2r)}{1+r} \end{bmatrix} \tag{4-26}$$

By using the Hencky proportional deformation theory, the plastic strain can be gotten as:

$$\bar{\varepsilon} = \left\{ [\varepsilon][P][\varepsilon]^{T} \right\}^{\frac{1}{2}} \tag{4-27}$$

where, $[\varepsilon] = [\varepsilon_{xx} \quad \varepsilon_{yy} \quad \varepsilon_{xy}]$. Suppose the material is subject to the pre-strain constant law as follow:

49

$$\overline{\sigma} = K\left(\varepsilon_0 + \overline{\varepsilon}\right)^n \tag{4-28}$$

In the presented study only normal anisotropy is taken into account, and thus the constitutive relation is as follows:

$$\left[\sigma\right]^T = \frac{\overline{\sigma}}{\overline{\varepsilon} + \varepsilon_0}\left[P\right]^{-1}\left[\varepsilon\right]^T \tag{4-29}$$

This gives the stress distribution of the part.

4.4 Implementation Procedure

The implementation procedure consists of three steps: (1) Finding the geometric surface based on the punch positions; (2) Finding the final shape based on the minimum energy principle (as given in Section 2), and (3) Finding the strain and stress distribution using the inverse FEM (as given in Section 3).

4.4.1 Finding the Geometric Surface

The geometric surface can be obtained based on the geometric relations of the blank holder, the sheet metal, and the punch locations. Assume the punch is spherical and its radius is r_t. For a given punch location (x_k, y_k, z_k), the punch surface is:

$$T_k(x,y) = z_k + r_t - \sqrt{\left(r_t^2 - (x_k - r_t)^2 - (y_k - r_t)^2\right)} \tag{4-30}$$

Given all the punch locations, the geometric surface $G(x, y)$ can be then determined as:

$$G(x, y) = \min\left(T_1(x, y) \cdots T_n(x, y)\right) \tag{4-31}$$

where, n is the total number of punches.

In summary, the implementation flowchart is given in Figure 4.5.

50
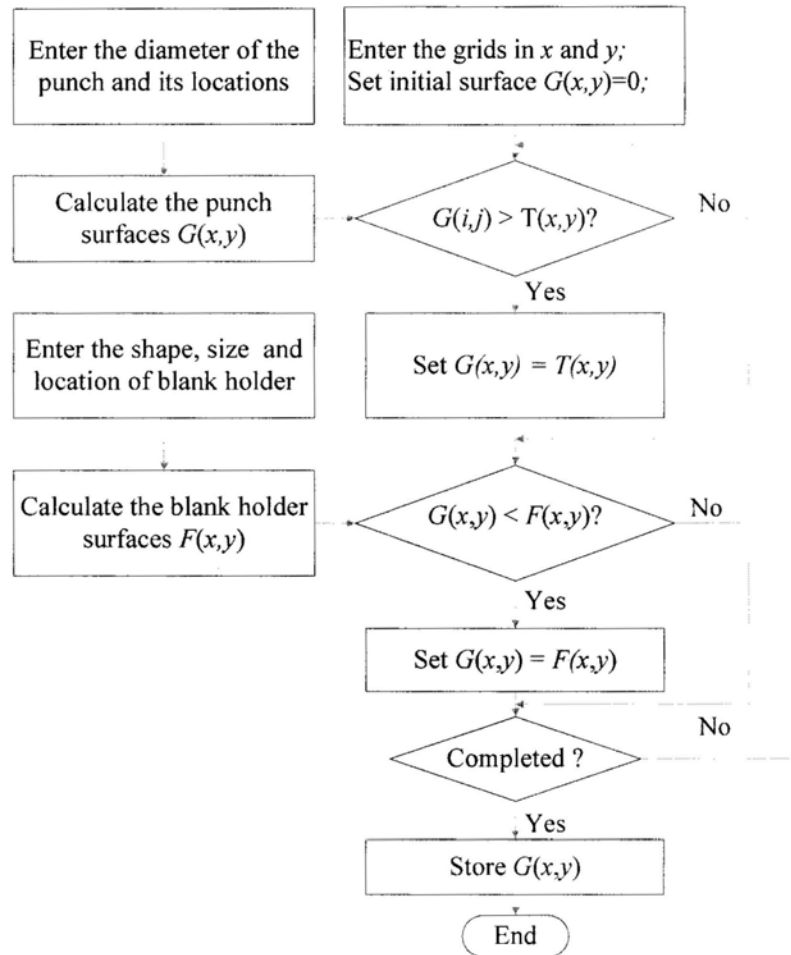
Figure 4.5: The flowchart for finding the geometric surface

4.4.2 Finding the Final Shape

Based on the method given in Section 2, the final shape of the part can be computed. The inputs include the geometric surface and boundary conditions, and the output is the final shape surface, which has the minimum energy position. Figure 4.6 illustrates the process of implementation of minimum energy principle to obtain the final shape in the final state of the process.
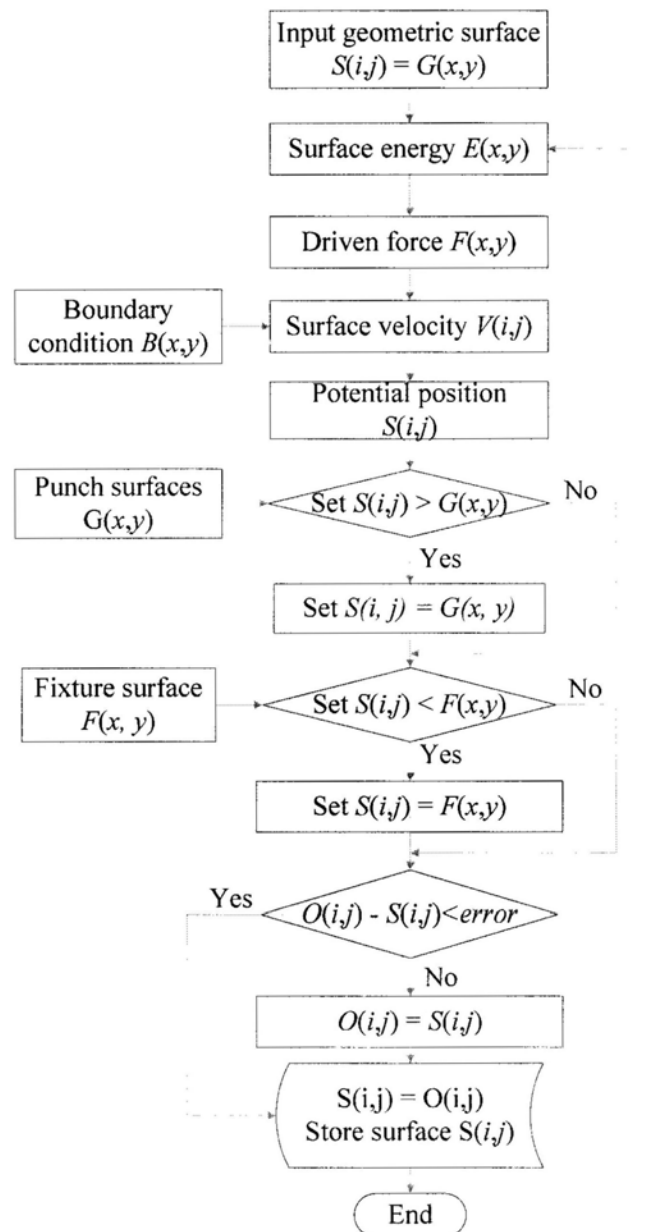
Figure 4.6: The flowchart for finding the final shape

4.4.3 Finding the Strain and Stress Distributions

Based on the inverse FEM method given in Section 3, the strain and stress distributions can be found using the flowchart in Figure 4.7. Note that in the previous step, the final shape is known. However, its topological structure has not been constructed yet. Therefore, before applying the inverse FEM method, it is necessary to code the final

shape as a set of CST elements. This can be done using commercial FEM software systems.


```
┌─────────────────────────────────────────────────┐
│ 1. Initialize nodal points of the final shape   │
│ 2. Input the geometric topology information     │
└─────────────────────────────────────────────────┘
                        ↓
┌─────────────────────────────────────────────────┐
│ Find the nodal points in the "initial state"    │
└─────────────────────────────────────────────────┘
                        ↓
┌─────────────────────────────────────────────────┐
│ Increase the number of element: n := n +1       │
└─────────────────────────────────────────────────┘
                        ↓
┌─────────────────────────────────────────────────┐
│ 1. Compute the normal vectors for each element. │
│ 2. Find  angels between element normal vectors  │
│    in "final state" and "initial state" vector  │
│    (0 0 1)                                       │
│ 3.  Move the element to the XY plane            │
└─────────────────────────────────────────────────┘
                        ↓
┌─────────────────────────────────────────────────┐
│ 1. Compute the true strains                     │
│ 2. Compute the logarithmic strain for the       │
│    principle strains                            │
│ 3. Compute logarithmic strains in global        │
│    coordinate                                   │
└─────────────────────────────────────────────────┘
                        ↓
┌─────────────────────────────────────────────────┐
│ Find the equivalent strain and equivalent stress│
└─────────────────────────────────────────────────┘
                        ↓
┌─────────────────────────────────────────────────┐
│ Compute the stresses for the element            │
└─────────────────────────────────────────────────┘
                        ↓
    No        ◇ Is all element competed? ◇
                        │ Yes
┌─────────────────────────────────────────────────┐
│ 1. Compute the stresses and thickness in the    │
│    nodes                                        │
│ 2. Output the results                           │
└─────────────────────────────────────────────────┘
                        ↓
                    ( end )
```

Figure 4.7: The flowchart of for finding the strain and stress distributions

4.5 Numerical Examples

In order to demonstrate the presented method, two examples are presented herein. The numerical simulation results are given in this section, while the experiment validation will be given in Chapter 6.

In both examples, the material constants and the geometric parameters of the sheet metal are the same as listed below:

- Stress-strain hardening curve $\bar{\sigma} = 576 \cdot (1.0 \times 10^{-4} + \bar{\varepsilon}_p)^{0.23}$ MPa ($\bar{\varepsilon}_p$ is the effective strain)
- Lankford value $r = 1.87$;
- Initial sheet thickness $t_0 = 1$ mm;
- Original blank size 300.0×300.0 mm;
- Poisson's ratio $v = 0.3$;
- Yang's modulus $E = 206.00$ GPa.

4.5.1 Example 1: A Tank

The part is a simple tank as shown in Figure 4.8. The top is a square while the bottom is a circle. The punch head is spherical with the diameter of 15 mm. Figure 4.9 shows its geometric surface. It is seen that the center of the part is not being punched. However, the minimum energy model predicts the final shape just like the design, as shown in Figure 4.10. Moreover, Figure 4.11 gives the thickness strain distribution. It is seen that the highest the strain occurs in the four sides of the part. This result is similar when forming with a die. Also, it is interesting to see there is a local strain distribution in each punch location. This is due to the local deformation when the tool punches on the sheet. A comparison of the design and the simulation result in Section A-A (refer to Figure 4.8) are shown in Figure 4.12. It shows that the simulation matches the design well except around the edges. The error is caused by the sheet metal trying to reach the minimum energy state. It can be reduced by adding the bottom support.
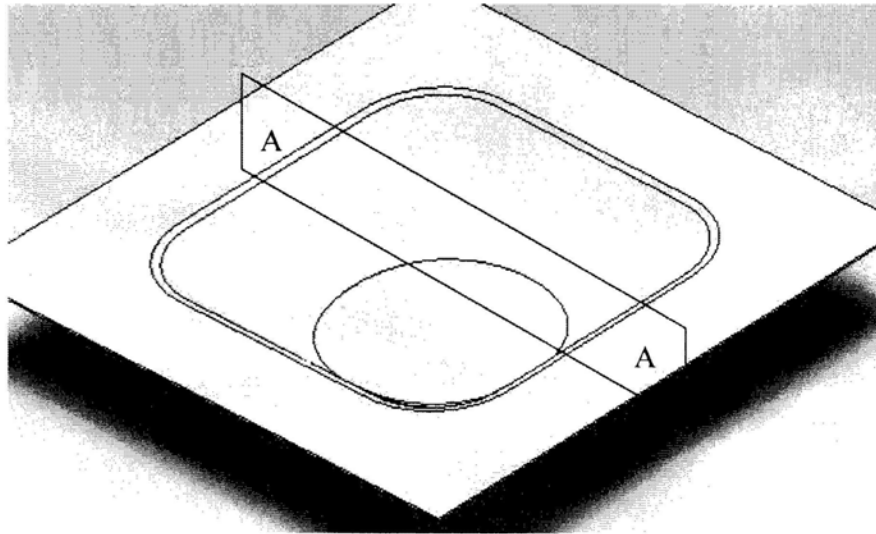
Figure 4.8: The CAD model of Example 1
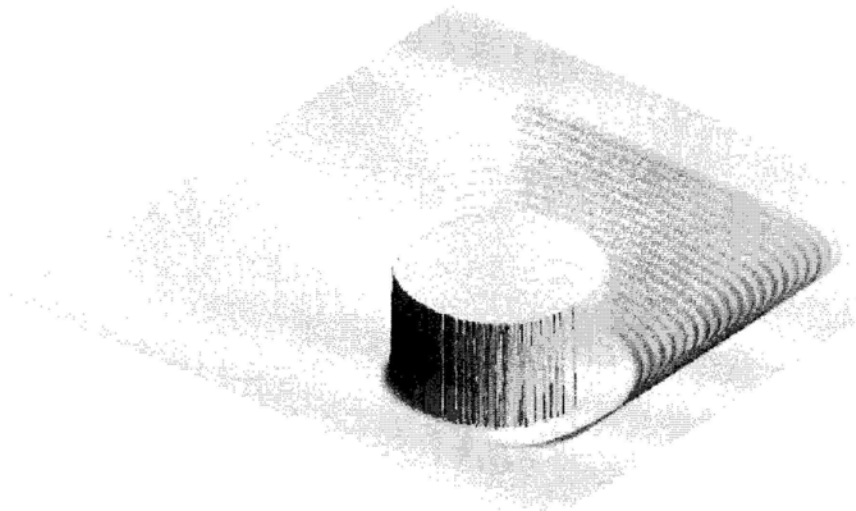
Figure 4.9: The geometric surface of Example 1

Figure 4.10: The predicted final shape of Example 1

Figure 4.11: The predicted strain distribution of Example 1
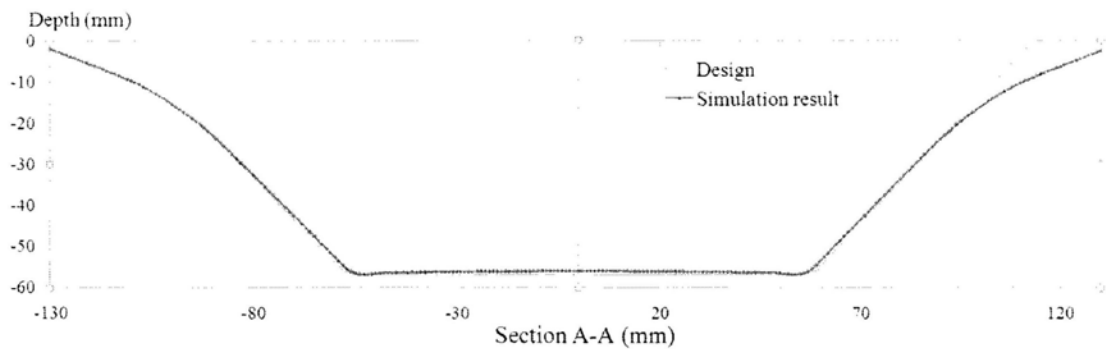
Figure 4.12: A comparison of experiment and simulation results of Example 1

4.5.2 Example 2: A Mask

The second example is a face mask. Figure 4.13 shows the CAD model of a face mask, which has many complex curves. A spherical punch with its radius of 15 mm was used. The geometric surface is shown in Figure 4.14 and the predicted final shape is shown in Figure 4.15. The predicted strain distribution is shown in Figure 4.16. The computations take only about 10 minutes to complete in a high end PC computer. A detailed study along the cross section B-B (refer to Figure 4.13) is shown in Figure 4.17. It is seen that the simulation matches the design well except around the edges. Similar to the previous example, the maximum error between the design and the simulation is attributed to the blank holding, near which the sheet metal tries to retain the minimum energy state. It can be reduced by adding a bottom support. The experimental studies will be presented in Chapter 6.

Figure 4.13: The CAD model of the face mask
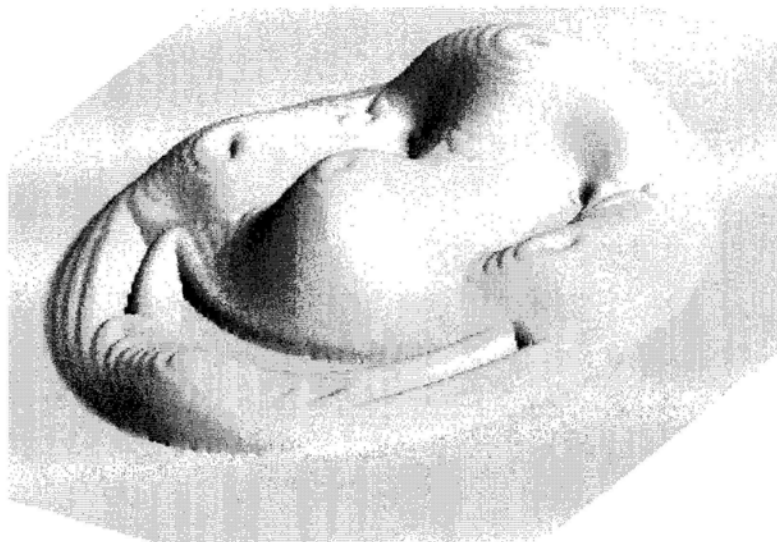
Figure 4.14: The geometric surface of Example 2

Figure 4.15: The predicted final shape of Example 2

Z Thickness strain
0.44082
0.39184
0.34286
0.29388
0.2449
0.19592
0.14694
0.097961
0.048998
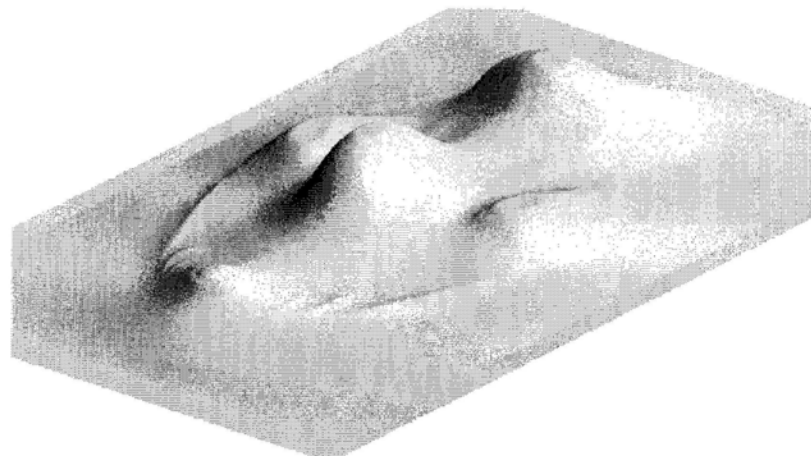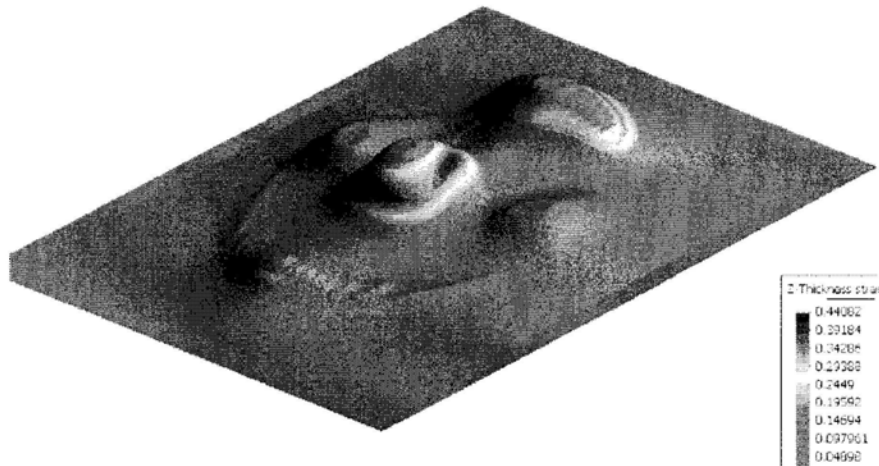
Figure 4.16: The predicted strain distribution of Example 2
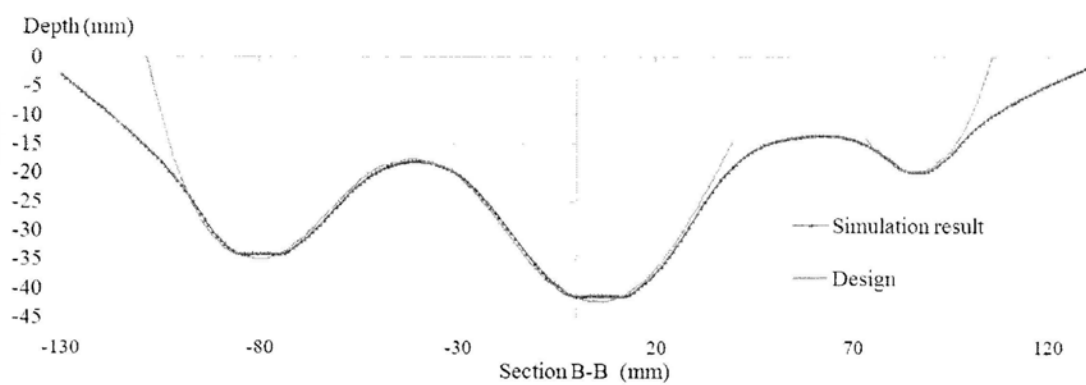
Figure 4.17: A comparison of the design and the simulation of Example 2

To evaluate the effectiveness of the fast mechanics, the computation time of the two examples is compared to the simulation results which are done in Dynaform®. Note that the first case presented in Section 3.5 is calculated by using Dynaform® with the conditions in Table 4-1. The computing time are also given in Table 4-1.

Table 4-1: The computation time of the old model and new model

Cases	Case of Section 3.5 using Dynaform®	Example 1 by our model	Example 2 by our model
Elements	5538	20000	20000
Nodes	3982	10201	10201
Punches	98	12807	8325
Applying boundary conditions	10 ~ 20 Hours	20min	20min
Finding final shape	~120 Hours	4.3 min	5.7 min
Finding strains		6.15 min	6.8 min

From the comparison results, it can be seen that the proposed mechanics model dramatically reduce the computing time. Such a significant improvement is probably caused by the follows:

- The procedure of applying boundary conditions is largely reduced.
- In our model, the contact between all of the punches and the workpiece is considered as a whole. While each punch is considered in one step in the old model using Dynaform®.
- The utilization of inverse FEM calculates the strains in one step. Therefore, it is an effective method but will cause an error.
- The Hill's 1979 criteria is used as the material model, it also reduce the computation time.

4.6 Summary

This chapter presents a fast computing model for predicting the forming process of Incremental Sheet Metal Forming (ISMF) based on incremental punching. Based on the results presented above, following conclusions can be drawn:

- The presented mechanics model can effectively predict the final shape of the part, as well as the strain and stress distributions of the part;

- The predictions of the final shape are generally accurate, though a significant error may occur around the edges near the blank holding positions;

- Compared to the simulations in commercial software, the commutation load is largely reduced to several minutes.

- Based on the simulation results, the dimples caused by punch applied on the sheet metal will be small when the feed step and layer thickness are less than 1 mm.

Chapter 5:

Design and Building of the Incremental Punching Machine

5.1 Introduction

It is well known that ISMF process is effective for small batch production and prototypes. Today, it has become one of the leading R&D topics in the industry. Nakajima [1979] first proposed the concept of flexible computer controlled forming process and anticipated the development of incremental forming based on NC control system. In subsequent years, a number of significant developments followed.

For example, Mori and Yamamoto [1996] proposed a new incremental forming method, in which a hemispherical hammer and a die were used to form the metal sheet into a 3D shape. Saotome and Okamoto [2001] designed an incremental microforming system to form 3D shell structures. Amino and Ro [2001] designed and built a CNC controlled ISMF system. The workpiece was held by a moving table under the pressing of a rotating forming tool. This method is further studied by Ambrogio *et al.* [2003], Kim and Park [2003], Ceretti *et al.* [2004], Kopac and Campus [2005], Micari *et al.* [2007], Ham and Jeswiet [2007], and Silva *et al.* [2009]. Callegari *et al.* [2007] compared the advantages of using robot cells and CNC machines. Allwood [2009] designed a close-loop system by integrating a vision system and a CNC ISMF machine. Also, Schafer and Schaft [2005] conducted experiments using an industrial robot and a hammer. Callegari *et al.* [2008] used a parallel kinematics machine and a rotating tool to carry on ISMF.

From point of view in machine building, existing ISMF systems can be roughly classified as either based on a 3-axis CNC machine with a rotating tool, or based on a robot with hammer. The former is rigid, while the later has more degree of freedom and large envelope. Presently, the former received much attention than the later.

Recently, Du's group in the Institute of Precision Engineering at the Chinese University of Hong Kong designed an incremental punching machine [Luo *et al.*, 2008; Luo, He and Du, 2009]. The machine is a 3 axes CNC machine with a high speed hydraulic punching head. Given a part, the punch path can be generated using commercial CAM systems with some modifications. Then, the machine takes over forming the part punch by punch. To fulfill the requirements of the proposed forming method, the design and control of the forming system will be described in details as following.

5.2 Overall Configurations

To further investigate the mechanics of the ISMF process, experimental studies are needed. Hence, a prototype machine is designed and built as shown in Figure 5.1. The machine was built based on a standard CNC machine. Mechanically, it consists of four components: an X-Y table, a Z slider, a fixture, and a high speed hydraulic punch. The workpiece is clamped by the fixture, while the fixture is fixed in a controllable X-Y table. Then the workpiece can be moved along X/Y direction with the X-Y table, which is controlled by the two servomotors. The slider moves in Z direction with the hydraulic punch head mounted on the top to provide sufficient punch force to deform the sheet metal. To balance the gravity force of the slider and the hydraulic punch head, a balancing weight is used. The work volume of the machine is 500 mm × 500 mm × 600 mm.

An industrial PC-based computer control system is developed for the prototype. The X-Y table and Z axis are controlled by a motion control card (GT400. After tuning the PID parameters, their position accuracies are about 0.01 mm. Figure 5.2 shows the control system. The high speed hydraulic punch head is a key component (manufacturer: Voith; model: Turbo H + L Hydraulic ECO 20), it can provide 10 tons force and has a maximum speed of 300 Strokes Per Minute (SPM) when the stroke is within 5 mm. It has its own closed-loop control system that can communicate with the PC computer. A PLC controller is utilized as the bridge to communicate the signal between hydraulic controller and the PC program.
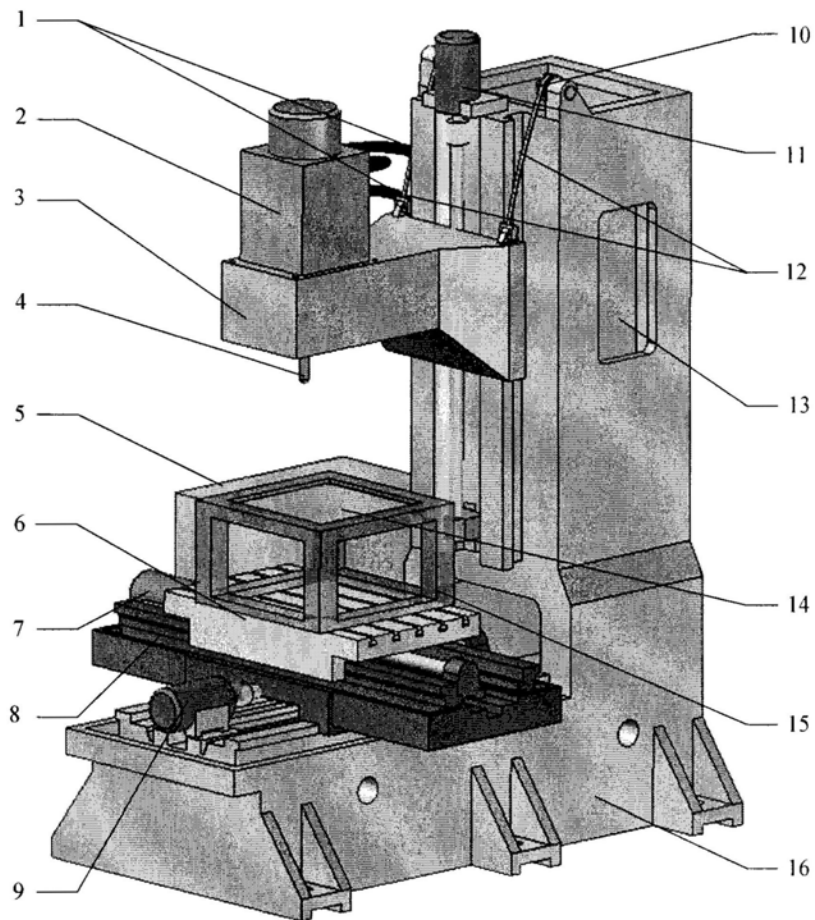
1- Hose, 2 - Hydraulic valve and hydraulic cylinder, 3 - Slider, 4 - Forming tool, 5- Hydraulic oil pump and oil tank, 6 - X-Y table, 7- X-axis servomotor and encoder, 8 - Bed, 9 - Y axis servomotor and encoder, 10 - Z axis servomotor and encoder, 11 – Balance wheel, 12 - Balance chain, 13 - Balance block, 14 - Workpiece, 15 - Fixture, 16- Mainframe

(a): Overall design
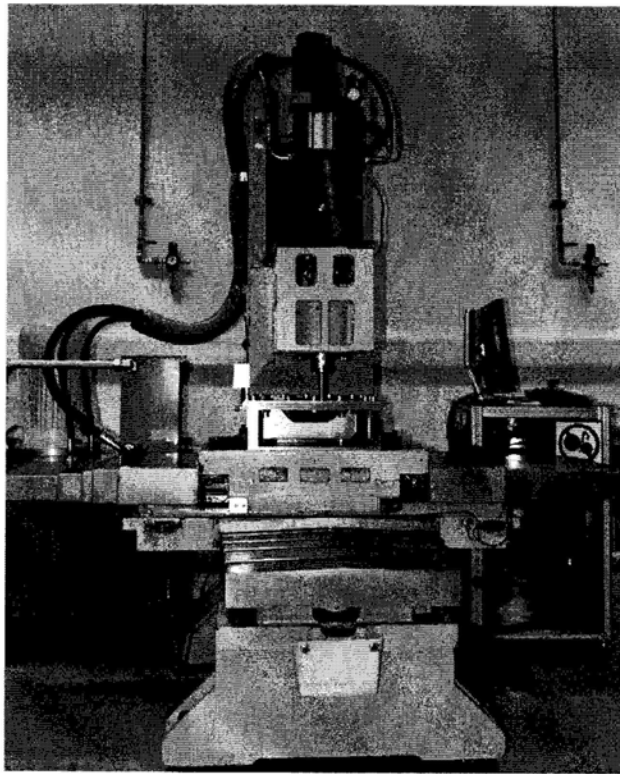
(b) Photo

Figure 5.1: Design and building of the ISMF machine
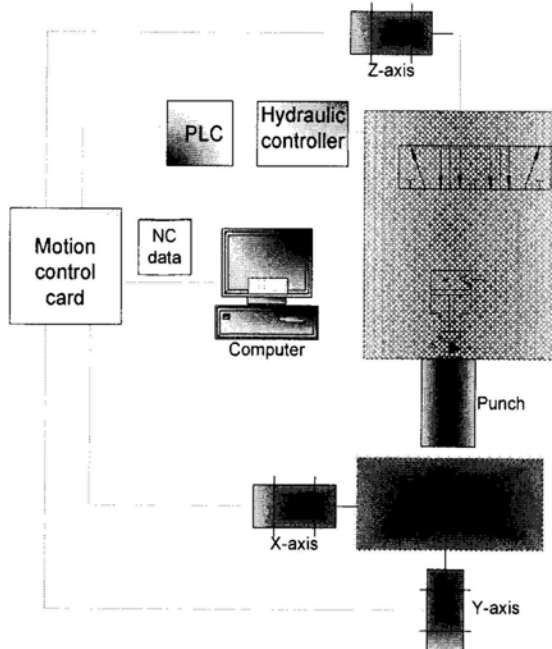
Figure 5.2 The control system of our ISMF machine

It is important to analyze the capability of the mechanical design and optimize of the control system to achieve the best performance of the machine. The dynamics analysis on the feeding system is presented in Section 2. The control system will play an important role in achieving good performance. The detailed design of the control system will be presented in Section 3. The hydraulic system is one of the key components of this system and it is presented in Section 4.

5.3 Dynamic of Motion System

5.3.1 Dynamic model of X-Y table

The X-Y table feed table is a two-layer stage. Figure 5.3 shows a dynamic model of the table including its base vibration dynamics in X direction [Erkorkmaz and Altintas, 2001; Matsubara *et al.*, 2004]. This model considers a feed drive driven by a rotary servo motor and a ball screw. The dynamics of the ball screw system can be modeled as a two-mass dynamic system with the natural frequency of 100~200Hz (only the longitudinal vibration mode is considered). The bed is a solid body supported by leveling blocks. Their dynamics is simply modeled by a spring and a damper.
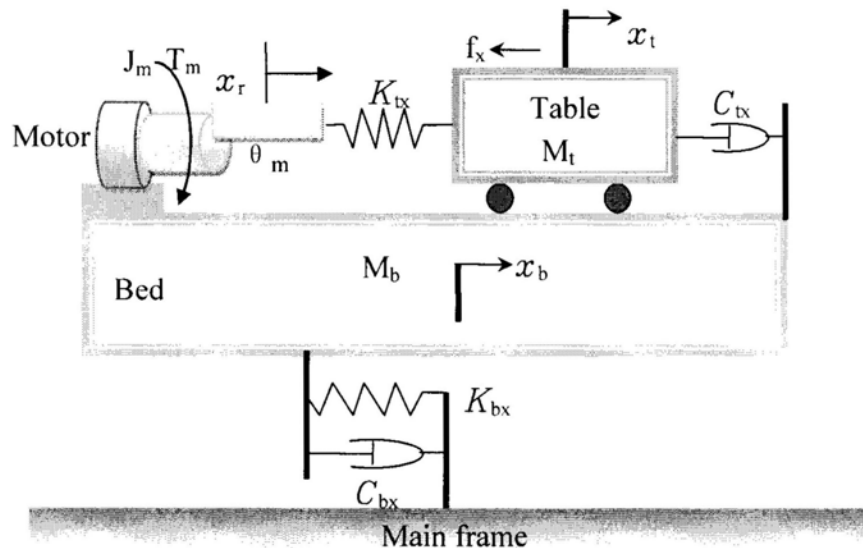
Figure 5.3: Dynamic model of X-Y table in X direction

In Figure 5.3, x_t: position of table, M_t: mass of the table, K_{tx}: stiffness of the table, C_{tx}: damping coefficient of guideway, J_m: inertia of the motors, P is the ballscrew pitch, θ_{mx}: angular position of the motor, f_x: is the friction force during forming, T_x: torque of the motor, x_r: is the nominal position of the table, x_b: position of the bed, M_b: mass of the bed, K_{bx}: stiffness of the bed, C_{bx}: damping coefficient, . Note that all of coefficients are in X direction. The equations of motion can be written as follows:

$$M_t \ddot{x}_t + C_{tx}(\dot{x}_t - \dot{x}_b) + K_{tx} x_t = K_{tx} x_r - f_x$$
$$M_b \ddot{x}_b + C_{bx} \dot{x}_b - C_{tx}(\dot{x}_t - \dot{x}_b) + K_{bx} x_b - K_{tx} x_t = -K_{tx} x \tag{5-1}$$

where, $x_r = \dfrac{P\theta_m}{2\pi}$, It can be rewritten as:

$$[M][\ddot{X}] + [C][\dot{X}] + [K][X] = [F] \tag{5-2}$$

where,

$$[X] = [x_t \quad x_b]^T$$

$$[M] = \begin{bmatrix} M_t & 0 \\ 0 & M_b \end{bmatrix}$$

$$[C] = \begin{bmatrix} C_{tx} & -C_{tx} \\ -C_{tx} & C_{bx} + C_{tx} \end{bmatrix}$$

$$[K] = \begin{bmatrix} K_{tx} & 0 \\ -K_{tx} & K_{bx} \end{bmatrix}$$

$$[F] = \begin{bmatrix} K_{tx} x_r - f_x \\ -K_{tx} x_r \end{bmatrix}$$

Figure 5.4 shows a dynamic model of the table including its base vibration dynamics in Y direction. With same assumptions in X direction, this model also considers a feed drive driven by a rotary servo motor and a ball screw. The dynamics of the ball screw system can be modeled as a two-mass dynamic system. The bed is a solid body supported by leveling blocks. Their dynamics is simply modeled by a spring and a damper.
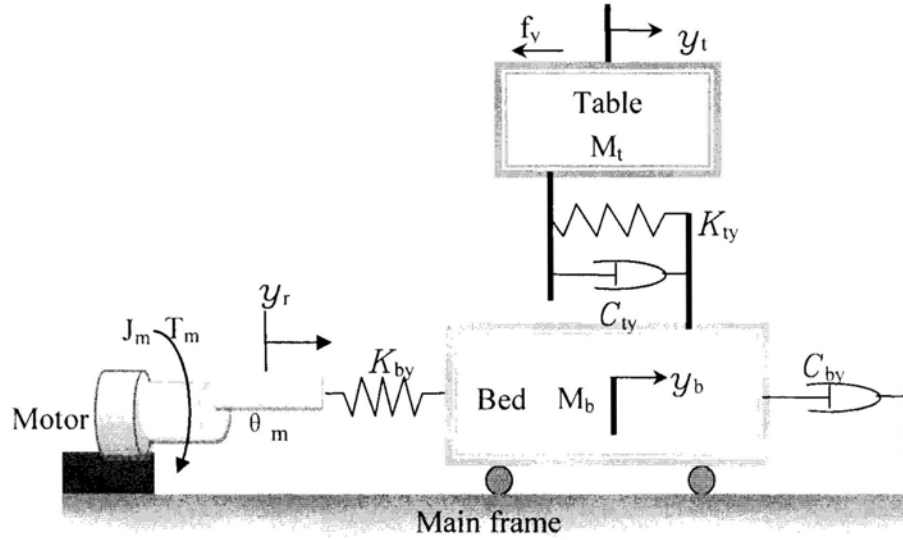
Figure 5.4: Dynamic model of X-Y table in Y direction

In Figure 5.4, y_t : position of table, M_t : mass of the table, K_{ty} : stiffness of the table, C_{ty} : damping coefficient of guideway, J_m : inertia of the motors, P is the ballscrew pitch, θ_{my} : angular position of the motor, T_y : torque of the motor, f_y : is the friction force during forming, y_r : is the nominal position of the table, y_b : position of the bed, M_b : mass of the bed, K_{by} : stiffness of the bed, C_{by} : damping coefficient. Note that all of coefficients are in Y direction. The equations of motion can be written as follows:

$$
\begin{aligned}
M_t \ddot{y}_t + C_{ty}(\dot{y}_t - \dot{y}_b) + K_{ty}(y_t - y_b) &= -f_y \\
M_b \ddot{y}_b + C_{ty}(\dot{y}_b - \dot{y}_t) + C_{by}\dot{y}_b + K_{by}y_b + K_{ty}(y_b - y_t) &= -K_{by}y_r
\end{aligned}
\tag{5-3}
$$

where, $y_r = \dfrac{P\theta_m}{2\pi}$, It can be rewritten as:

68

$$[M][\ddot{X}]+[C][\dot{X}]+[K][X]=[F]$$ (5-4)

where,

$$[X]=[y_t \quad y_b]^T$$

$$[M]=\begin{bmatrix} M_t & 0 \\ 0 & M_b \end{bmatrix}$$

$$[C]=\begin{bmatrix} C_t & -C_t \\ -C_t & C_t+C_b \end{bmatrix}$$

$$[K]=\begin{bmatrix} K_{ty} & -K_{ty} \\ -K_{ty} & K_{ty} \end{bmatrix}$$

$$[F]=\begin{bmatrix} -F_f \\ -K_{tx}x_{rx} \end{bmatrix}$$

With the above equations, the mechanical system is modeled in Matlab$^{®}$. The parameters of the system are given in Table 5.1. For testing the machine, assume that the table has the acceleration of the 10m/s^2. The error between the inputs (x_r, y_r) and outputs (x_t, y_t) is the most important factor that indicate the stiffness of the mechanical system.

Table 5-1: The parameters of the X-Y table

symbols	values	symbols	values
M_t	140Kg	K_{tx}	$1.21\times10^9 N/m$
M_b	300Kg	K_{ty}	$8.3\times10^9 N/m$
J_m	2.05×10^3 Kgm	T_{max}	23 Nm
K_{by}	$8.3\times10^9 N/m$	K_{bx}	$1.21\times10^9 N/m$
C_{by}	7000N/(m/sec)	C_{bx}	7000N/(m/sec)
C_{tx}	7000N/(m/sec)	C_{ty}	7000N/(m/sec)
μ	0.15	P	6mm

69

The dynamic simulation is conducted in Matlab®. Figure 5.5 (a) shows the errors between input and output in X direction while Figure 5.5 (b) shows the results in Y direction. It's noted that the vibration in both X and Y directions are proportional to the punch force. The maximum error will be 0.012 mm and 0.015 mm in X and Y direction respectively.
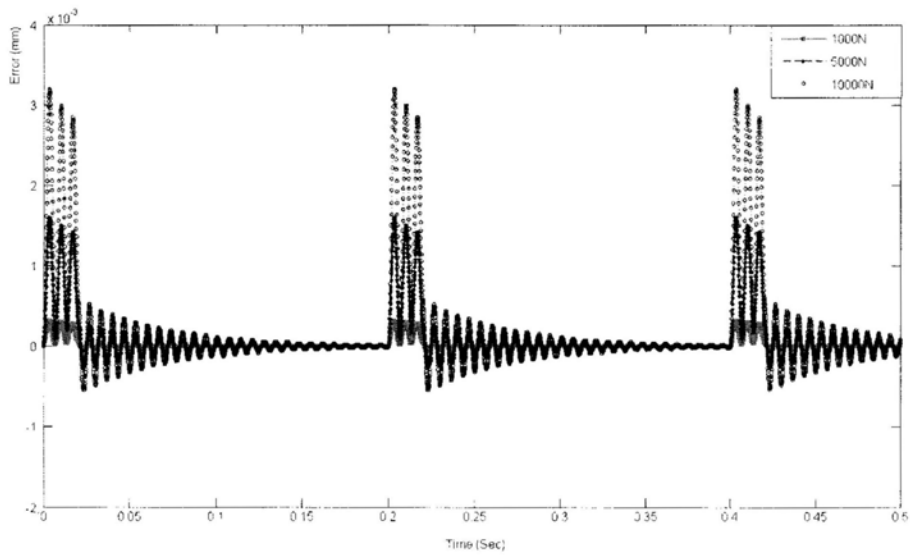
(a) X direction
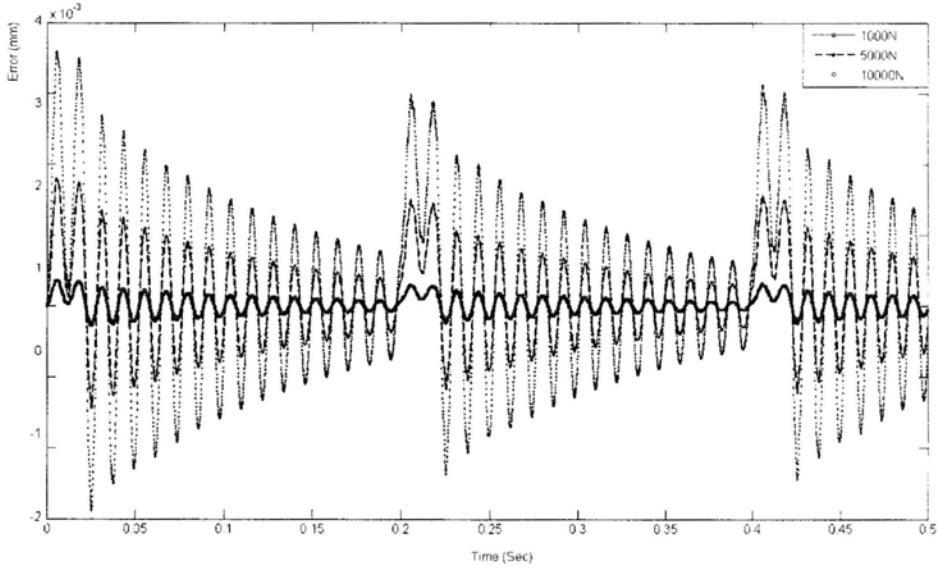
(b) Y direction

Figure 5.5: Errors between input and output: $F_p = 1000N$; $F_p = 5000N$; $F_p = 10000N$

From the presented simulation results, it can be seem that the accuracy is largely depended on the impact force. IF the punch force is less than 10000N, the position error is less than ±0.005mm. In that case, it will satisfy the requirement of the ISMF machine.

5.3.2 Dynamic model of the slider

The slider system consists of a motor, a ballscrew, a balance block, and a hydraulic cylinder mounted on the slider. A dynamic model of the system is shown Figure 5.6. It considers a feed drive driven by a rotary servo motor and a ball screw. Note that a pulley system is designed to balance the gravity of the slider and hydraulic cylinder.
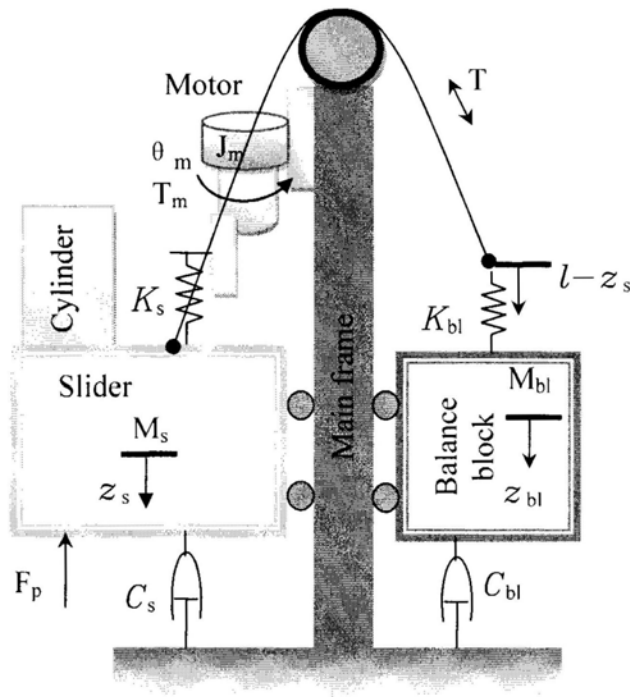
Figure 5.6: Dynamic model of slider

In Figure 5.6, z_t: position of slider, M_s: mass of the slider and punch system, M_{bl}: mass of the balance block, K_s: stiffness of the slider, C_s: damping coefficient of guideway, J_m: inertia of the motors, P is the ballscrew pitch, $\theta_{m\varepsilon}$: angular position of the motor, T_z: torque of the motor, T is the tension of the balance chain, F_p: is the punch force during forming, x_{rz}: is the nominal position of the slider, z_s: position of the

slider, C_s: damping coefficient slider, C_{bl}: damping coefficient balance block. Note that all of coefficients are in Z direction. The equations of motion can be written as follows:

$$M_s\ddot{z}_s + C_s\dot{z}_s + K_s z_s = K_s z_r - F_p - T + M_s g$$
$$M_b\ddot{z}_{bl} + C_{bl}\dot{z}_{b1} = T - M_{bl}g$$

(5-5)

where, $z_r = \dfrac{P\theta_m}{2\pi}$ and $T = K_{bl}(l - z_s - z_{bl})$.

It can be rewritten as:

$$[M][\ddot{X}] + [C][\dot{X}] + [K][X] = [F]$$

(5-6)

where,

$$[X] = [z_s \quad z_{bl}]^T$$

$$[M] = \begin{bmatrix} M_s & 0 \\ 0 & M_{bl} \end{bmatrix}$$

$$[C] = \begin{bmatrix} C_s & 0 \\ 0 & C_{bl} \end{bmatrix}$$

$$[K] = \begin{bmatrix} K_s & 0 \\ 0 & 0 \end{bmatrix}$$

$$[F] = \begin{bmatrix} -K_s z_r + F_p + T \\ T \end{bmatrix}$$

With the above equations, the mechanical system is modeled in Matlab®. The parameters of the system are given in Table 5.2. Assume that the table has the acceleration of the 10m/s², the error between the inputs (x_r, y_r) and outputs (x_t, y_t) is the most important factor that indicate the stiffness of the mechanical system. Table 5.1 shows the parameters used in this simulation and the result are shown in Figure 5.7.

Table 5-2: The parameters of Z direction feeding system

symbols	values	symbols	values
M_s	$350Kg$	K_s	$1.21 \times 10^9 N/m$
M_b	$350Kg$	K_{bl}	$8.3 \times 10^9 N/m$
J_m	$2.05 \times 10^3\ Kgm$	T_{max}	$23\ Nm$
C_s	$7000N/(m/sec)$	C_{bl}	$500N/(m/sec)$
l	$800mm$	P	$6mm$
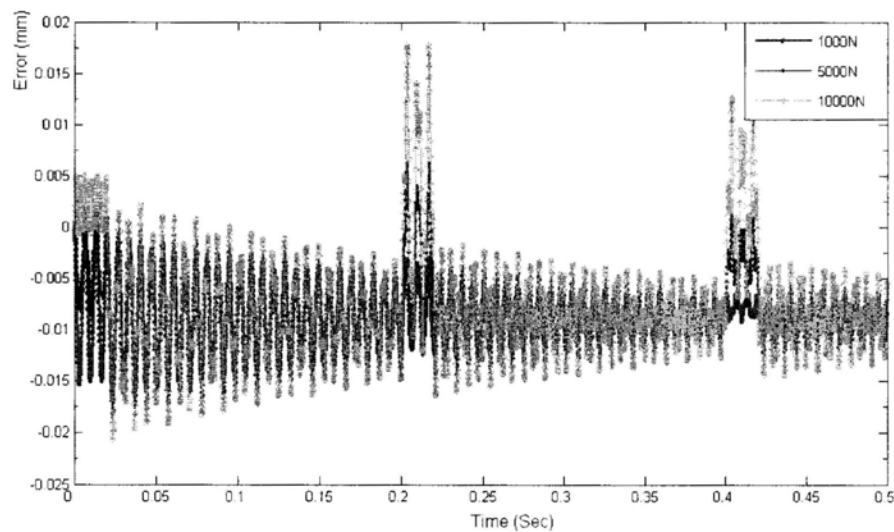
Figure 5.7: Errors between input and output: $F_p = 1000N$; $F_p = 5000N$; $F_p = 10000N$

The simulation results shows that the dynamic performance is largely depended on the impact force, when the force is less than 10000N, the position error of the punch will less than ±0.02mm, which will satisfy the requirement of the ISMF machine.

5.4 Control System

The purpose of control system is to control the motion system and movement of the hydraulic cylinder. One PC-based motion controller card is used to manipulate the ISMF system. The control software is with a friendly user interface, from which the G code can be input and sent to the control card. The details will be presented as following.

The ISMF machine is based on a typical three axis CNC milling machine. Its motion system consists of a computer, a motion control card, amplifiers and three servo motors. Since the position accuracy required in sheet metal forming is about 0.02mm, which is quite larger than milling, the control of the feed system is essentially a partial close loop control system. The feedbacks of X-Y table position (x, y) and the slider (z) are from the three encoders which are connected to the three driven motors respectively. To simplify the use of the forming system, the motion of the feed system designed is compatible with ISO NC code. The illustration of motion system is shown in Figure 5.8.
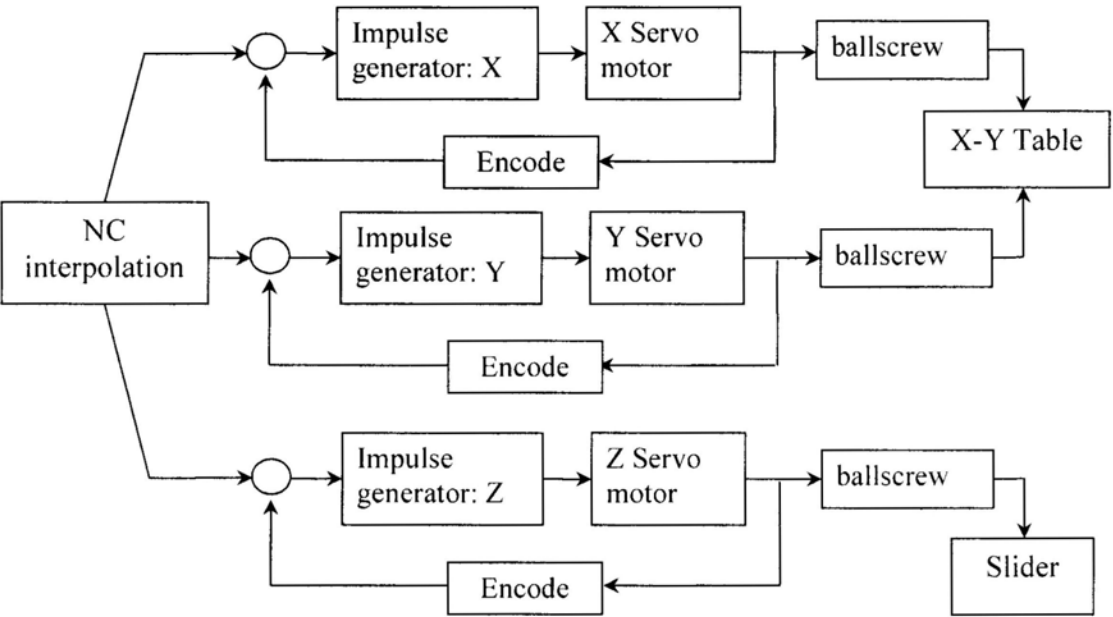
Figure 5.8: Illustration of motion control system

The function of NC decoding in a plane can be classified as: linear interpolation and circular interpolation. For example, two axes X, Y are moved at different lengths form start position to end position, it is necessary to use interpolation to regulate their speeds:

$$V_x = \frac{\Delta x}{\left(\Delta x^2 + \Delta y^2\right)} V_f$$

$$V_y = \frac{\Delta y}{\left(\Delta x^2 + \Delta y^2\right)} V_f$$

(5-7)

where, V_x and V_y are the interpolation speed in X axis and Y axis respectively, Δx, Δy are the length between start position and end position in X axis and Y axis respectively, V_f is the required feed speed.

The circular interpolation is to break down a curve profile into many segments. The accuracy of the circular profile is largely depended on the sampling period. In each sampling period, λ_i, the feed step (length of each segments) is:

$$f = v\lambda_i \tag{5-8}$$

where, v is the average velocity in the current feed step.

If current position is (x_i, y_i), the feed step for next position in X and Y direction can be derived form the geometric relation:

$$\begin{aligned}
\Delta x_{i+1} &= \frac{v}{R}\lambda_i\left(y_i - \frac{v}{2R}x_i\right) \\
\Delta y_{i+1} &= \frac{v}{R}\lambda_i\left(x_i + \frac{v}{2R}y_i\right)
\end{aligned} \tag{5-9}$$

Hence, the next position will be:

$$\begin{aligned}
x_{i+1} &= x_i + \Delta x_{i+1} \\
y_{i+1} &= y_i + \Delta y_{i+1}
\end{aligned} \tag{5-10}$$

Linear interpolation will be applied to control the motion between the current position (x_i, y_i) to next position (x_{i+1}, y_{i+1}).

The PC-based motion controller card is used to manipulate the motion system, which s manufactured by the Googoltech Technology Limited and the model number is GT-400-SV [http://www.googoltech.com]. The control card is capable of controlling up to four

axes during independent motion and up to three axes during coordinated motion. It is with 8 digital input channels and 16 output channels. The maximum encoder sampling rate for each axis is 2 MHz. It is integrated with an industrial PC as shown in Figure 5.9. A control program is developed with the user interface shown in Figure 5.10.
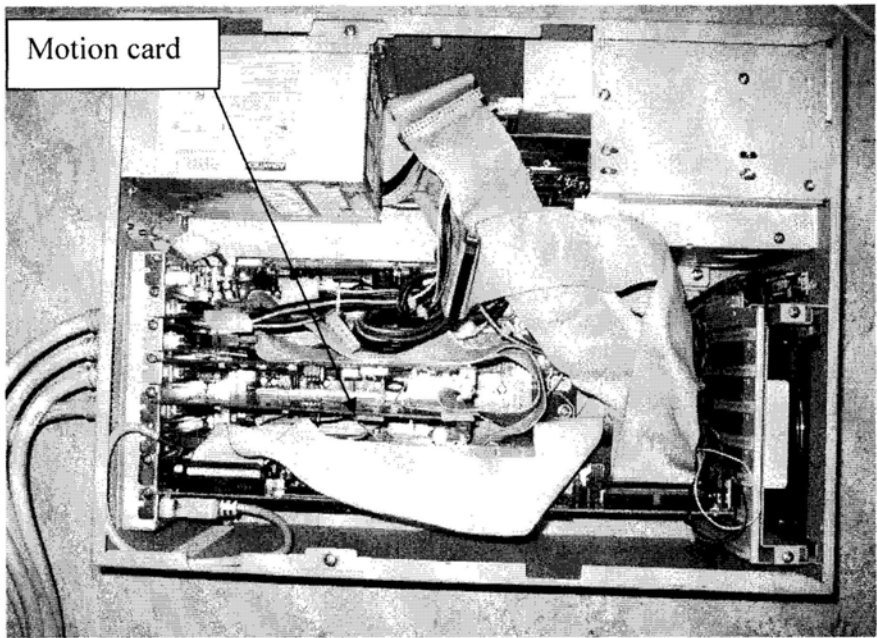
Figure 5.9: The PC-based control system and GT-400-SV motion card
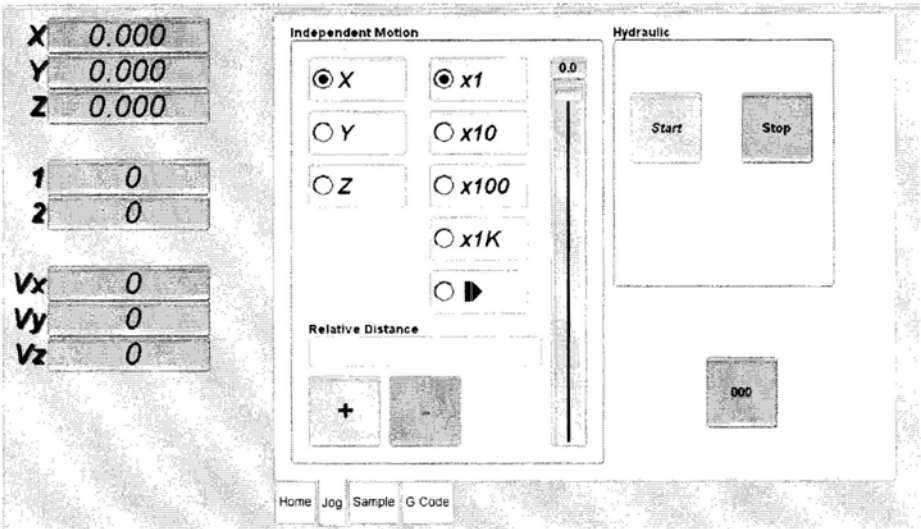
Figure 5.10: User interface of the control system

5.5 Hydraulic System

The hydraulic cylinder is mounted on the slider. It can provide 10 ton punch force that is satisfied the requirements in deforming of the sheet metal with large size of forming tool. Figure 5.11 shows the hydraulic circuit of the punch system. A PLC controller is used to control the hydraulic system. The punch moves up and down between the two sensors. The hydraulic punch can move between the two limit sensors in a high frequency. The distance of the two sensors is adjustable. If the distance is small, the punch will reach a higher frequency. The maximum frequency of the punch can be 300 *SPM*, and it makes the experimental equipment more efficiency.

The motion of punch is controlled by the hydraulic controller. The speed is determined by the hydraulic flow rate. In this hydraulic system, the flow rate is a constant value which depends on the setting of the hydraulic system and the flow control gate. A couple of approximate switches are mounted on the mainframe to detect whether the ram moves in the safety range. If the limiters detect the ram approximates, the hydraulic controller is initiated by the signal from the sensors and send out the command to change direction of the pilot valve. Figure 5.12 shows the hydraulic controller.
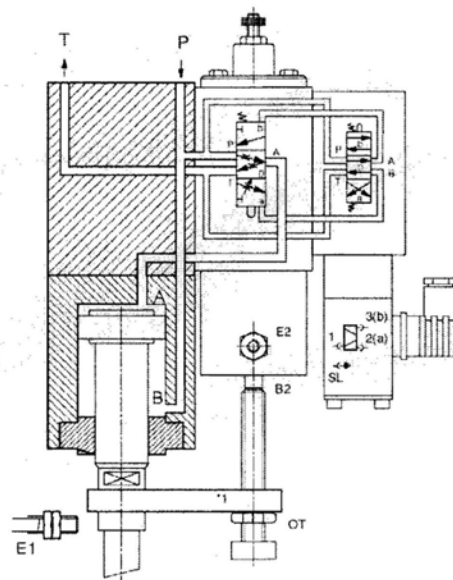
Figure 5.11: Illustration of hydraulic circuit of high frequency punch system
[http://www.voithturbo.com]
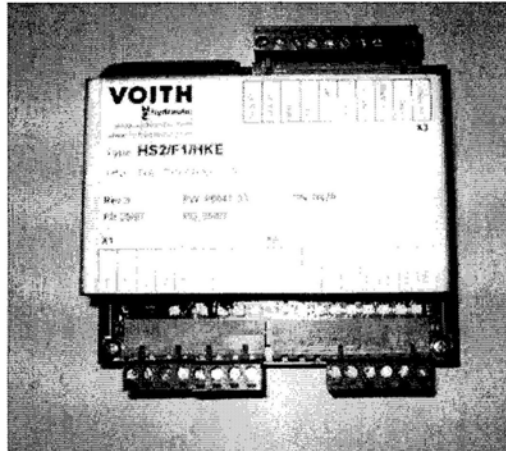
Figure 5.12: Hydraulic controller [http://www.voithturbo.com]

5.6 Summary

This chapter presents a completed design and control of the incremental punching machine including mechanical design, electrical design, hydraulic design, safety design, *etc.* The mechanical system is based on CNC milling machine with some modifications. The dynamics analysis of the system is conducted to investigate the vibration of the system under the large punching force. The control system is based on an industry PC and a motion card, a control system is developed to control system. The control program is compatible with standard NC code, which makes the system is easier to use. The hydraulic design is based on H+L punching system, which provides sufficient forming force in a high frequency. The PLC controller is applied to control the hydraulic system. The other designs of this machine, such as the limit sensors, lubrication system, *etc.*, were also done while will omitted in this thesis.

Chapter 6:

Experimental and Simulative Studies on the Incremental Punching Process

6.1 Introduction

During the past decade, several ISMF processes have received wide development. It consists of a simple hemispherical tool that, moving along a defined path by means of either a CNC machine or a robot or a self designed device, locally deforms a metal sheet. A lot of experimental and simulative studies have been conducted in ISMF process with different aims: to study relations between the formability and process parameters; to develop models to forecast the final sheet thickness and shape; to understand how the sheet deforms and how formability limits can be defined. Nowadays, a lot of these topics are still open.

For example, Cerro *et al.* [2006] conducted FEM simulation of the ISMF. A simple FEM model which gives accurate prediction of some characteristics of the formed parts. Minutolo *et al.* [2007] used LS-DYNA® code to evaluate of the maximum slope angle of frustums of pyramids and cones beginning from aluminum alloy 7075T0 sheets. Ambrogio *et al.* [2007] built an analytical model for improving precision in single point incremental forming through a reliable statistical analysis. As mentioned before, the incremental punching system is a new process that is with a different forming mechanism in comparing to existing processes. It's difficult to simulate the whole process. Recently, Luo *et al.* [2010] proposed a new method based on minimum energy principle and inverse FEM, which has already been presented in Chapter 4 in details. An in-house program was developed accordingly. It can predict the forming process in about 10 minutes.

With the in-house simulation program, a large number of examples have been simulated. These examples were also validated experimentally using our prototype machine. In this

chapter, two experiments are presented in details. To evaluate the proposed mechanics model, comparative studies on numerical results and experiment results are also conducted considering final sheet thickness, geometrical errors of the final part. The rest of the Chapter is organized as following. Section 2 describes the experimental setup and the mechanical properties of the sheet metal. Section 3 presents two examples with two experimental setups. Finally, Section 4 includes discussions and conclusions.

6.2 Experimental Setup and Material Properties

From the simulation on the forming process presented in Chapter 4, the fixture and the support will play an important role on the final shape of the parts. A simple fixture, also called blank holder, is used for this study. The square workpiece is simply mounted on the fixture along the edges and there is no additional support. As shown in Figure 6.1, in the experiments, two different configurations are used: L = 220 mm (Setup A), and L = 260 mm (Setup B).
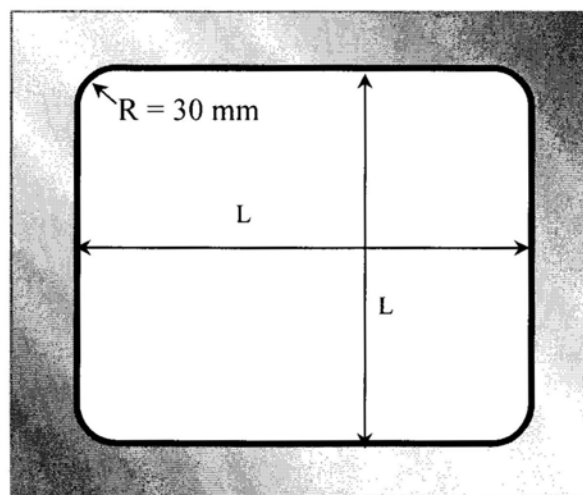
Figure 6.1: Illustration of the fixture size

To facilitate the operation, four different ball-end punch heads are made, as shown in Figure 6.2. Their diameters are 5 mm, 10 mm, 15mm, and 20 mm respectively. The size of the ball end punch head determines not only the minimum curvature of the part but also the surface roughness of the part. It also affects the punch force.
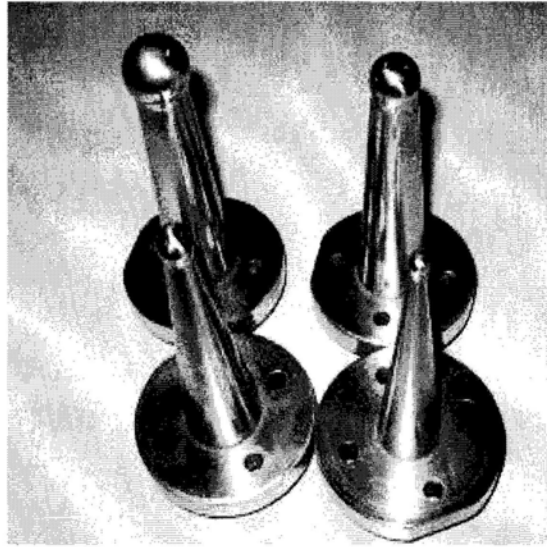
Figure 6.2: The ball-end punch heads

Using our prototype machine, a large number of experiments were carried out. In this section, following the previous paper, two experiments are presented in details. In both experiments, the size of the punch we applied here is 10 mm. The workpiece material is SPCC steel. Its mechanical properties are summarized as follows:

- Workpiece size 300.0×300.0 mm;
- Workpiece thickness $h_0 = 1$ mm;
- Yang's module $E = 206.0 \text{GPa}$;
- Poisson ratio $v = 0.3$;
- Stress-strain hardening curve $\sigma = 576 \cdot (1.0 \times 10^{-4} + \bar{\varepsilon}_p)^{0.23} \text{MPa}$ ($\bar{\varepsilon}_p$ is the effective strain);
- Lankford value $r = 1.87$;

6.3 Examples

6.3.1 Example 1: A Tank

In this example, two parts were made with the Setup A and Setup B, which will be referred to as Case 1 and Case 2. The parts are with the same design, as shown in Figure 6.3; however, different control parameters are used. In Case 1, the layer thickness is 1 mm and the feed step varies from 1 mm to 4 mm. In Case 2, the layer thickness is 3 mm and the feed step is uniform (3 mm). Figure 6.4 shows the simulation and experiment results, in which (a) is the punch path, (b) is the geometric surface based on the punch path, (c) is the predicted part surface using the minimum energy method given in Part 1 of the paper, (d) is the predicted thickness strain distribution using the inverse FEA method given in Part 1 of the paper, and (e) is the experiment results. It is interesting to note that the center of the part is not being punched. Though, it deforms to its lowest energy position as predicted. Moreover, both cases result in similar thickness strain distribution pattern. However, the part in Case 2 has large punch marks, as predicted. In short, the computer simulations and the experiment results are well matched.
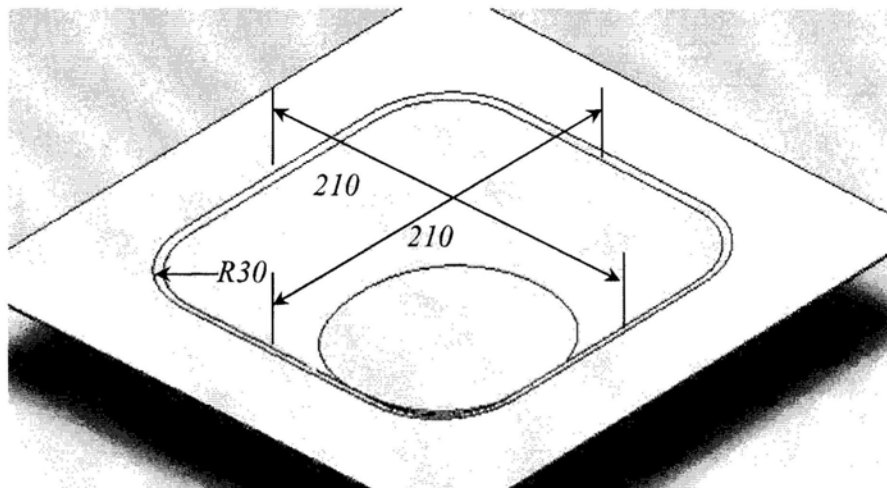
Figure 6.4: CAD Model of the Tank (unit: mm)
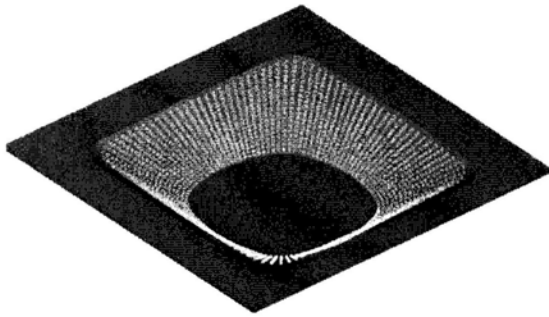
Case 1   Case 2
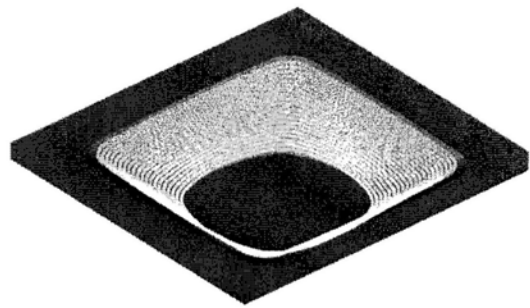
(A1) Punch path in Case 1   (B1) Punch path in Case 2
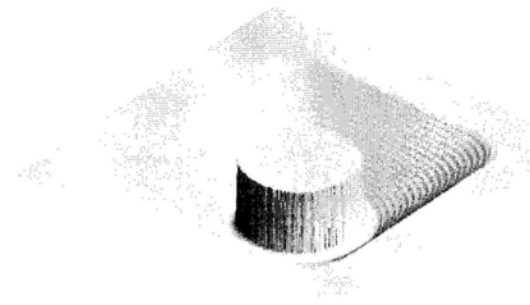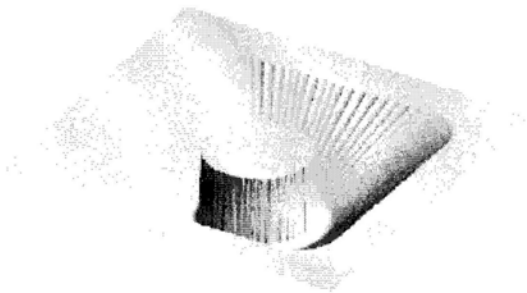
(A2) Geometric surface based on the punch path in Case 1   (B2) Geometric surface based on the punch path in Case 2
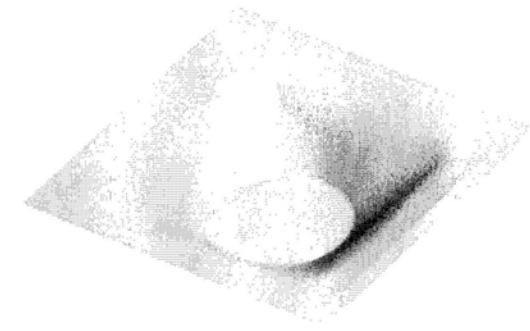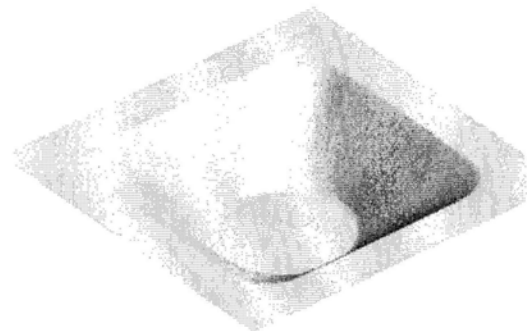
(A3) Predicted surface based on minimum energy method in Case 1   (B3) Predicted surface based on minimum energy method in Case 2
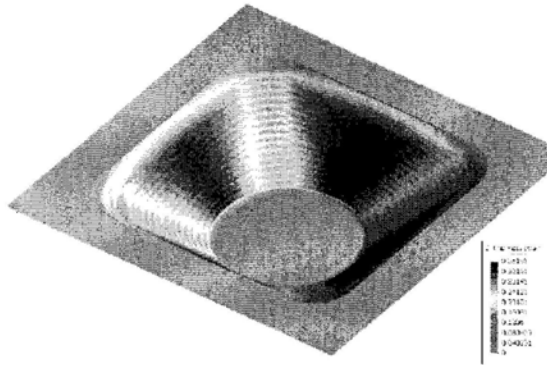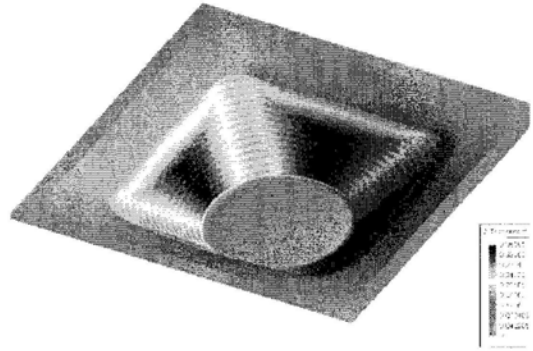
(A4) The thickness strain distribution in Case 1   (B4) The thickness strain distribution in Case 2
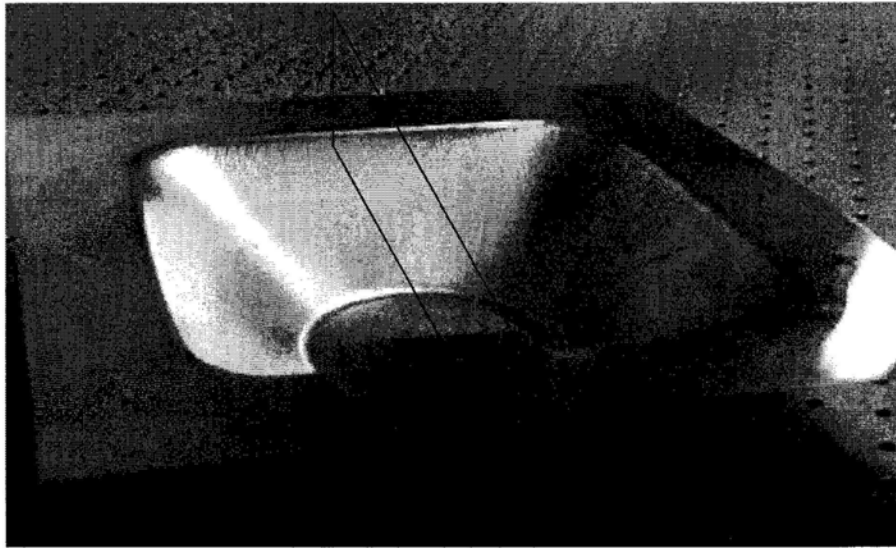
(A5) The experimental result in Case 1
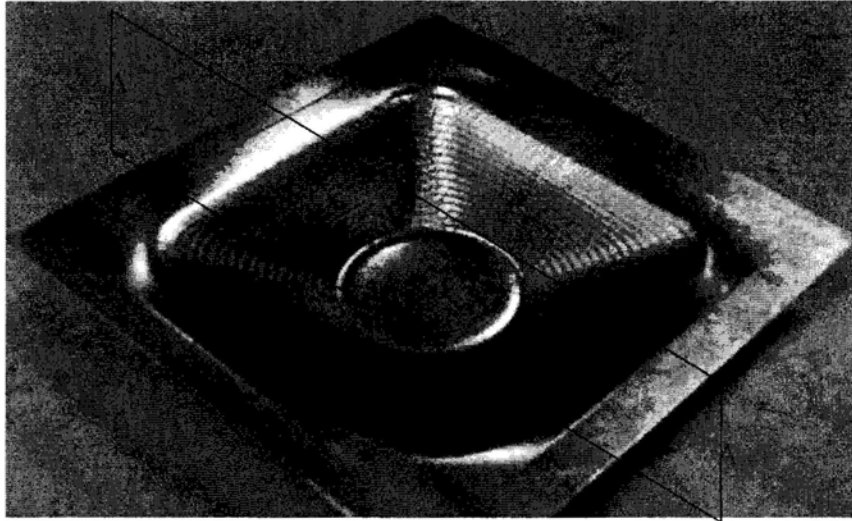
(B5) The experimental result in Case 2

Figure 6.4 Experiment results in Example 1

Figure 6.5 and Figure 6.6 show more detailed studies. A cross section is selected as shown in Figure 6.5, and then measure the geometry using a CMM machine. From Figure 6.5, it is seen that the part quality in Case 1 is better. This is because the uniform step size is not as effective as the variable step size, which can better accommodate the curvatures. In both cases, the experiment results match the simulation results very well. Though comparing to the design, they both have significant errors around the edges. It is noted that the error in Case 2 is much larger because of the offset in holding the sheet metal blank. Also, it is seen that at the bottom of the part, there is a blending causing by the stress of the metal. Figure 6.6 shows the errors along the cross section. From the figure, it is seen that the maximum error occurs at the blank holding edge. In the other regions, the errors are typically about 1 mm.
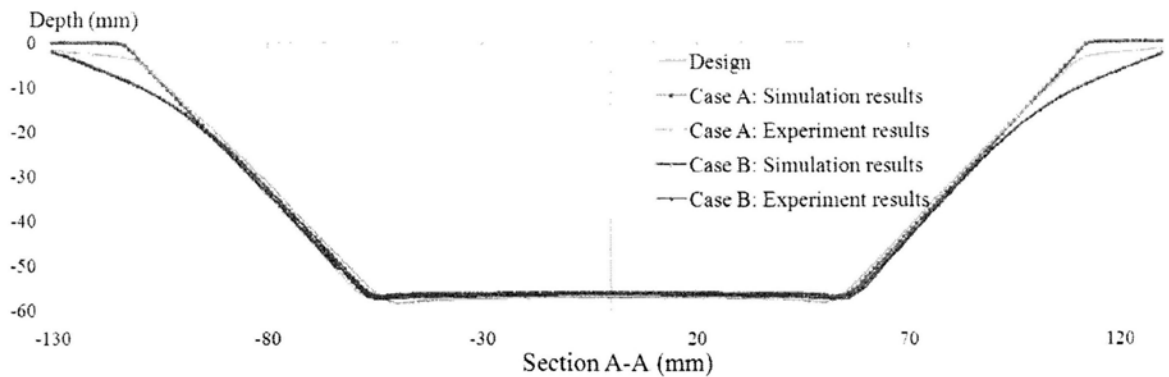
Figure 6.5: The cross section geometric profile of the parts
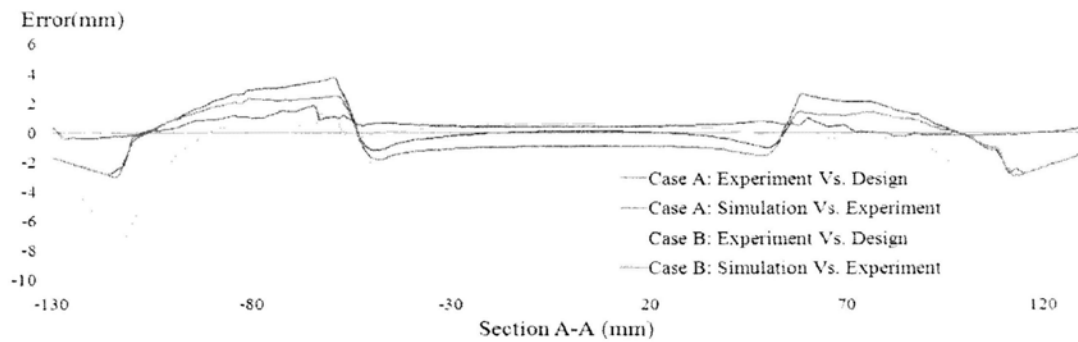
Figure 6.6: The cross section error distributions of the parts

The thickness change of the part is another important issue in stamping, as it may cause quality problems. An EDM machine is utilized to cut part along Section A-A and Figure 6.7(a) shows the photo of the cross section. In Regions A and C, the thickness of the part is reduced, which is necessary to accommodate the bending. In region B, the thickness is further reduced because of large deformation. This result matches the simulation result well. Figure 6.7(b) shows the thickness measurement along the cross section. The thickness of the final part in ISMF process was usually computed by the so-called Sine law [Gao *et al*, 2007]. Figure 6.7(c) compares the simulation result, the experiment result and the Cosine law. It is seen that the Cosine law does not work for ISMF very well. This is perhaps due to the fact that the conventional stamping results in large deformation around the corner while the incremental punches produce more even deformation.
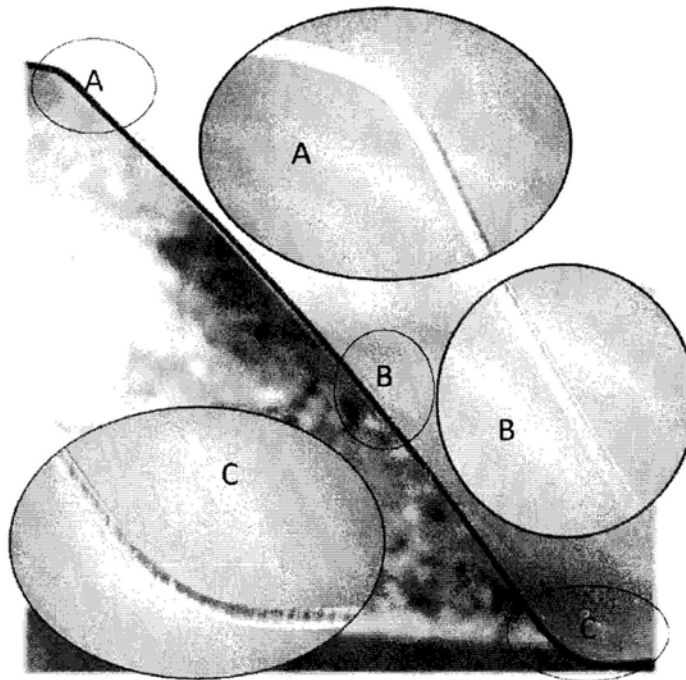
(a) Section view of the sheet metal part

(b) The measured thickness of the part
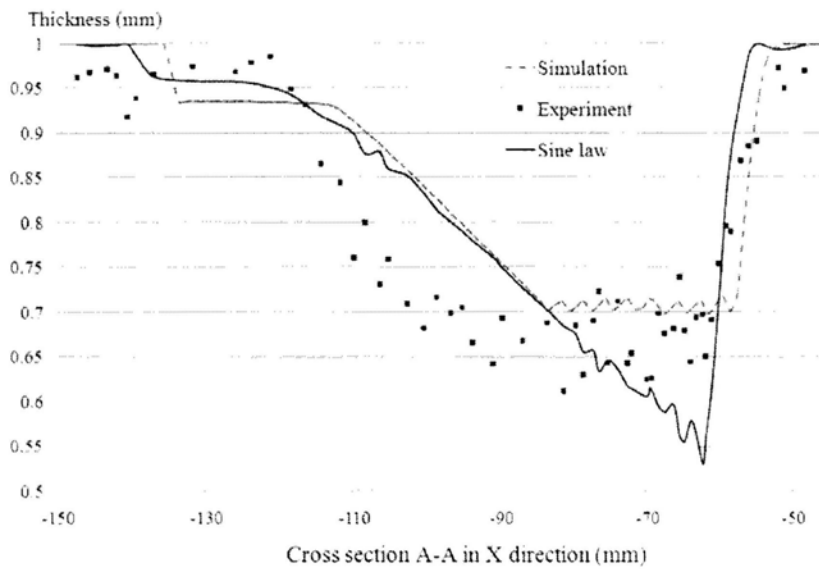
Thickness (mm)

Cross section A-A in x direction (mm)

(c) A comparison of the thickness distribution: simulation, experiment and Cosine law

Figure 6.7: The thickness distribution in Case 1

(a) Section view of the sheet metal part

88

(b) The measured thickness of the part

(c) A comparison of the thickness distribution: simulation, experiment and Cosine law

Figure 6.8: The thickness distribution in Case 2

The setting may affect the thickness too. The cross section A-A in Case 2 is shown in Figure 6.8(a). From the figure, it is seen that in Region A, there is a large deformation, but little thickness reduction. This is due to the fact that the deformation is caused not by the punch, but by the materials trying to retain the minimum energy state. In Regions B

and C, the thickness is significantly reduced due to the punches. In Region D, the thickness of sheet is reduced, which is similar to Case 1. Figure 6.8(b) summarizes the thickness variation. The variation in thickness is also different form the Sine law as shown in Figure 6.8(c).

Additionally, it is interesting to note that the surface finish is a function of the step size. In Case 2, the punch marks are clearly seen while such marks are not seen in Case 1. Considering the fact that the layer thickness is 3 mm in Case 2 while it is 1 mm in Case 1, it is apparent that the smaller the step size, the better the surface finish.

The other important observation is on the variation of the thickness. In both cases, the thickness variation occurs only in the bending area. This justifies the assumption that the x and y positions of the sheet metal blank are invariant during the incremental punching, as stated in Section 2 Chapter 4.

6.3.2 Example 2

The second example is a face mask as shown in Figure 6.9. Its shape is much more complex containing multiple peaks and valleys. Similar to Example 1, two experiments are conducted using different blank holders: Case 1 uses a small blank holder while Case 2 uses a large blank holder. Though, the punch path is the same as shown in Figure 6.10 and hence, the geometric surface is the same as shown in Figure 6.11. The use of different blank holders results in different boundary conditions and hence, different results. Figure 6.12 shows the experiment results of the two cases. From the figure, it is seen that the computer simulation matches the experiment result well. In addition, it is seen that Case 1 will result in a fracture, which is proved experimentally. This is because the deformation of the sheet metal exceeds its forming limit in this region. Therefore, larger blank holder is needed, which unfortunately scarifies the accuracy as shown below.

Figure 6.9: The design of Example 2

Figure 6.10: The punch path of Example 2
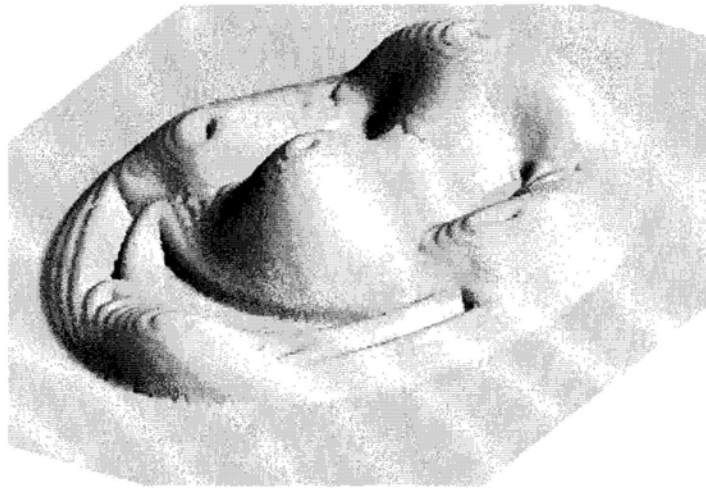
Figure 6.11: The geometric surface of Example 2

(A1) Predicted surface in Case 1	(B1) Predicted surface in Case 2
(A2) The thickness strain distribution in Case 1, the circle indicates a fracture	(B2) The thickness strain distribution in Case 2
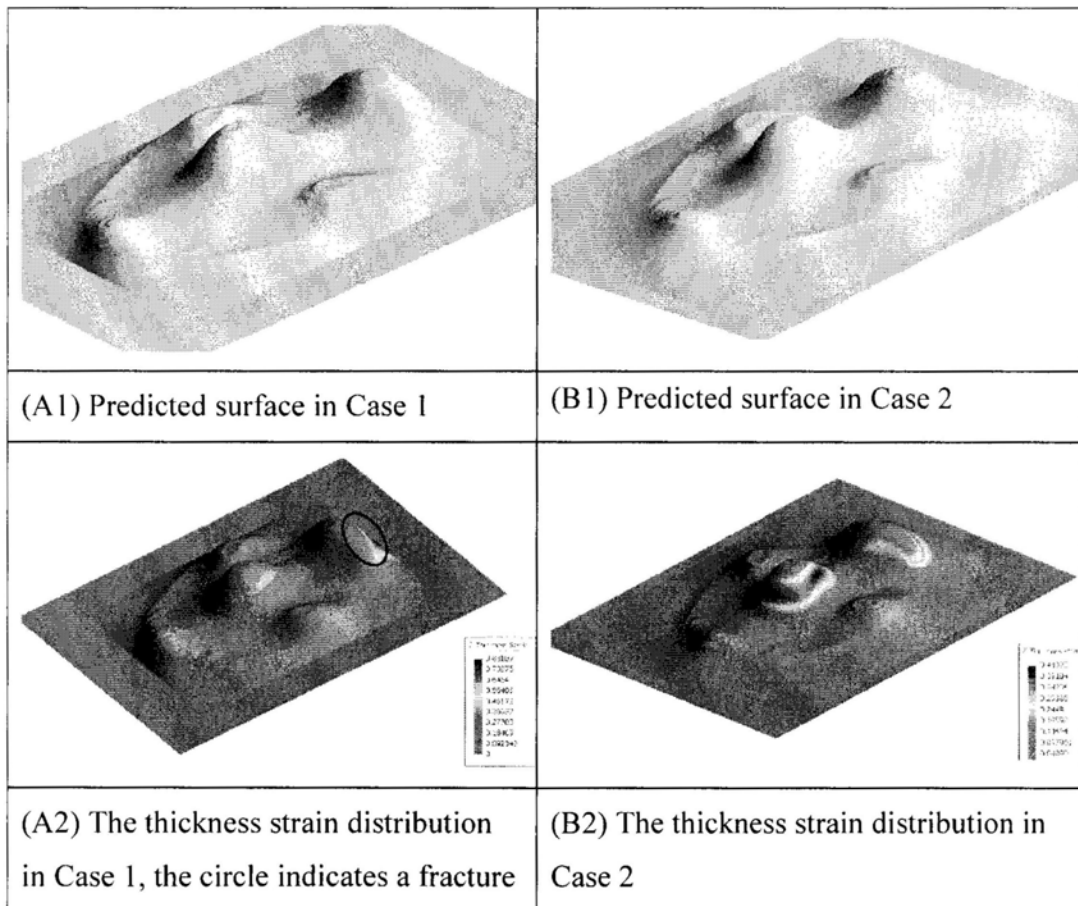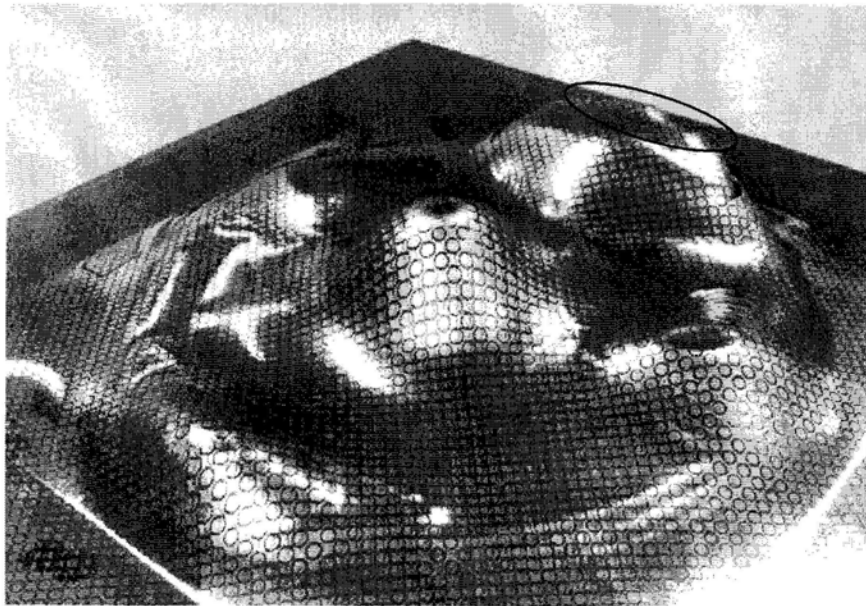
(A3) The experiment result in Case 1
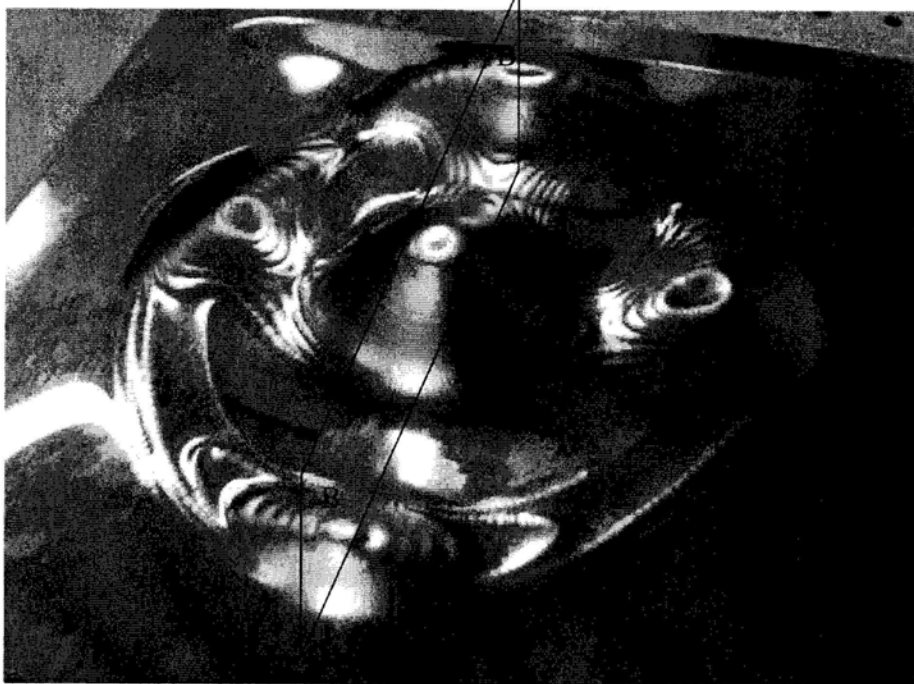
(B3) The experiment result in Case 2

Figure 6.12: The experiment results of Example 2

Figure 6.13 shows a more detailed study on the cross section, B-B, along the center line of the mask (refer to Figure 6.12(B3)). From the figure, it is seen that the computer simulation matches the experiment results well. Though, comparing to the design, they both have a significant error (the maximum error is about 15 mm) around the edges. Figure 6.14 shows the error profiles. It is believed that the error is caused by the loose blank holding. Since the tie blank holding would result in fracture (as in Case 1) and the loose blank holding would result in large error, additional effort is necessary. It is believed that adding a bottom support will solve the problem, which will be a topic of future study.
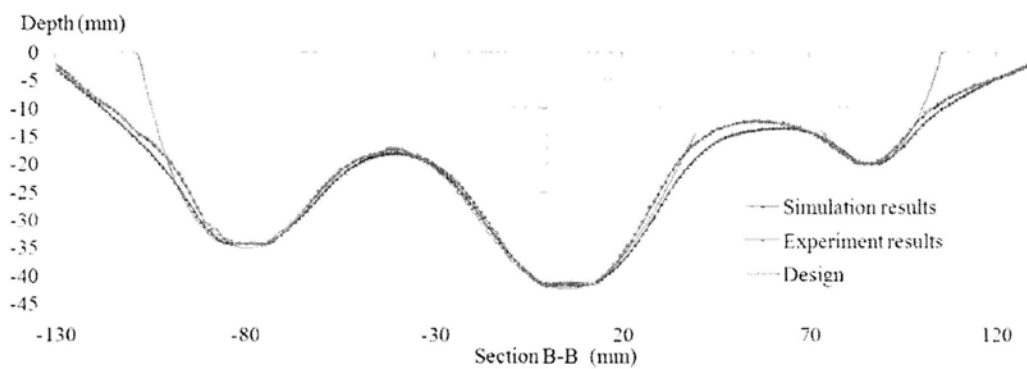
Figure 6.13: A comparison of the cross section profile in Example 2: computer simulation and experimental result (note that the curve in design is a broken line)
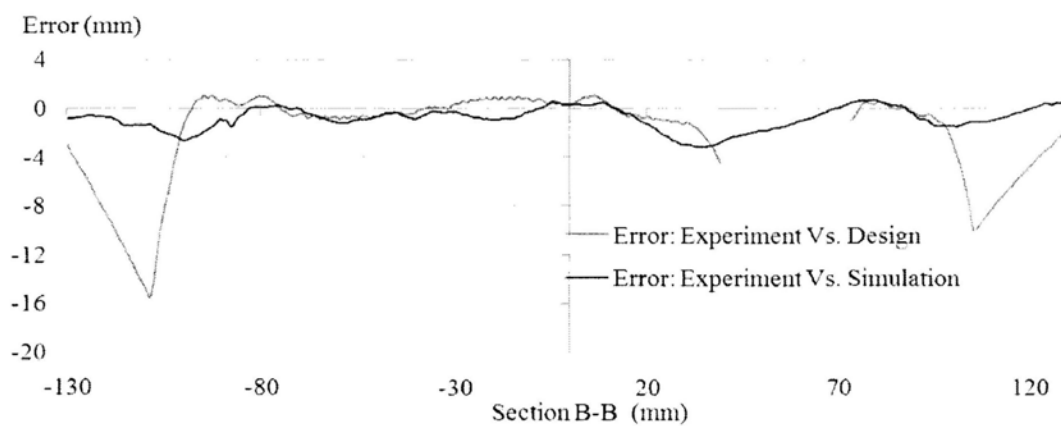
Figure 6.14: Error distributions along the cross section

To further study the behavior of the incremental punch, the part is divided along the cross section B-B using EDM. The section photo is shown in Figure 24(a). In particularly, the four regions A, B, C and D are studied, which have different bending angles. Table 6-1 summarizes the relationship between the bending angle and the thickness variation. From the table, it is seen that large angle usually results in large thickness variation.

Table 6-1: The effect of the geometric angle

Region	Geometric angle	Thickness
A	45°	0.58 mm
B	63°	0.45 mm
C	50°	0.64 mm
D	20°	0.76 mm

Figure 6.15(b) shows the thickness distribution along the section. Figure 6.15(c) shows a comparison among the simulation, the experiment and the Cosine law. It is seen that both the simulation and the Cosine law can predict the thickness, but the errors are significant.
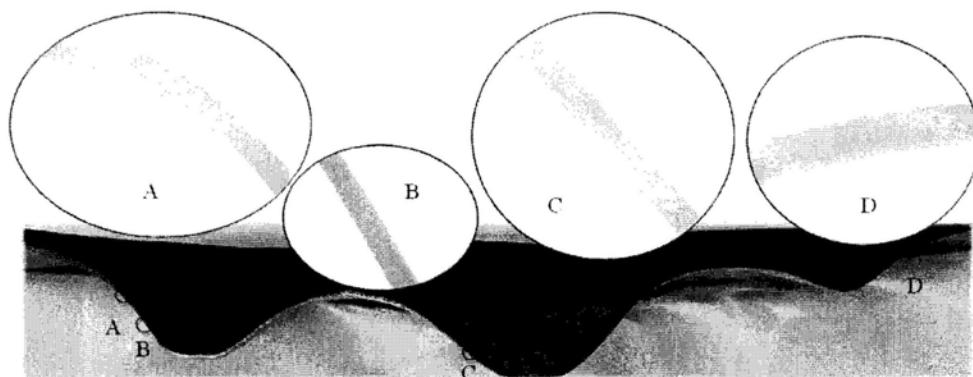
(a) The photo of the cross section B-B
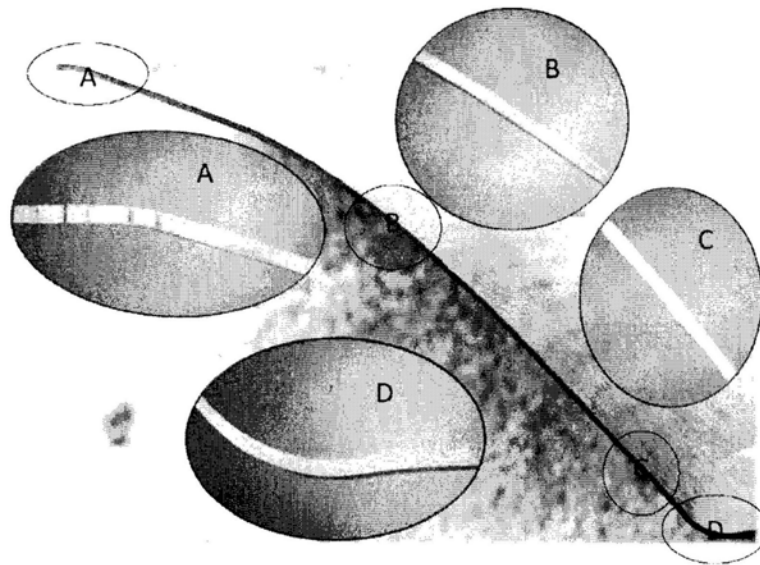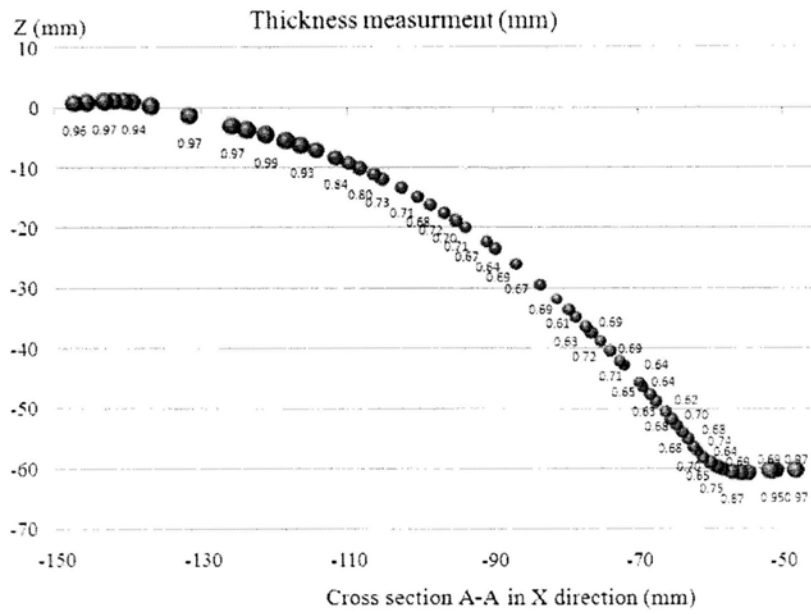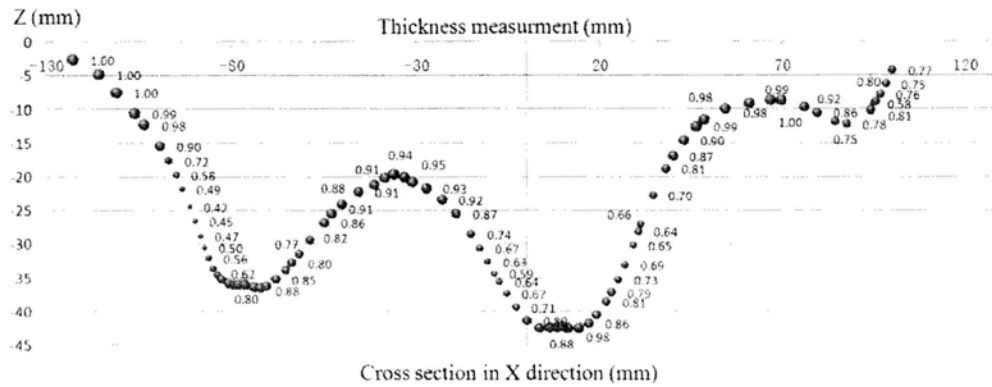
(b) Thickness measurement
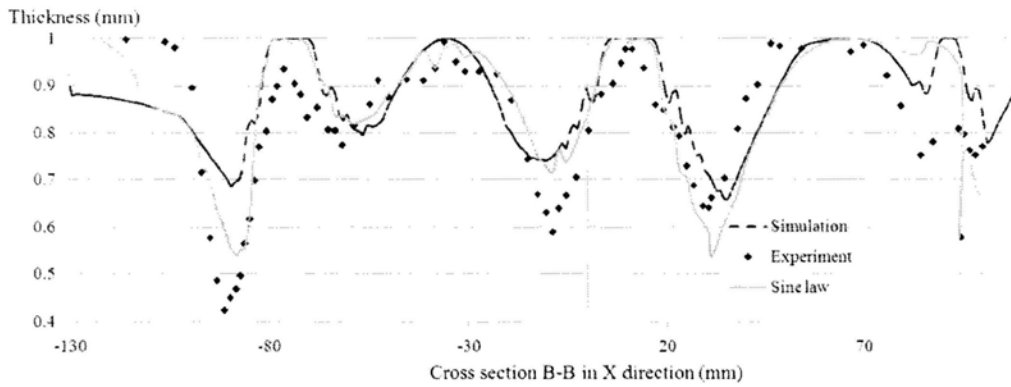
(c) A comparison of the thickness distribution: simulation, experiment and Cosine law

Figure 6.15: Thickness distributions in cross Section B-B

6.4 Discussions

When predicting the strain and stress using the inverse FEM method, the strain in a punch, except the first one, is dependent on the previous punches. Though, the inverse FEM method assumes the strains are independent and hence, will cause an error. Such an error is an inevitable trade off of the computation speed. Form the comparisons of the four cases of the two examples, it can be seen that the magnitude of the errors between the simulations and experiments is about 3mm. This error can be reduced by consideration of the springback.

96

The strains of the two examples are compared by the means of the thickness of the cross section. Note that the thickness is measured by a Mitutoyo® CMM machine. Its accuracy is 0.005mm. Hence, the errors between the simulations and experiments are caused by the punch marks. It can be easily checked in the cross sectional views, for example, Figure 6.8 (a).

6.5 Summary

This chapter presents two examples studied by our fast numerical model and experiments. Based on the results presented above, the following conclusions can be drawn:

- Compared to the existing ISMF systems, it has a number of unique features. First, it is backed by a mechanics model, based on which the formation of the part as well as the strain and stress of the part can be well predicted.

- The prediction error in the final shape is usually well within 2 to 3 mm. The computation can usually be done in several minutes using a PC computer.

- Similar to existing incremental forming methods, the presented incremental punching method is effective in making free form sheet metal parts. Though, it does not need bottom support and hence, is relatively simpler. Also, it can provide increased strength to the part like the shot peening process.

- Though, the presented system may suffer large errors around the edges. The error is largely dependent on the holding of the sheet metal blank. The error can be reduced by adopting small layer thickness and feed step size, which however will result in longer production time.

Chapter 7:

Studies on the Formability of Incremental Punching Process

7.1 Introduction

As we known, the mechanism of incremental punching process is quite different from the conventional stamping. The forming process is a discrete process in which the sheet metal is incrementally deformed along the punch path. The dimples (punch marks) on the final product indicate that the local deformations are obvious and the strains path is more complicated. Hence, its formability has received much attention. Based on literature survey, there are two variants to define the formability: (1) maximum forming angle, and (2) forming limit diagram (FLD).

In order to measure the formability, Iseki [2001] developed a process called incremental sheet metal bulging, which he used to derive an empirical FLD for ISMF. Several other authors also published articles related to the development of similar types of FLDs based on an experimental investigation of the fracture occurring during the forming of various shapes [Silva *et al.*, 2008]. Park *et al.* [Shim and Park, 2001; Kim and Park, 2003] pointed out that the forming limit curve is quite different from that in conventional forming. Several possible explanations of this phenomenon of higher formability can be found:

- It was suggested that this formability was due to the non-monotonic, serrated strain paths to which the material is subjected during the ISMF process [Eyckens *et al.*, 2007].
- The through-thickness shear postpones failure in ISMF processes [Eyckens *et al.*, 2009].
- The triaxiality ratio occurring during SPIF is smaller than that during a classic stamping process [Martins *et al.*, 2008].

- It has been proposed that the bending-under-tension allow large uniform straining [Emmens and van den Boogaard, 2008; Emmens and van den Boogaard, 2009].

Silva *et al.* [2008] formed analytical model into a theoretical framework to investigate the formability limits of SPIF in terms of ductile damage mechanics. The fracture forming limit in SPIF can be approximately expressible in the form $\varepsilon_1 + \varepsilon_2 = q$, where $\varepsilon_t = q$ is the thickness strain at the onset of fracture in plane.
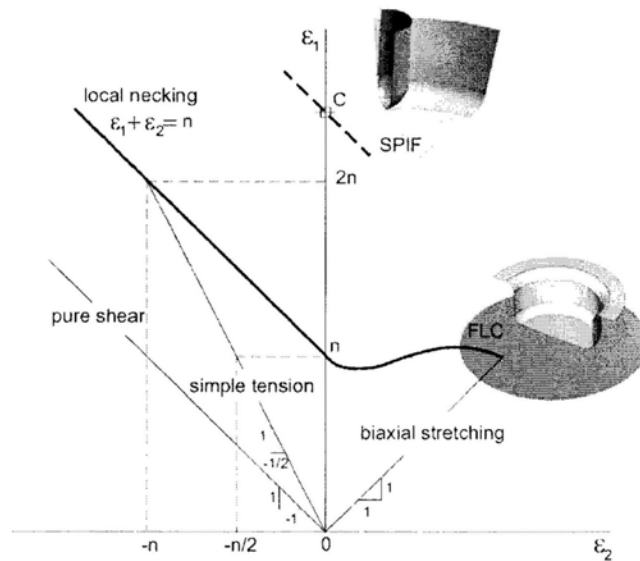
Figure 7.1: FLC of ISMF against to deep drawing processes [Silva *et al.*, 2008]

Also, some authors conducted experiments to investigate the maximum forming angle of the ISMF processes. For example, Gao *et al.* [2007] conducted experiments to evaluate the forming angle of aluminum in the condition described in the article. The maximum forming angle is 66°. It was also reported by Takano *et al.* [2008] that the forming angle of aluminum is 65°~70° in CNC ISMF process.

The objective of this chapter is to study the formability of the forming process in the two above mentioned methods. The FLC is integrated into the proposed numerical simulation program. The rest of the paper is organized as follows. Section 2 presents a

modified M-K analysis to determine FLC and its implementation procedure. Section 3 gives one numerical example as well as the experiment result. Section 4 presents the experimental studies on maximum forming angle of incremental punching. Finally, Section 5 contains conclusions.

7.2 FLD of Incremental Punching

The traditional way of treating possible instabilities in sheet metal forming processes are the comparison of resulting strains in the final stage with a Forming Limit Curve (FLC). In conventional stamping, the FLC usually does not take into account any changes in strain path as it considers only the final stage of deformation. But for some special cases, the strain path is with two or three steps. The effect of the proportional strain and pre-strain on the shape of FLC has been studied by many researches either theoretically or experimentally [Chan and Lee, 1990]. However, the Incremental Punching is rather complicated that the sheet will undergo many of times of deformations before being formed to the final shape. The deformation zone of sheet is small in each punch, and it will change to next position by the movement of the tool along its path. Each point of the sheet is then subjected to elasto-plastic loading and unloading depending on the distance from the tool location. This is quite different from the conventional stamping. Based on the numerical simulation program of incremental punching in our previous research [Luo, He and Du, 2010], the forming limit diagram is therefore needed to predict the potential fracture of workpiece during the forming process.

An example of such a strain path is shown in Figure 7.2. It represents the evolution of the major principal strain and minor principal strain of an element located in the region of the wall of a cone on the top layer of brick elements. This strain path evolution is due to the deformed region in each step is small, progressively increasing the level of plastic deformation.
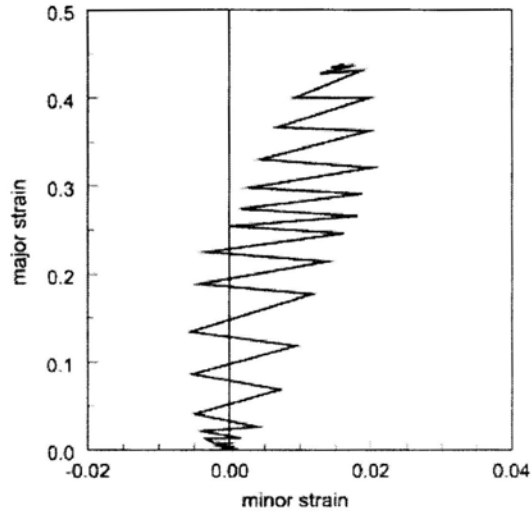
Figure 7.2: Example of cyclic strain history [Eyckens *et al.*, 2007]

7.2.1 Yield Criterion

The yield criterion is usually used in the FEM simulation of sheet metal forming processes. It describes the relationship between the stress components in the region where the sheet metal is undergoing plastic yielding. If the local deformation is pure tension, the yield point is easily expressed by using the tensile stress-strain curve of material. In most of cases, the sheet metal experiences multiaxial stress state. It cannot be easily modeled by the tensile stress-strain curve. The maximum shear stress criterion (Tresca) and strain energy criterion (von-Mises) are usually used as the yield criteria. However, the properties of sheet metal are anisotropic due to the complex production process that is from crystallization to the rolling process. Hill (1948) proposed the relation for the plastic yielding creation for the deformation of planar isotropy sheet metals [Hill, 1948].

$$f = \sigma_x^2 + \sigma_y^2 + r(\sigma_x + \sigma_y)^2 - (1+r)X^2 = 0 \qquad (7\text{-}1)$$

where, r is the Lanford factor, X is the equivalent yield stress.

Follow by the inverse FEM method, the Hill's [1979] criteria is utilized in our model. Hill [1979] non-quadratic normal anisotropic plastic potential is a generalization of the

101

normal anisotropic potential. However, a special case [Zhu *et al.*, 1987] will be considered in the study which is shown in Equation 7-1. The yield function is with normal anisotropic coefficient, *r*, and additional material constant *a*, which is usually larger than 2.

$$f = \left|\sigma_x + \sigma_y\right|^a + 2(1+r)\left|\sigma_x - \sigma_y\right|^a - 2(1+r)X^a = 0 \qquad (7\text{-}2)$$

7.2.2 Modified M-K Analysis

The localized necking and diffuse necking are common failure methods in sheet metal forming. Maricniak and Kuczynski [1967] proposed an analysis method (M-K analysis) to calculate the right side of FLD. Hutchinson and Neale [1978] extended M–K theory using a J2 deformation theory. Therefore, the left and right hand sides of the forming limit diagram can be calculated by M–K analysis. It assumes that the test sheet metal is with a week region A and a strong region B, which is shown in Figure 7.3. However, the traditional M-K method is used for calculate the conventional stamping, in which the strain ration is a constant. In incremental forming process, the sheet metal will experience many times of loading and unloading in forming a typical part. Hence, the strain ratio will not be a constant during the whole process. This has already been shown in Figure 7.2.
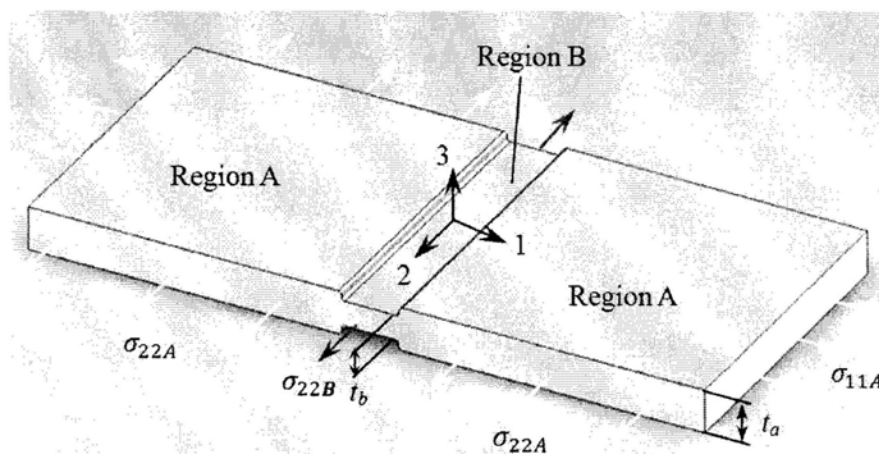
Figure 7.3: Schematic representation of M - K analysis

During the entire process, the groove force balance must be respected. Therefore, the force balance condition requires:

$$F_{1A} = F_{1B} \tag{7-3}$$

where, F_{1A} and F_{1B} stand for the force on one direction inside and outside the groove region respectively. Therefore,

$$\sigma_{11A} t_A = \sigma_{11B} t_B \tag{7-4}$$

Characterizing the initial imperfection by $f = k_B t_{B0} / k_A t_{A0}$ and using $t = t_0 \exp \varepsilon_{33}$, substitute these value into the Equation 7-4. We can obtain

$$\sigma_{11A} = f \exp(\varepsilon_{33B} - \varepsilon_{33A}) \sigma_{11B} \tag{7-5}$$

Defining the slope of principle stress $\xi = \dfrac{\overline{\sigma}}{\sigma_{11}}$, Equation 7-5 can be rewritten as

$$\frac{\overline{\sigma}_A}{\xi_A} = \frac{f \exp(\varepsilon_{33B} - \varepsilon_{33A}) \overline{\sigma}_B}{\xi_B} \tag{7-6}$$

The ratio of the principal stress and strain are defined as

$$\alpha = \frac{\sigma_{22}}{\sigma_{11}} \tag{7-7}$$

$$\rho = \frac{d\varepsilon_{22}}{d\varepsilon_{11}} \tag{7-8}$$

According to the yield function in Equation 7-2, the slope of the principle stress is

$$\xi = \frac{\bar{\sigma}}{\sigma_{11}} = \left[\frac{(\alpha+1)^a + (1+R)(1-\alpha)^a}{2(R+1)} \right]^{1/a} \tag{7-9}$$

Based on the yield criteria in Equation 7-2, the effective stress and plastic work rate yield functions are

$$\bar{\sigma} = \left[\frac{\left|\sigma_{11} + \sigma_{22}\right|^a + (1+R)\left|\sigma_{11} + \sigma_{22}\right|^a}{2(1+R)} \right]^{1/a} \tag{7-10}$$

and

$$\dot{\bar{\varepsilon}} = \frac{[2(1+R)]^{1/a}}{2} \left(\left|\dot{\varepsilon}_{11} + \dot{\varepsilon}_{22}\right|^{a/(a-1)} + \left(\frac{\left|\dot{\varepsilon}_{11} - \dot{\varepsilon}_{22}\right|^a}{(1+2R)} \right)^{1/(a-1)} \right)^{(a-1)/a} \tag{7-11}$$

Assume the deformation is proportional during the deformation step, and then the effective strain is

$$\bar{\varepsilon} = \int \dot{\bar{\varepsilon}} dt \tag{7-12}$$

The relationship between the strain ratio and stress ration are

$$\rho = \frac{(1+\alpha)^{a-1} - (1+2R)(1-\alpha)^{a-1}}{(1+\alpha)^{a-1} + (1+2R)(1-\alpha)^{a-1}} \tag{7-13}$$

and its inverse

$$\alpha = \frac{[(1+2R)(1+\rho)]^{1/(a-1)} - (1-\rho)^{1/(a-1)}}{[(1+2R)(1+\rho)]^{1/(a-1)} + (1-\rho)^{1/(a-1)}} \tag{7-14}$$

The slope of ratio of strain rate and major ration is

104

$$\lambda = \frac{\left[2(1+R)\right]^{1/a}}{2}\left(\left(1+\rho\right)^{a/(a-1)} + \left(\frac{(1-\rho)^{a}}{(1+2R)}\right)^{1/(a-1)}\right)^{(a-1)/a}$$ (7-15)

Assuming the hardening effects of the material are represented as

$$\bar{\sigma} = K\bar{\varepsilon}^{n}\dot{\bar{\varepsilon}}^{m}$$ (7-16)

where K is a material constant $\bar{\sigma}$ and $\bar{\varepsilon}$ are the effective stress and strain. The strain rate sensibility parameter is given by m, while n is the strain coefficient.

Since the cross section areas of region A is normal while it thinner in region B, $\varepsilon_1^A = \varepsilon_1$ and $\varepsilon_1^B > \varepsilon_1$. And the elastic strain will recovered in both of A and B when the punch released from the sheet metal.

$$\varepsilon_{ij}^{e(t)} = \frac{1}{E}(1+v)\sigma_{ij}^{(t)} - v\delta_{ij}\sigma$$ (7-17)

where E is the Young's modulus, v is the Poisson's ratio, 'e' and '(t)' denotes the elastic recovered after the t times punch released. Therefore, the plastic deformation reached by both the nominal and weak areas can be calculated as:

$$\bar{\varepsilon}^{p(t)} = \bar{\varepsilon}^{(t)} - \bar{\varepsilon}^{e(t)}$$ (7-18)

where superscript 'p' denotes the plastic deformation during 't' stage. The strain hardening power law used for next stage is modified as:

$$\bar{\sigma}^{(t+1)} = K\left(\bar{\varepsilon} + \bar{\varepsilon}^{p(t)}\right)^{n}\dot{\bar{\varepsilon}}^{m}$$ (7-19)

where $\dot{\bar{\varepsilon}}$ is defined as Equation 7-11., $\bar{\varepsilon}^{p(t)}$ and $\bar{\varepsilon}$ are the effective plastic strains defined in Equation 7-12 for the prestraining stage and currents stage respectively.

If the prestrain results in a strain state ($\varepsilon_{11}^{p(t)}, \varepsilon_{22}^{p(t)}$), where the index t denotes t time strain, and the current stage results in final strain state ($\varepsilon_{11}^{p(t+1)}, \varepsilon_{22}^{p(t+1)}$), then the principal stresses at the end of current stage are given by [Stoughton, 2000]:

$$\sigma_{11} = \frac{\overline{\sigma}\left(\overline{\varepsilon}\left(\varepsilon_{11}^{p(t)}, \varepsilon_{22}^{p(t)}\right) + \overline{\varepsilon}\left(\varepsilon_{11}^{p(t+1)} - \varepsilon_{11}^{p(t)}, \varepsilon_{22}^{p(t+1)} - \varepsilon_{22}^{p(t)}\right)\right)}{\xi\left(\alpha(\varepsilon_{22}^{p(t+1)} - \varepsilon_{22}^{p(t)})/\left(\varepsilon_{11}^{p(t+1)} - \varepsilon_{11}^{p(t)}\right)\right)} \tag{7-20}$$

and

$$\sigma_{22} = \alpha\left(\frac{\varepsilon_{22}^{p(t+1)} - \varepsilon_{22}^{p(t)}}{\varepsilon_{11}^{p(t+1)} - \varepsilon_{11}^{p(t)}}\right)\sigma_1 \tag{7-21}$$

where $\overline{\sigma}(\overline{\varepsilon})$, $\overline{\varepsilon}(\varepsilon_{11}, \varepsilon_{22})$ and $\xi(\alpha)$ are defined as Equation 7-16, Equation 7-12 and Equation 7-9 respectively, and $\alpha(\rho)$ is the inverse function of Equations 7-13 and 7-14.

$$\frac{1}{\lambda_A} \frac{\overline{\sigma}\left(\overline{\varepsilon}\left(\varepsilon_{11A}^{p(t)}, \varepsilon_{22A}^{p(t)}\right) + \overline{\varepsilon}\left(\varepsilon_{11A}^{p(t+1)} - \varepsilon_{11A}^{p(t)}, \varepsilon_{22A}^{p(t+1)} - \varepsilon_{22A}^{p(t)}\right)\right)}{\xi\left(\alpha(\varepsilon_{22A}^{p(t+1)} - \varepsilon_{22A}^{p(t)})/\left(\varepsilon_{11A}^{p(t+1)} - \varepsilon_{11A}^{p(t)}\right)\right)}$$
$$= \frac{f \exp(\varepsilon_{33B}^{(t+1)} - \varepsilon_{33A}^{t+1})}{\lambda_B} \frac{\overline{\sigma}\left(\overline{\varepsilon}\left(\varepsilon_{11B}^{p(t)}, \varepsilon_{22B}^{p(t)}\right) + \overline{\varepsilon}\left(\varepsilon_{11B}^{p(t+1)} - \varepsilon_{11B}^{p(t)}, \varepsilon_{22B}^{p(t+1)} - \varepsilon_{22B}^{p(t)}\right)\right)}{\xi\left(\alpha(\varepsilon_{22B}^{p(t+1)} - \varepsilon_{22B}^{p(t)})/\left(\varepsilon_{11B}^{p(t+1)} - \varepsilon_{11B}^{p(t)}\right)\right)} \tag{7-22}$$

Hence, with a given stain path in region A, the stresses in strong region A can be calculated. Also, the stresses (σ_{11A}^{t+1}, σ_{11B}^{t+1}) can be obtained by using the balance equation. Using the compatibility requirement $d\varepsilon_{22A}^{t+1} = d\varepsilon_{22B}^{t+1}$, we can get $\varepsilon_{22B}^{t+1} = \varepsilon_{22A}^{t+1}$. The major strain in region B can be obtained by [Stoughton, 2000]:

$$\varepsilon_{11B}^{t+1} = \varepsilon_{11B}^{t} + \frac{\overline{\varepsilon}\left(\overline{\sigma}\left(\sigma_{11B}^{t+1}, \sigma_{22B}^{t+1}\right)\right) - \overline{\varepsilon}\left(\varepsilon_{11B}^{t}, \varepsilon_{22B}^{t}\right)}{\lambda\left(\rho\left(\sigma_{11B}^{t+1}/\sigma_{22B}^{t+1}\right)\right)} \tag{7-23}$$

Though, it's too complicated to compute the FLC using analytical method. It can be solved in numerical method by using Equations 7-22 and 7-23. The computing procedure can be summarized in Figure 7.4.
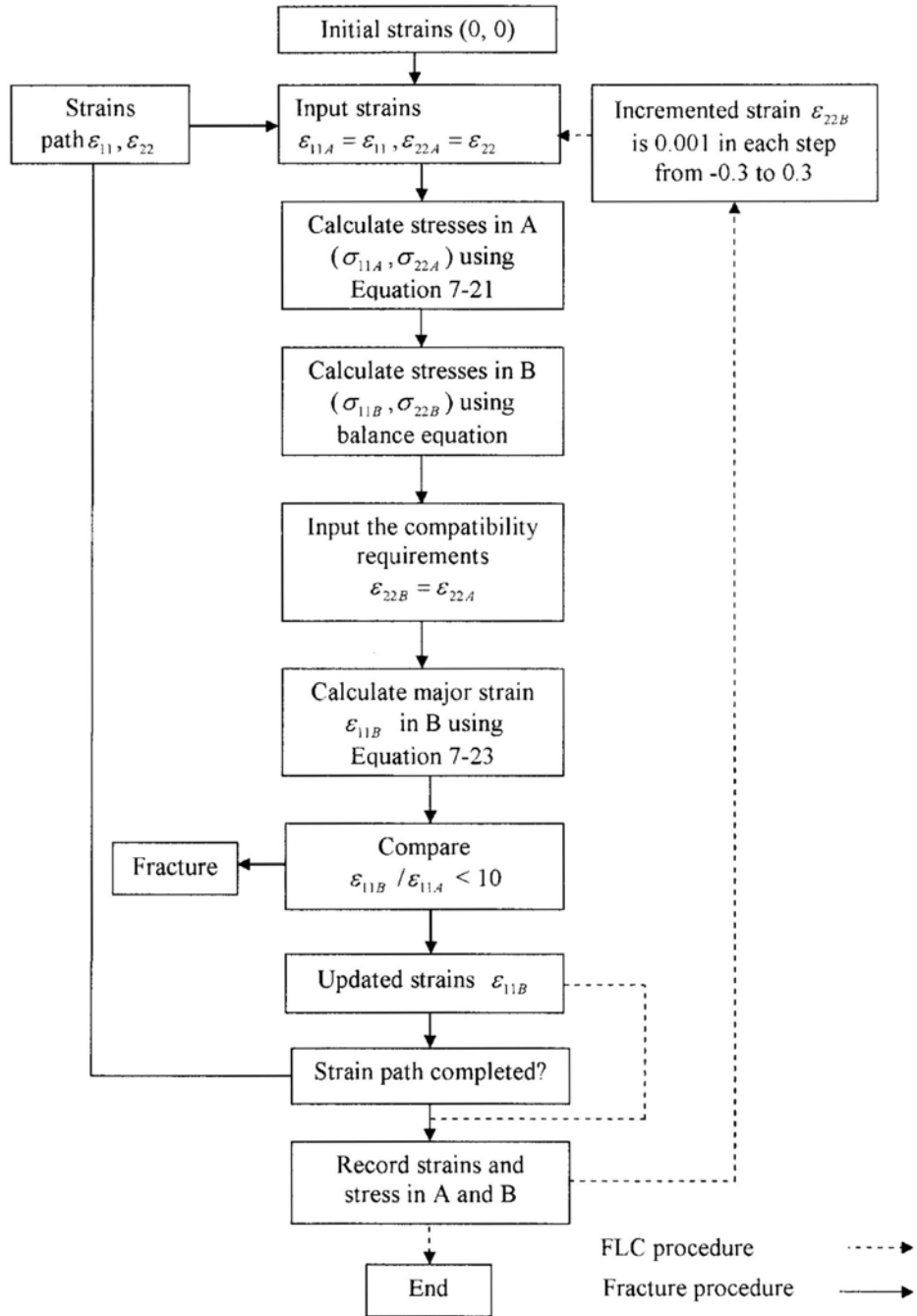
Figure 7.4: The computing procedure of FLC

First, defining strains in the first step is (0, 0). Next step is to estimate the final status using the computing procedure of fracture. If it is success to finish the strain path, then it will go to the FLC procedure with the stresses and strains in final step. It should for

given increase the value of the minor strain form -0.3 to 0.3. Also, in each loop, the incremented strain ($\Delta\varepsilon_{11a}$) out side of the groove is 0.001 in each step. The presented algorithm was implemented in Matlab®.

Figure 7.5 show a given strain path (solid line), and with the assumption of f=0.999, the strain in region B can be obtained (dot line). If the strain path only goes to the point (0.4, -0.02), the FLC can be obtained as shown in Figure 7.6.
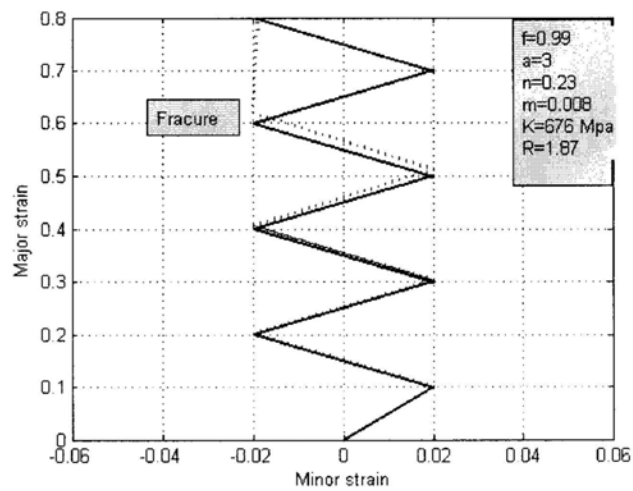
Figure 7.5: A typical strain path in incremental punching and its fracture
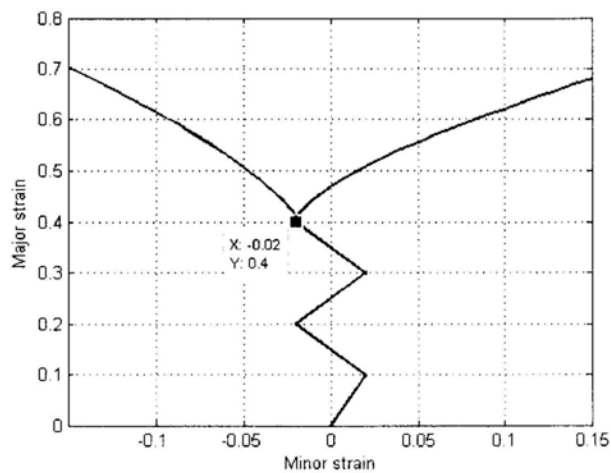
Figure 7.6: FLC with complex pre-strain path

7.3 Ductile Fracture Analyses

According to previous research [Kim and park, 2002; Siva $et\ al$, 2008; Eyckens $et\ al.$, 2009], the forming limits of ISMF is possible to conclude that plastic deformation takes place by uniform thinning (without necking) until fracture. The fracture forming limit in ISMF causes by ductile damage mechanics based on void growth models [Siva $et\ al$, 2009]. The fracture forming limit can be approximately expressible in the form $\varepsilon_1 + \varepsilon_2 = -q$, where $\varepsilon_t = -q$ is the thickness strain at the onset of fracture in plane. Based on Tresca yield criterion, the slope is defined as:

$$q = -\frac{5(r_{tool}/t)+2}{3(r_{tool}/t)+6} \tag{7-24}$$

A special point $(\varepsilon_{11}, \varepsilon_{22})$ on the fracture limit can be obtained by using biaxial stretching and the incompressibility condition.

7.4 A Case Study

Since Case A of Example 2 is cracked, it can be used to study the forming limit. SPCC steel sheet was used in this work. Its mechanical properties are summarized in Table 7-1. The power-law material model, as shown in Equation 7-16, is introduced to describe the stress-strain relationship.

Table 7-1: Mechanical properties of SPCC

σ_y (MPa)	K (MPa)	n	m	Poisson ratio v	Lankford value r
206	576	0.23	0.008	0.3	1.87

The thickness of initial sheet metal is 1mm and its size is 310mm×310 mm. The forming tool is with the hemispherical end of 15mm diameter punched on the sheet metal at a speed of 300rpm. In this experiment, a facial mask is designed. The tool path is generated based on the design of part in MasterCAM® using contour method. The feed step changes from 1mm to 3 mm based on the curvature of current contour. However,

the layer thickness is uniformed with 1 mm. The punch locations map is shown in Figure 7.7 and the blank holder is with the inner size of 220×220 mm.

Figure 7.7: The punch locations map

7.4.1 Simulation results

A mechanics model that combined the minimum energy principle and inverse FEM is developed to predict the final shape of the part, as well as the strain and stress distributions of the part. The predictions of the final shape are accurate and effectively. In this experiment, the mechanics model and its program are used to simulate the forming process. The thickness strain distribution of the experiment is predicted as shown in Figure 7.8. Its maximum thickness strain is 0.82. The risk of crack is predicted in Figure 7.9.
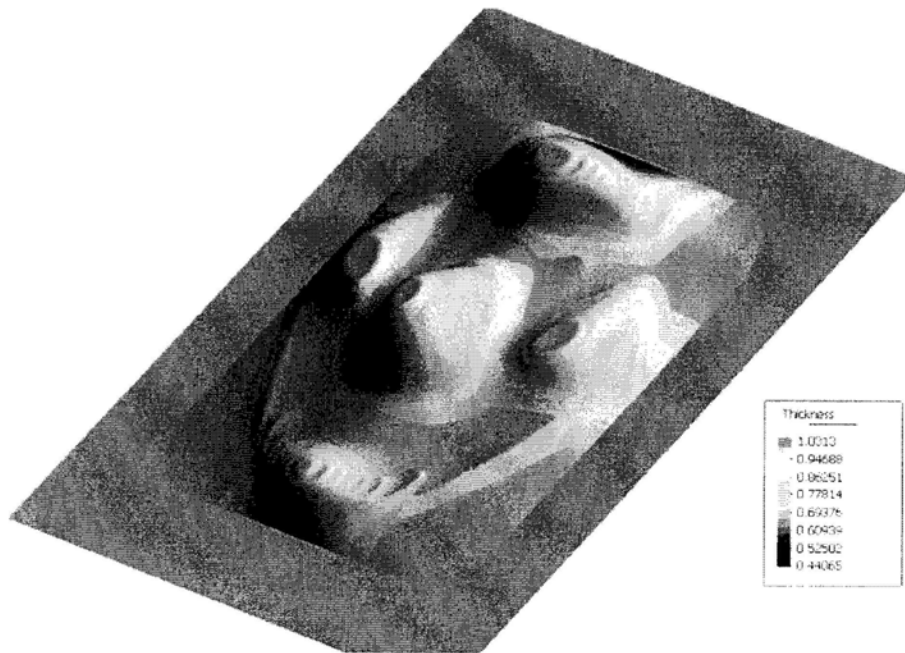
Figure 7.8: Predicted thickness distribution
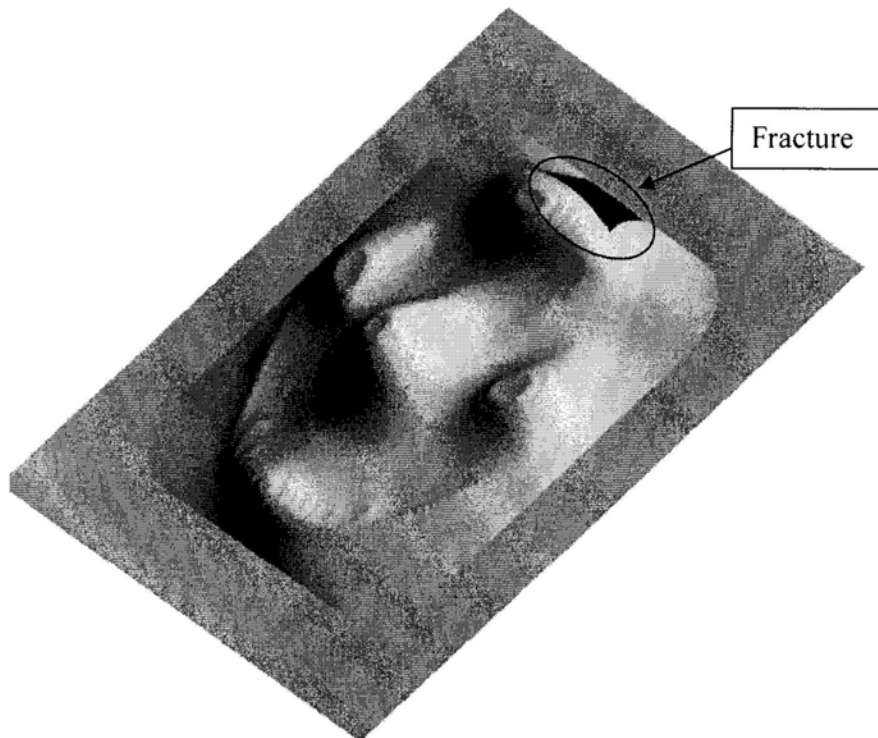
Figure 7.9: Predicted risk of forming part

7.4.2 Experiment Result

In order to evaluate the formability of the SPCC sheet in Incremental Punching, two tests were carried to investigate the strains on the sheet metal. The former test is with a small blank holder that cracks will probably happen. For measurement of the strain distributions on the deformed sheet metal, circular grids are marked on sheet before being clamped on the blank holder. To effectively measure the local deformations, the diameter of the circle is 3 mm. The circular grids were deformed as ellipsoids in the region where the sheet metal deformed in the forming process. The strains are measured from the formed part to evaluate the Forming Limit Diagram (FLD). In sheet metal forming, the sheet can be described as shell element, and logarithmic strains are used. Hence, the major strains ε_1 and minor strains ε_2 are:

$$\varepsilon_1 = \ln\frac{l_1}{l_0} \text{ and } \varepsilon_2 = \frac{l_2}{l_0} \tag{7-25}$$

where, l_1 is the major axis of the ellipse, l_2 is the minor axis of the ellipse, and l_0 is the diameter of the initial circle.
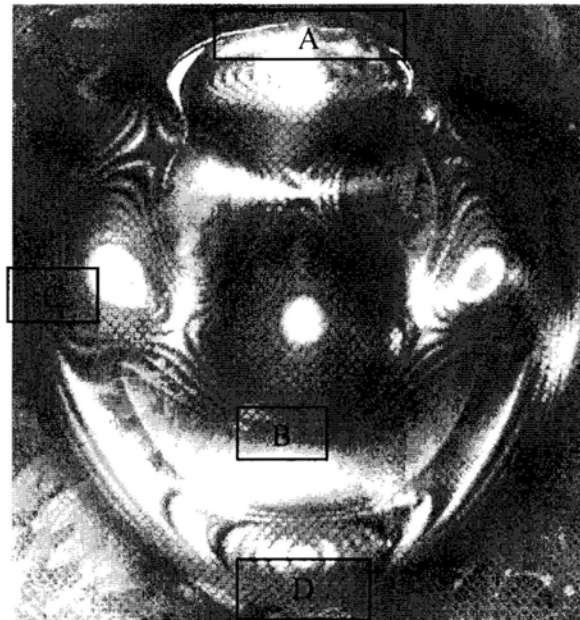
Figure 7.10: The Experiment results

Figure 7.10 shows the experiment part, and four interested regions are selected for further analysis. In region A, the angel of the wall is 80°, and hence, the sheet metal cracked. No crack happened in others region. The strains distributions in the four interested regions were measured and summarized in Table 7-2. Form Table 7-2, it can be seen that the effective strains are extremely large in region B and they are basically reasonable in the other regions.

Table 7-2: The measured strain distributions

#	ε_1	ε_2	Thickness	#	ε_1	ε_2	Thickness
1	0.73	0.087	0.44	9	0.068	0.02	0.92
2	0.78	0.003	0.46	10	0.05	0.006	0.93
3	0.81	0.017	0.44	11	0.25	0.049	0.74
4	0.63	-0.05	0.56	12	0.22	0	0.81
5	0.46	-0.03	0.65	13	0.48	0.03	0.60
6	0.44	-0.05	0.68	14	0.48	-0.01	0.62
7	0.46	0.02	0.62	15	0.39	0.02	0.67
8	0.46	0.03	0.61	16	0.36	0	0. 70

The FLC presented in Figure 7.6 is used. Then the data from the experiments and simulations, the Forming Limit Diagram (FLD) is shown in Figure 7.11. It can be seen that the strains of points 1-3 exceed the forming limit of the material. Ductile fracture analysis is more closed to the experiment results.
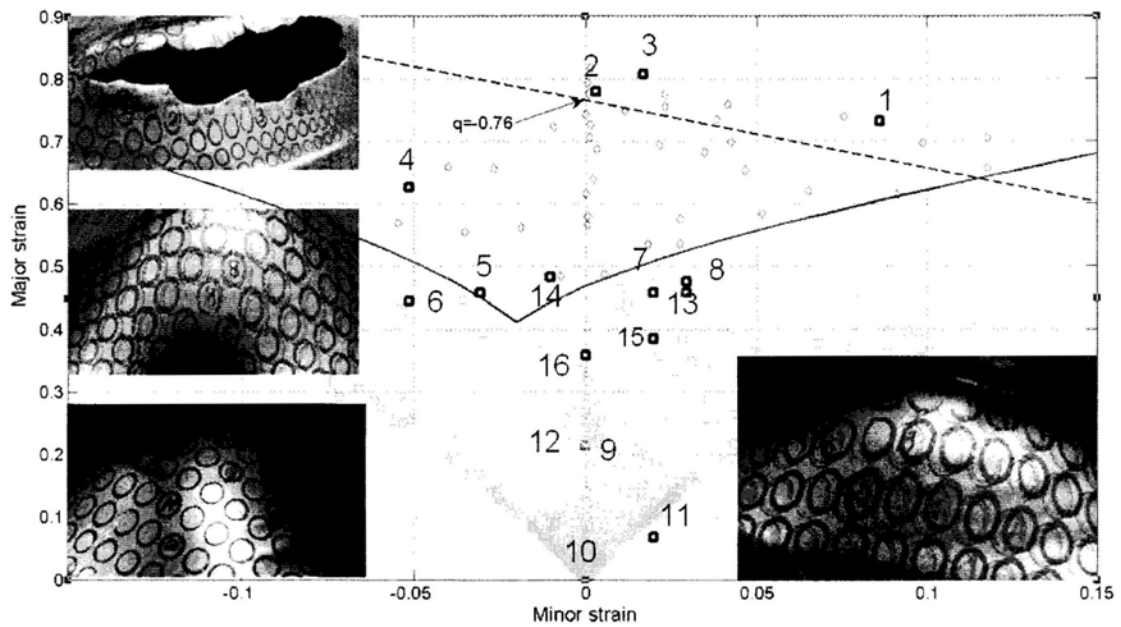
Figure 7.11: Comparison of simulation and experiment results in FLD

7.5 Experimental Study on the Maximum Forming Angle

In sheet metal forming, the formability is an important concern. The formability is expressed as the maximum forming angle, θ_{max}, that a sheet would endure without fracturing. Gao *et al.* [2007] designed a new method to evaluate the forming angle. Jeswiet *et al.* [2005] summarized the maximum forming angle in CNC ISMF and Robot ISMF. According to literatures, the maximum forming angle of an 1 mm mild steel sheet of DC04 is about 65°. The material used in this study is SPCC which has similar mechanical properties as that of DC04.

In the test, the vertical feed rate (the layer thickness) is set at 1 mm, the horizontal feed rate is set 1 mm and the punch diameter is 10 mm. The blank thickness is 1 mm and the size is 150.0 × 150.0 mm. The size of the fixture is 80.0 × 80.0 mm. The experiment setup is shown in Figure 11. The experiment results are summarized in Figure 12. The testing result is rather similar to that of in [Jeswiet, 2005].
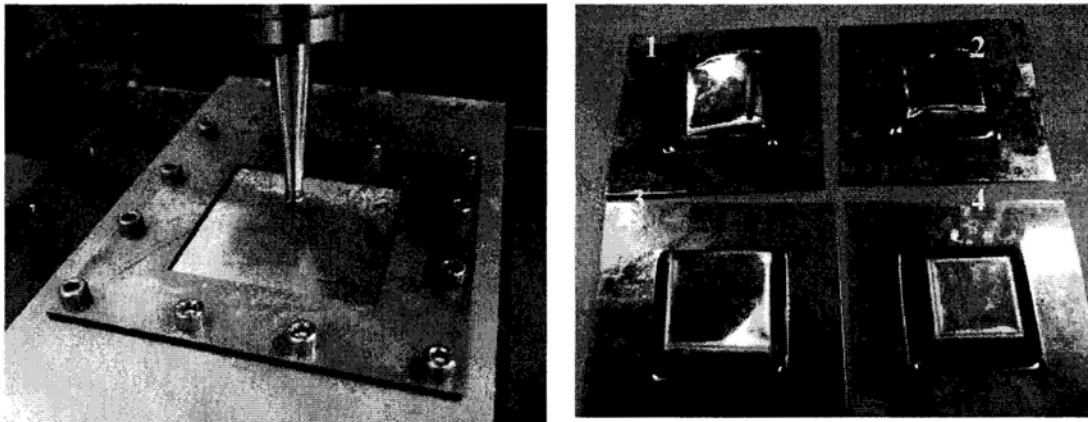
(a) Configuration of the test

(b) Testing part with different forming
angle: $1 - 80°$; $2 - 75°$, $3 - 68°$, $4 - 63°$

Figure 7.12: The experiments for testing the formability of SPCC
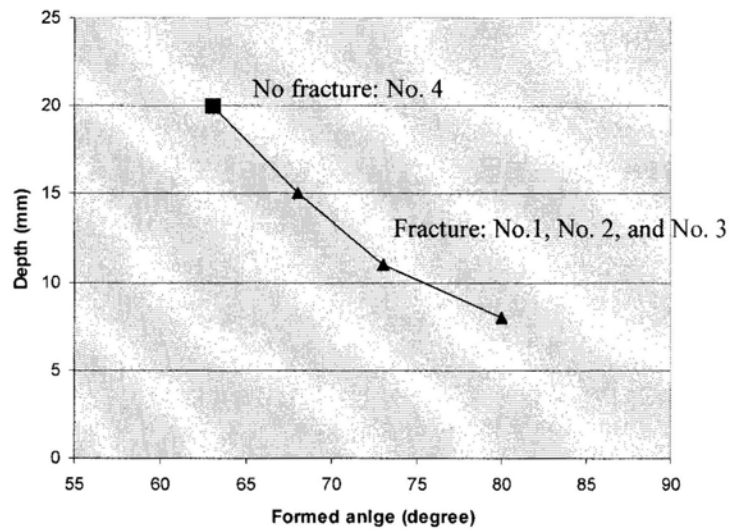
Figure 7.13: The maximum forming angle test results

The final thickness of the sheet metal can be computed by the forming angle using the Sine law:

$$t = t_0 \sin(\frac{\pi}{2} - \theta) \qquad (7\text{-}26)$$

where, t_0 is the initial thickness of the blank, θ is the forming angle.
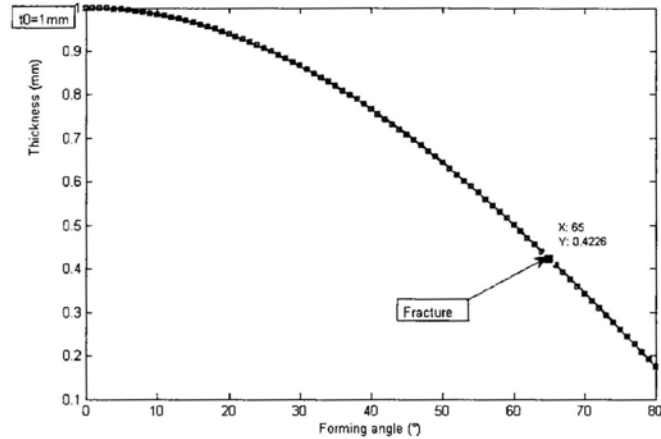
Figure 7.14: The predicted thickness using Sine law

7.6 Summary

This chapter presents a modified M-K method to determine the FLC for incremental punching in which the material will experience a complex strain path. Also the maximum forming angle is experimentally studied. Based on the results presented above, following conclusions can be drawn:

- Similar to the CNC ISMF process, the failure of this process is largely depended on the ductile limit.

- The forming limit of multi-steps strain path is higher than that of conventional stamping. That means the forming process will have higher formability than conventional sheet forming.

- The maximum forming angle of this process can reach the same value as existing incremental forming method.

- The forming parameters, feeding speed, layer thickness, punch velocity *e.g.*, should be related to the failure of the process, and future work will investigate the effects of these parameters.

- Note that Hill's 1979 criteria is used in this study. Therefore, the modified M-K model is with the limitation of isotropic yield criteria which can not well predict the formability of sheet with a high plastic. It should be considered with the utilization of anisotropy model in the future research.

116

Chapter 8:

Concluding Remarks and Future Work

8.1 Concluding Remarks

This thesis is devoted to a new Incremental Sheet Metal Forming (ISMF) system based on incremental punching. Although the basic concept of incremental forming was proposed almost 40 years ago by Leszak [1967], it became one of the leading R&D topics in the sheet metal forming industry and was put into practice only recently. This is probably because of the development of the Numerically Controlled (NC) technology and the increasing need of the low volume production. The thesis presents a new ISMF system. Moreover, a mechanics model is developed for simulating the forming process. The integration of the new ISMF system and the mechanics model provides an effective solution for low volume production and prototypes.

The research presented in this thesis is partially supported by a grant from the Research Grants Council of Hong Kong (No. 411808), entitled "A New Technology for Die-less Sheet Metal Stamping." The main contributions of this research can be summarized as follows:

- **A new ISMF method based on incremental punching:** The new method uses a generic tool punching the sheet metal along the path controlled by the CNC machine. The method is backed by a FEM software system. The software system helps to choose forming process parameters, such as punch diameter, feed step, layer thickness, and *etc*. The new system is effective in making free form sheet metal parts like existing ISMF methods. It has several features: First, it punches the sheet metal in discrete manner and hence, is not be affected by friction and does not need lubrication and cooling. Second, it does not need bottom support and hence, is relatively simpler. Third, the punch applies local deformations on workpiece and the

compression in thickness direction provides increased strength to the part like the shot peening process.

- **Deign and build a new IMSF machine:** Most studies on ISMF forming use either a milling machine with a rotating tool or an industrial robot with a hammer. Our new machine is designed and built based on a 3-axis CNC milling machine framework and a high speed hydraulic punch. A PC based control system is used to control the motion during the forming process. In order to ensure the accuracy of the machine, the dynamic models are built for 3-axis milling machine framework respectively. The simulation results indicate that maximum loading of the machine is below 10000 N. Such stiffness is much better than that of the robot based ISMF system. The machine is inexpensive to build as all its major components, including the 3-axis CNC milling machine framework, the high speed hydraulic punch head, and the PC based controller, are all standard parts. Also, the machine is easy to use as it uses standard NC code.

- **Modeling of the incremental punching process:** Using commercial FEM software system will take very long time to model the incremental forming process. In this thesis, a new mechanics model is developed based on minimum energy principle and inverse FEM method. The computer software system is written using Matlab®. It provides a quick and accurate prediction of the geometric shape well as the strain and stress distribution of the part. The prediction error in the geometric shape is usually well within 2 mm. The computation is usually done in several minutes using a PC computer. The computer software also helps to optimize the forming process parameters.

- **Study the quality of the ISMF formed parts:** The effects on the quality of the final part are studied by the means of experiments and simulations. The results indicate that the error is largely dependent on the blank holder and the punch path. Better results can be achieved by improving the design of fixture and adopting small layer thickness and feed step size, which however will result in longer production time.

- **Formability of the new ISMF process:** The mechanics of incremental forming process is rather different form the conventional stamping, in which the sheet metal experiences a large number of small step deformations. This allows the incremental forming process to achieve higher formability than that of conventional forming method. A modified M-K methods is developed for computing the Forming Limit diagram (FLD). The FLD is integrated to our computer software system to predict the risk of failure. The maximum forming angle is also investigated. These studies pave the road for practical applications.

8.2 Future Work

It believed that the new ISMF system will find many practical applications in the near future. Though, it should be pointed out that the new system is still in its infancy and further research and development are needed. The future research includes:

- **Experiment study on the forming process:** More experimental studies should be conducted. In the thesis, two parts are studied extensively. It is believed that they are representative. Also, it is believed that the computer simulation model is accurate. However, more experiments are useful, especially for studying the effect of blank holding. In addition, a comparative study in the cases with and without bottom support should be conducted to find out how does the bottom support effect the accuracy. Finally, the surface finish of the parts is an important concern for practical applications. The optimized parameters for achieving good surface finish can be obtained by means of experimental studies.

- **Improve the design of the incremental punching system:** It is desirable to design and build a new machine that uses mechanical punch system instead of the hydraulic system to improve efficiency. Currently, our machine runs at the speed of 300 Shot Per Minute (SPM) limited by the performance of the hydraulic system. If the punch system uses a servo motor, it is expected to reach the high speed of 3000 SPM. This

will greatly improve the productivity of the machine. In this case, though, the dynamic performance of the new system should be carefully calculated. Moreover, to improve the accuracy of the part, a moving bottom support system should be designed and built. In this case, the control system needs to be improved to achieve 4-axis synchronous motion.

- **Improve the mechanics model:** Currently, the mechanics model does not consider the springback. As a result, the regions that undergo large bending cannot be well predicted (e.g., the region near the blank holder). Moreover, the effect of the bottom support can be modeled. It is desirable to consider these factors in the future research.

- **Study effects on the formability:** Currently, the fracture mechanics in the ISMF process is still not clear. More experimental and theoretical studies on this aspect are needed. The formability is a function of material properties, forming parameters and geometric shape of the part. A formability model will facilitate the use of the new ISMF system.

Bibliography

[1]   Abbott, D., "Laser forming of titanium alloys", *Materials World,* Vol. 7, No. 6, pp. 328-30, 1999.

[2]   Aggarwal, M.L., Agrawal, V.P. and Khan, R.A., "A stress approach model for predictions of fatigue life by shot peening of EN45A spring steel", *International Journal of Fatigue*, Vol. 28, Issue 12, pp 1845-1853, 2006.

[3]   Allwood, J., Houghton, N. E., and Jackson, K. P., "The design of an incremental sheet forming machine", *Advanced Materials Research*, Vol. (6 - 8), pp. 471- 478, 2005.

[4]   Allwood, J. M. and Utsunomiya, H., "A survey of flexible forming processes in Japan", *International Journal of Machine Tools and Manufacture*, Vol.46, Issue 15, pp1939-1960, 2006.

[5]   Allwood, J.M., Shouler, D.R. and Tekkaya, A.E., "The increased forming limits of incremental sheet forming processes", *SheMet 2007 International Conference on Sheet Metal*, Palermo, Italy, pp. 621–628, 2007.

[6]   Allwood, J., Music, O., Raithathna, A and Duncan S. R., "Closed-loop feedback control of product properties in flexible metal forming processes with mobile tools", *CIRP Annals - Manufacturing Technology*, Vol. 58, Issue 1, pp287-290, 2009.

[7]   Ambrogio, G., De Napoli, L., Filice, L., Gagliardi, F. and Muzzupappa, M., "Application of Incremental Forming process for high customised medical product manufacturing", *Journal of Materials Processing Technology*, Vol.162-163, pp156-162, 2005.

[8]   Ambrogio, G., Cozza, V., Filice, L. and Micari, F., "An analytical model for improving precision in single point incremental forming", *Journal of Materials Processing Technology,* Vol.191, Issues 1-3, pp92-95, 2007.

[9]   Amino, H., Lu, Y., Ozawa, S., Fukuda, K. and Maki, T., "Dieless NC forming, prototype of automotive service parts", *Proceedings of the second international conference on rapid prototyping & manufacturing*, Beijing, pp 179-185, 2002.

[10] Araghi, B. T., Manco, G. L., Bambach, M., Hirt, G., "Investigation into a new hybrid forming process: Incremental sheet forming combined with stretch forming", *CIRP Annals – Manufacturing Technology,* Vol. 58, Issue 1, pp225-228, 2009.

[11] Arai, H., "Robotic metal spinning -Forming asymmetric products using force control", *Proceedings of 2005 IEEE International Conference on Robotics and Automation* , Barcelona, Spain, pp. 2702–2707, 2005.

[12] Arnet, H. and Vollertsen, F., "Extending laser bending for the generation of convex shapes", *Journal of Engineering Manufacturing,* Vol. 209, pp. 433–442, 1995.

[13] Batoz, J.L., Guo, Y.Q. and Mercier, F., "The inverse approach with simple triangular shell elements for large strain prediction of sheet metal forming parts", *Journal of Engineering Computation,* Vol.15, No.7, pp864-92, 1998.

[14] Becker, A.A., *An introduction to finite element method,* Professional Engineering Publishing, London and Bury Edmuds, UK, 2004.

[15] Cai, Z. Y., Wang, S. H., Xu, X. D. and Li, M. Z., "Numerical simulation for the multi-point stretch forming process of sheet metal", *Journal of Materials Processing Technology,* Vol. 209, Issue 1, pp396-407, 2009.

[16] Callegari, M., Amodio, D. Ceretti, E., and Giardini, C., "Sheet incremental forming: Advantages of robotised cells vs. CNC machines," *Industrial Robotics: Programming, Simulation and Applications,* ARS, Vienna, pp. 493–514, 2007.

[17] Callegari, M.,Gabrielli, A., Palpacelli, M. C. and Principi, M, "Incremental forming of sheet metal by means of parallel kinematics machines", *Journal of Manufacturing Science and Engineering,* Vol.130, Issue 5, 054501, 2008.

[18] Ceretti, E., Giardini, C. and Attanasio, A., "Experimental and simulative results in sheet incremental forming on CNC machines", *Journal of Materials Processing Technology,* Vol. 152, Issue 2, pp176-184, 2004.

[19] Cerro, I., Maidagan, E., Arana, J., Rivero, A. and Rodríguez, P.P., "Theoretical and experimental analysis of the dieless incremental sheet forming process", *Journal of Materials Processing Technology,* Vol.177, No.1-3, pp404-408, 2006.

[20] Chan, K. C. and Lee, W. B., "A theoretical prediction of the strain path of

anisotropic sheet metal deformed under uniaxial and biaxial stress state", *International Journal of mechanical Sciences,* Vol. 32, No. 6, pp.497-511, 1900.

[21] Cui, Z. and Gao, L., "Studies on hole-flanging process using multistage incremental forming", *CIRP Journal of Manufacturing Science and Technology,* In Press, Available online 2 March 2010

[22] Dai, K., Wang, Z.R. and Fang, Y., "CNC incremental sheet forming of an axially symmetric specimen and the locus of optimization", *Journal of Materials Processing Technology,* Vol.102, pp 164-167, 2000.

[23] Dejardin, S., Thibaud, S., Gelin, J.C. and Michel, G., "Experimental investigations and numerical analysis for improving knowledge of incremental sheet forming process for sheet metal parts", *Journal of Materials Processing Technology,* Vol. 210, Issue 2, pp363-369, 2010.

[24] Duflou, J. R., Verbert, J., Belkassem, B., Gu, J., Sol, H., Henrard, C. and Habraken, A. M., "Process window enhancement for single point incremental forming through multi-step toolpaths", *CIRP Annals - Manufacturing Technology,* Vol. 57 pp. 253-256, 2008.

[25] Emmens W. C. and van den Boogaard, A. H., "Tensile tests with bending: a mechanism for incremental forming", *International Journal of Material Forming,* Vol. 1, Issue 1, pp. 1155-1158, 2008.

[26] Emmens W. C. and van den Boogaard, A. H., "Incremental forming by continuous bending under tension—An experimental investigation", *Journal of materials processing technology,* Vol. 209, No.14, pp. 5456-5463, 2009.

[27] Edwards, k. R., Edwardson, S. P., Carey, C., Geoff, D., Watkins, K. G., "Laser micro peen forming without a tamping layer", *International Journal of Advanced Manufacturing Technology,* Vol. 47, Issues 1-4, pp191-200, 2010.

[28] Erkorkmaz, K. and Altintas, Y., "High speed CNC system design. Part II: modeling and identification of feed drives", *International Journal of Machine Tools and Manufacture,* Vol.41, Issue 10, pp1487-1509, 2001.

[29] Eyckens, P., Van Bael, A., Van Houtte, P. and Duflou, J. R., "Forming limit predictions for the serrated strain paths in single point incremental forming", *Proceedings Numiform 07 Portugal, AIP CP908,* pp. 141–146, 2007.

[30] Eyckens, P., Moreau, J. D., Duflou, J. R. , Bael, A. V. and Houtte, P. V., "MK modelling of sheet formability in the incremental sheet forming process, taking into account through-thickness shear", *International Journal of Material Forming,* Vol. 2, pp 379-382, 2009.

[31] Eyckens, P., Van Bael, A., Aerens, R., Duflou, J. R., and Van Houtte, P., "Small-scale finite element modelling of the plastic deformation zone in the incremental forming process", *International Journal of Material Forming,* Vol. 1, No.1 , pp1159-1162, 2008.

[32] Filice, L., Fratini, L. and Micari, F., "Analysis of material formability in incremental forming", *Annals of CIRP,* Vol. 51, No.1, pp. 199–202, 2002.

[33] Filice, L., Ambrogio, G. and Micari, F., "On-line control of single point incremental forming operations through punch force monitoring", *CIRP Annals - Manufacturing Technology,* Vol. 55, Issue 1, pp 245-248, 2006.

[34] Geiger, M. and Vollertsen, F., "The mechanisms of laser forming", *CIRP Annals - Manufacturing Technology,* Vol. 42, No. 1, pp 301-304, 1993.

[35] Geiger, M., Merklein, M. and Pitz, M., "Laser and forming technology—an idea and the way of implementation", *Journal of materials processing technology,* vol. 151, pp3-11, 2004.

[36] Geiger, M., Duflou, J., Kals, H. J .J., Shirvani, B. and Singh, U. P., "Incremental sheet forming with an industrial robot - forming limits and their effect on component design", *Advanced Materials Research,* Vol. 6-8, pp.457-464, 2005.

[37] Ham, M. and Jeswiet, J., "Forming limit curves in single point incremental forming", *CIRP Annual- Manufacturing Technology,* Vol. 56, pp277-280, 2007.

[38] Hardt, D.E., Olsen, B.A., Allison, B.T. and Pasch, K., "Sheet metal forming with discrete die surfaces", *Proceedings of Ninth American Manufacturing Research Conference* pp. p140–p144, 1981.

[39] Hardt, D.E., Webb, R.D. and Suh, N. P., "Sheet metal die forming using closed loop shape control", *Annual of CIRP,* Vol. 31, pp. 165–169, 1982.

[40] Henrard C., 2008, *Numerical Simulations of the Single Point Incremental Forming Process,* PhD thesis, Université de Liège., 2008

[41] Hirt, G., Ames, J., Bambach, M. and Kopp, R., "Forming strategies and process

modeling for CNC incremental sheet forming", *CIRP Annals—Manufacturing Technology*, Vol. 53, No.1, pp. 203–206, 2004.

[42] Hill R., "A theory of yielding and plastic flow of anisotropic metals", *International Journal of Mathematical, Physical and Engineering Sciences*, Vol. 193, pp281-297, 1948.

[43] Hill R., "Theoretical plasticity of textured aggregates," *Mathematical Proceedings of the Cambridge Philosophical Society*, Vol. 85, pp179-191, 1979.

[44] Hong, T., Ooi, J.Y., Shaw, B., "A numerical simulation to relate the shot peening parameters to the induced residual stresses", *Engineering Failure Analysis*, Vol.15, pp1097-1110, 2008.

[45] Huang, Y., Chen, Y.P. and Du, R., "A new approach to solve key issues in multi-step inverse finite element method in sheet metal stamping", *International Journal of Mechanical Science*, Vol.48, No.6, pp591-600, 2006.

[46] Hu, S., Li, Y.F., Ju, T. and Zhu, X., "Modifying the shape of NURBS surfaces with geometric constraints", *Computer Aided Design*, Vol.33, pp903-912, 2001.

[47] Hu, Z.Q., Li, M.Z., Cai, Z.Y. and Gong, X.P., "Continuous flexible forming of three-dimensional surface parts using bendable rollers", *Materials Science and Engineering: A*, Vol. 499, Issues 1-2, pp 234-237, 2009.

[48] Hussain, G., Gao, L. and Dar, N.U., "An experimental study on some formability evaluation methods in negative incremental forming", *Journal of Materials Processing Technology*, Vol.186, Issues 1-3, pp45-53, 2007.

[49] Hussain, G. and Gao, L. , "A novel method to test the thinning limits of sheet metals in negative incremental forming", *International Journal of Machine Tools and Manufacture*, Vol. 47, Issues 3-4, pp419-435, 2007.

[50] Hussain, G., Gao, L., Hayat, N., Cui, Z., Pang, Y.C. and Dar, N.U., "Tool and lubrication for negative incremental forming of a commercially pure titanium sheet", *Journal of Materials Processing Technology*, Vol.203, pp193-201, 2008.

[51] Hussain, G., Gao, L. Hayat, N., and Dar, N.U "The formability of annealed and pre-aged AA-2024 sheets in single-point incremental forming", *International Journal of Advanced Manufacturing Technology*, Vo. 37, pp496-503.

[52] Hwang, Y. M and Altan, T., "Finite element analysis of tube hydroforming

processes in a rectangular die", *Finite Elements in Analysis and Design*, Vol. 39, pp1071–1082, 2002.

[53] Iseki, H., Shioura, T. and Sato, K., "Practical development of press-molding machine with small punching tool", *Proceedings of the Fifth International Conference on Technology of Plasticity*, pp. 935–938, 1996.

[54] Iseki H., "An approximate deformation analysis and FEM analysis for the incremental bulging of sheet metal using a spherical roller", *Journal of Materials Processing Technology,* Vol.111, pp 150-154, 2001.

[55] Iseki, H. and Naganawa, T., "Vertical wall surface forming of rectangular shell using multistage incremental forming with spherical and cylindrical rollers", *Journal of Materials Processing Technology,* Vol.130-131, 675-679, 2002.

[56] Jackson, K., Allwood, J., "The mechanics of incremental sheet forming", *Journal of Materials Processing Technology*, Vol. 209, pp1158-1174, 2009.

[57] Jie, L., Jianhua, M. and Shuhuai, H., "Sheet metal dieless forming and its tool path generation based on STL files", *International Journal Advanced Manufacturing Technology*, Vol. 23, pp696-699, 2004.

[58] Jeswiet, J., Micari, F., Hirt, G., Bramley, A., Duflou, J., Allwood, J., "Asymmetric single point incremental forming of sheet metal", *CIRP Annals - Manufacturing Technology*, Vol.54, Issue 2, pp88-114, 2005.

[59] Jeswiet, J., Geiger, M., Engel, U., Kleiner, M., Schikorra, M., Duflou, J., Neugebauer, R., Bariani, P. and Bruschi, S., "Metal forming progress since 2000", *CIRP Annals - Manufacturing Technology,* Vol.1, pp2-17, 2008.

[60] Kawai, K., Yang, L.N. and Kudo, H., "A flexible shear spinning of axi-symmetrical shells with a general-purpose mandrel", *Journal of Materials Processing Technology,* Vol.192-193, pp 13-171, 2007.

[61] Kim, T. J. and Yang, D. Y., "Improvement of formability for the incremental sheet metal forming process", *International Journal of Mechanical Sciences,* Vol.42, pp 1271-1286, 2000.

[62] Kim, Y. H. and Park, J. J., "Effect of process parameters on formability in incremental forming of sheet metal", *Journal of Materials Processing Technology*, Vol. 130-131, pp 42-46, 2002.

[63] Kim, Y. H. and Park, J. J., "Fundamental studies on the incremental sheet metal forming technique", *Journal of Materials Processing Technology*, Vol. 140, pp 447-453, 2003.

[64] Kim, H., Nargundkar, N. and Altan, T., "Prediction of bend allowance and springback in air bending", *Journal of Manufacturing Science Technology*, Vol. 129, pp342-351, 2007.

[65] Kim, T. Y., Lee, J. H., Lee, H. and Cheong, S. K., " An area-average approach to peening residual stress under multi-impacts using a three-dimensional symmetry-cell finite element model with plastic shots", *Materials & Design*, Vol. 31, Issue 1, pp 50-59, 2010.

[66] Kitazawa, K., Wakabayashi, A., Murata, K. and Seino, J., "A CNC incremental sheet metal forming method for producing the shell components having sharp components", *Journal of Japan Society for Technology of Plasticity*, Vol. 35, No.406, pp. 1348–1353, 1994.

[67] Kopp, R. and Schulz, J., "Flexible sheet forming technology by double-sided simultaneous shot peen forming", *CIRP Annals - Manufacturing Technology*, Vol.51, Issue 1, pp195-198, 2002.

[68] Kopac, J. and Campus, Z., "Incremental sheet metal forming on CNC milling machine tool", *Journal of Materials Processing Technology*, Vol. 162–163, pp622–628, 2005.

[69] Kulkarni, K. M. , Schey J. A. and Badger D. V., "Investigation of shot peening as a forming process for aircraft wing skins", *Journal of Applied Metalworking*, Vol. 1, No.4, pp 34-44, 1981.

[70] Lamminen, L., Tuominen, T. and Kivivuori S., "Incremental sheet forming with an industrial robot", *Materials Forum*, Vol. 29, 331-335, 2005.

[71] Lan, J., Dong, X.H. and Li, Z.G., "Inverse finite element approach and its application in sheet metal forming", *Journal of Material Processing Technology*, Vol.170, No.3, pp624-631, 2005.

[72] Lee, C.H. and Huh, H., "Blank design and strain estimates for sheet metal forming processes by a finite element inverse approach with initial guess of linear

deformation", *Journal of Material Processing Technology*, Vol. 82, No.1-3, pp145-155, 1998.

[73] Levers, A.and Prior, A., "Finite element analysis of shot peening," *Journal of Material Processing Technology*, Vol. 80-81, pp304-308, 1998.

[74] Leszak, E., "Apparatus and process for incremental dieless forming", Patent US3342051A1, 1967.

[75] Li, M. Z., Cai, Z. Y., Sui Z. and Yan, Q. G., "Multi-point forming technology for sheet metal", *Journal of Materials Processing Technology*, Vol. 129, Issues 1-3, pp333-338, 2002.

[76] Liu, C. G., Li, M. Z. and Fu, W. Z., "Principles and apparatus of multi-point forming for sheet metal", *The International Journal of Advanced Manufacturing Technology*, Vol.35, No.11-12, pp1227-1233, 2008.

[77] Liu, J. and Mo, J., "Tool path generation based on STL file for sheet metal dieless forming", *Chinese Journal of Mechanical Engineering*, Vol. 17, pp. 230-232, 2004.

[78] Logan, R. W. and Hosford, W. F., "Upper-bound anisotropic yield locus calculations assuming <111> pencil glide", *International Journal of Mechanical Sciences*, Vol. 22, pp. 419-430, 1980.

[79] Luo, Y., He, K. and Du, R., "Studies on a new incremental sheet metal forming process: using geometric, FEM and experiments", *Proceedings of DET2009*, Hong Kong, 2009.

[80] Luo, Y., He, K. and Du, R., "A new sheet metal forming system based on incremental punching, Part 1: Modeling and simulation", *International Journal of Advanced Manufacturing Technology*, available online, 2010.

[81] Luo, Y., He, K. and Du, R., "A new sheet metal forming system based on incremental punching, Part 2: machine building and experiment results", *International Journal of Advanced Manufacturing Technology*, available online, 2010.

[82] Marciniak, Z. and Kuczynski, K., "Limits strains in the processes of stretch-forming sheet metal, *International Journal of Mechanical Sciences*, Vol. 9, pp. 609-620, 1967.

[83] Marciniak, Z., Duncan, J. L. and Hu, S. J., *Mechanics of sheet mental forming*, Butterworth Heinemann, Oxford, England, 2002.

[84] Martins, P., Bay, N., Skjoedt, M., and Silva, M., "Theory of single point incremental forming," *CIRP Annals - Manufacturing Technology*, Vol. 57, pp. 247–252, 2008.

[85] Matsubara, S., "Development of dieless spinning machine having single roller", *Proceedings of the 1994 Japanese Spring Conference on Technology of Plasticity*, pp. 387, 1994.

[86] Matsubara, A, Lee, K, Ibaraki, S, Kakino, Y, and Endo, M, "Enhancement of feed drive dynamics of NC machine tools by actively controlled sliding guideway", *JSME International Journal Series C*, Vol. 47, No. 1, pp.150-159, 2004.

[87] Meier, H., Buff, B., Laurischkat, R. and Smukala, V., "Increasing the part accuracy in dieless robot-based incremental sheet metal forming", *CIRP Annals - Manufacturing Technology*, Vol. 58, Issue 1, pp233-238, 2009.

[88] Micari, F., Geiger, M., Duflou, J., Shirvani, B., Clarke, R., Lorenzo, D. R. and Fratini, L., "Two point incremental forming with two moving forming tools", *Key Engineering Materials*, Vol. 344, pp. 599-605, 2007.

[89] Micari, F., Ambrogio, G. and Filice, L., "Shape and dimensional accuracy in single point incremental forming: State of the art and future trends", *Journal of Materials Processing Technology*, Vol.191, pp. 390-395, 2007.

[90] Micari, F., Ambrogio, G. and Filice L., "Shape and dimensional accuracy in single point incremental forming: State of the art and future trends", *Journal of Materials Processing Technology*, Vol. 191, pp. 390-395.

[91] Minutolo, F. C., Durante, M., Formisano, A., Langella, A., "Evaluation of the maximum slope angle of simple geometries carried out by incremental forming process", *Journal of Materials Processing Technology*, Vol.194, Issues 1-3, pp145-150, 2007.

[92] Mori, K. I., Yang, G. and Osakada, K., "Determination of optimal motion of tools in metal forming processes by controlled FEM simulation", *International Journal of Machine Tools and Manufacture*, Vol. 35 , Issue 6, pp851-859, 1995.

[93] Mori, K., Yamamoto, M. and Osakada,K., "Determination of hammering sequence

in incremental sheet metal forming using a genetic algorithm", *Journal of Materials Processing Technology*, Vol. 60, pp.463–468, 1996.

[94] Murata, A., "A new trial on incremental forming of sheet metal parts", *R&D Review of Toyota CRDL*, Vol. 34 No. 3 1999.

[95] Naceur, H., Delamiere, A., and Batoz, J.L., "Some improvements on the optimum process design in deep drawing using the inverse approach", *Journal of Material Processing Technology*, Vol.46, No.2, pp250-262, 2004.

[96] Nakajima, N., "Numerical control for traditional manual forming of sheet metal", *Journal of Japan Society for Technology of Plasticity*, Vol.23, pp. 696–700, 1979.

[97] Na1, S. J. and Kim, J. T., "3D laser forming strategies for sheet metal by geometrical information", *International Journal of Material Forming*, Vol.1, No. 1, pp1367-1370, 2008.

[98] Ong, S. K, De Vin, L. J, Neeand, A. Y. C. and Kals, H. J .J, "Fuzzy set theory applied to bend sequencing for sheet metal bending", *Journal of Materials Processing Technology*, Vol. 69, No.1-3, pp29-36,1997.

[99] Park J. J and Kim Y. H., "Fundamental studies on the incremental sheet metal forming technique", *Journal of Materials Processing Technology*, Vol. 140, Issues 1-3, pp447-453, 2003.

[100] Pearce, R., *Sheet metal forming*, Bristol, Philadelphia and New York, IOP Publishing Ltd Techno House, 1991.

[101] Pohlak, M., Küttner, R., Majak, J., Karjust, K. and Sutt, A., "Simulation of incremental forming of sheet metal products", *Proceeding of 4th International DAAAM Conference*, Tallinn, Estonia, pp143-145, 2004.

[102] Pohlak, M., Küttner, R. and Majak, J., "Modelling and optimal design of sheet metal RP&M processes", *Rapid Prototyping Journal*, Vol.11, No. 5, pp: 304-311, 2005.

[103] Puzik, A., "Incremental sheet forming with a robot system for an industrial application", *The 41st CIRP Conference on Manufacturing Systems*, Tokyo, Japan, pp. 421-424, 2008.

[104] Raithatha, A., Jackson, K., Duncan, S. and Allwood, J., "New method for nodeling plastic deformation in incremental sheet forming", *Proceedings of the 2006 IEEE*

International Conference on Control Applications, Munich, Germany, 2006.

[105] Rauch, M., Hascoet, J. Y., Hamann, J. C. and Plenel, Y., "Tool path programming optimization for incremental sheet forming applications", *Computer-Aided Design,* Vol. 41, Issue 12, pp877-885, 2009.

[106] Schafer, T. and Schraft, R. D., "Incremental sheet metal forming by industrial robots", *Rapid Prototyping Journal,* Vol. 11, pp278-286, 2005.

[107] Shankar, R., Jadhav, S., Goebel, R., Homberg, W. and Kleiner, M., "Incremental sheet metal forming of preformed sheets", *Proceeding of the 8th International Conference on Technology of Plasticity,* Verona, Italy, 2005.

[108] Shi, Y. J., Yao, Z. Q., Shen, H. and Hu, J., "Research on the mechanisms of laser forming for the metal plate", *International Journal of Machine Tools and Manufacture,* Vol. 46, No. 12-13, pp689-1697, 2006.

[109] Shima, S., Kotera, H., Murakami, H., Nakamura, N., "Development of flexible spinning – a fundamental study", *Advanced Technology of Plasticity (Proceedings of the Fifth ICTP),* pp. 557–560, 1996.

[110] Shim, M. S. and Park, J. J., "The formability of aluminum sheet in incremental forming", *Journal of Material Processing technology*, Vol.113, pp 654-658, 2001.

[111] Shimizu, I., "Asymmetric forming of aluminum sheets by synchronous spinning", *Journal of Materials Processing Technology,* Vol. 210, Issue 4, pp585-592, 2010.

[112] Strano, M., Ruggiero, M. and Carrino, L., "Technological representation of forming limits for negative incremental forming of thin aluminum sheets", *Journal of Manufacturing Processing Technology,* Vol.7, pp122-129, 2005.

[113] Silva, M. B., Skjoedt, M., Martins, P.A.F. and Bay, N., "Revisiting the fundamentals of single point incremental forming by means of membrane analysis," *International Journal of Machine Tools & Manufacture*, Vol. 48, pp. 73–83, 2008.

[114] Silva, M.B., Skjoedt, M., Bay, N. and Martins, P.A.F., "Revisiting single-point incremental forming and formability/failure diagrams by means of finite elements and experimentation ", *Journal of Strain Analysis for Engineering Design*, Vol. 44, No. 4, pp 221-234, 2009.

[115] Skjoedt, M., Bay, N., Endelt, B. and Ingarao, G., "Multi stage strategies for single

point incremental forming of a cup", *International Journal of Material Forming*, Suppl. 1, pp. 1199–1202, 2008.

[116] Stoughton, T. B, "A general forming limit criterion for sheet metal forming", *International Journal of Mechanical Sciences,* Vol. 42, pp1-27, 2000.

[117] Strano, M., Ruggiero, M. and Carrino, L., "Technological representation of forming limits for negative incremental forming of thin aluminum sheets", *Journal of Manufacturing Processes*, Vol. 7, pp. 122-129, 2005.

[118] Takano, H., Kitazawa, K. and Goto, T., "Incremental forming of nonuniform sheet metal: Possibility of cold recycling process of sheet metal waste", *International Journal of Machine Tools and Manufacture*, Vol. 48, Issues 3-4, pp477-482, 2008.

[119] Tanaka, S., Nakamura, T., and Hayakawa, K., "Incremental sheet metal forming using elastic tools", *Advanced Technology of Plasticity (Proceedings of the Sixth ICTP),* Erlangen, Germany, pp.1477–1482, 1999.

[120] Tang, B.T., Zhao, Z., Lu, X.Y., Wang, Z.Q., Zhao, X.W. and Chen, S.Y., "Fast Thickness Prediction and Blank Design in Sheet Metal Forming Based on an Enhanced Inverse Analysis Method", *International Journal Mechanical Science,* Vol. 49, pp1018-1028, 2007.

[121] Tang, B.T., Zhao, Z., Lu, X.Y., Wang, Z.Q., Zhao, X.W. and Chen, S.Y., "Fast thickness prediction and blank design in sheet metal forming based on an enhanced inverse analysis method", *International Journal Mechanical Science,* Vol. 49, pp1018-1028, 2007.

[122] Tuomi, J. and Lamminen, L., "Incremental sheet forming as a method for sheet metal component prototyping and manufacturing", *Proceeding of 10th European Forum on Rapid Prototyping*, 2004.

[123] Verbert, J., Belkassem, B., Henrard, C., Habraken, A.M., Gu, J., Sol, H., Lauwers, B. and Duflou, J.R., "Multi-step toolpath approach to overcome forming limitations in single point incremental forming", *International Journal of Material Forming*, Suppl. 1, pp. 1203–1206, 2008.

[124] Vihtonen, L., Puzik, A. and Katajarinne, T., "Comparing Two Robot Assisted Incremental Forming Methods: Incremental Forming by Pressing and Incremental Hammering", *International Journal of Material Forming,* Vol.1, Sup. 1, 2008.

[125] Walczyk, D.F. and Hardt, D.E., "Design and analysis of reconfigurable discrete dies for sheet metal forming", *Journal of Manufacturing System,* Vol.17, pp. 436–454, 1998.

[126] Walczyk, D.F., Lakshmikanthan, J. and Kirt, D.R., "Development of a reconfigurable tool for forming aircraft body panels", *Journal of Manufacturing System,* Vol. 17, pp. 287–296, 1998.

[127] Wang, T., Platts, M.J. and Levers, A., "A process model for shot peen forming", *Journal of Materials Processing Technology,* Vol. 172, Issue 2, pp159-162, 2006.

[128] Wong, C. C., Dean, T. A. and Lin, J., "A review of spinning, shear forming and flow forming processes", *International Journal of Machine Tools and Manufacture,* Vol. 43, Issue 14, pp 1419-1435, 2003.

[129] Xia, Q. X., Cheng, X. Q., Hu, Y. and Ruan, F., "Finite element simulation and experimental investigation on the forming forces of 3D non-axisymmetrical tubes spinning", *International Journal of Mechanical Sciences,* Vol. 48, Issue 7, pp 726-735, 2006.

[130] Yamashita, M., Gotoh, M. and Atsumi, S. Y., "Numerical simulation of incremental forming of sheet metal", *Journal of Materials Processing Technology,* Vol.199, Issues 1-3, pp163-172, 2008.

[131] Yang, M. and Shima, S., "Development of new bending die—development of an intelligent flexible bending system", *Journal of Japan Society for Technology of Plasticity,* Vol. 32, No.370, pp. 1377–1382, 1991.

[132] Yang, M., Manabe, K. and Nishimura, H., "Development of an intelligent tool system for flexible L-bending process of metal sheets", *Smart Materials and Structures,* Vol. 7, pp. 530–536, 1998.

[133] Yoon, S. J. and Yang, D. Y., "An incremental roll forming process for manufacturing doubly curved sheets from general quadrilateral sheet blanks with enhanced process features", *CIRP Annals - Manufacturing Technology,* Vol. 54, Issue 1, pp221-224, 2005.

[134] Zhu, Y., Dodd, B., Caddell, R. M., and Hosford W. F., "Convexity Restrictions on non-quadratic anisotropic yield criteria", *International Journal of Mechanical Sciences,* Vo. 29, pp.733-741, 1987.

Instruction for Collection of Graduation Certificate

If you collect your graduation certificate in person, please fill in Section A. If you authorize a representative to collect it on your behalf, please fill in both Sections A and B.

(The personal data of the graduate or the representative will be used for collection of the certificate and record purpose only. This Instruction and copy of the graduate's ID document will be kept in the Graduate School for not less than 7 years.)

Section A: Personal data of the graduate

Name (in English): _____   Name (in Chinese): _____

Year of Graduation: _____   HKID Card No.*: _____

Degree: _____   Programme: _____

Time Basis: ☐ Full-time ☐ Part-time

* If you do not have a HKID card, please present your CU student ID card, or passport/ID document, the name and date of birth printed on which must match with those in your student record, for verification.

Section B: Letter of Authorization
(Please bring along the copy of ID document of the graduate for verification)

I (the Graduate) hereby authorize the following person to collect my graduation certificate on my behalf:

Personal data of my representative

Name (in English): _____   Name (in Chinese): _____

Name of ID Document of
Representative: _____

ID Document No. of
Representative: _____

Signature of Graduate: _____   Date: _____

For Graduate School Office use only:

Acknowledgement of receipt of the graduation certificate

Signature of
Graduate/Representative: _____   Date: _____

Staff: _____   Date: _____

THE CHINESE UNIVERSITY OF HONG KONG
Graduate School

<u>Application for Certifying Letter</u>

(Please read the Notes for Application at the back before completing this form.)

A. Personal Particulars

Name (in English) : _____   (in Chinese, if any) : _____

Student ID No. : _____   HKID Card No. # : _____

Date of Birth (DD/MM/YYYY) : _____   Division: _____

Programme: _____   Degree/Diploma: _____

Time Basis : ☐ Full-time   ☐ Part-time   Study Year / Year of Graduation : _____

Correspondence Address : _____

_____

Contact Tel. No(s). : _____   E-mail: _____

(# The HKID Card No. is for verification of the identity of the applicant.)

B. No. of copies applied for : _____

C. Purpose of Application (Please put a "✓" as appropriate)

☐ for application for visa to other countries
☐ for other purposes (please specify): _____

D. Payment Method (Please put a "✓" as appropriate)

☐ by ATM (please attach original receipt)   ☐ by PPS (payment reference No. _____)
☐ by e-banking   ☐ by EPS   ☐ by cheque / bankdraft

E. Method of Despatch (Please put a "✓" as appropriate)

☐ Please send the certifying letter(s) by mail (Please fill in the address slip to which your Certifying Letter is to be sent.):
    ☐ air/surface (no additional postal charge)   ☐ registered (HK$13)
    ☐ express (overseas only, HK$6)   ☐ Others (please specify) _____

☐ I will collect in person.

☐ To be collected by the person authorized in the letter attached.

Signature : _____   Date : _____

FOR OFFICE USE ONLY:

1. _____ Copy/copies at $40.00 each HK$ _____   2. For inter-departmental transfer
    Postage   HK$ _____   Postage involved HK$ _____
    <u>Total :</u>   HK$ _____

	Date	Signature
Application received on		
Certifying letter(s) despatched on		
Certifying letter(s) collected on		_____ (Applicant's Signature)